Winter 12-15-2021

Causal Function and Bias Correlation of the Orbitofrontal Cortex in Economic Choices

Shi Weikang
Washington University in St. Louis

WASHINGTON UNIVERSITY IN ST. LOUIS
Division of Biology and Biomedical Sciences
Neurosciences

Dissertation Examination Committee:
Camillo Padoa-Schioppa, Chair
Todd Braver
Adam Kepecs
Ilya Monosov
Lawrence Snyder
Joni Wallis

Causal Function and Bias Correlation of the Orbitofrontal Cortex in Economic Choices

by

Weikang Shi

A dissertation presented to
The Graduate School
of Washington University in
partial fulfillment of the
requirements for the degree
of Doctor of Philosophy

May 2022
St. Louis, Missouri

Table of Contents

List of Figures ..... **v**

List of Tables ..... **vii**

Acknowledgments ..... **viii**

Abstract ..... **x**

Chapter 1: Introduction **1**

1.1 Economic choices and the orbitofrontal cortex 1

1.1.1 Economic choices 1

1.1.2 The orbitofrontal cortex 3

1.2 Value signals in the OFC 6

1.3 Decision mechanism of the OFC 10

1.4 Summary 13

Chapter 2: Values encoded in orbitofrontal cortex are causally related to economic choices **15**

2.1 Introduction 16

2.2 Results 17

2.2.1 Experiment 1: high-current stimulation 17

2.2.2 Experiment 2: low-current stimulation 22

2.3 Discussion 26

2.4 Methods 27

2.4.1 Choice tasks 28

2.4.2 Electrical stimulation 30

2.4.3 Data analysis 32

2.4.4 Predicting the range-dependent bias 33

2.4.5 Interpretation of the order bias 35

2.4.6 Data and code availability 39

2.5 Supplementary figures 39

Chapter 3: Economic choices under simultaneous or sequential offers rely on the same neural circuit **50**

3.1 Introduction 52
3.2 Results 54
3.2.1 Comparing choices across tasks 54
3.2.2 Neuronal classification in each choice task 60
3.2.3 Matching classifications across choice tasks 65
3.2.4 Matching maximum selectivity windows across choice tasks 71
3.3 Discussion 72
3.4 Methods 76
3.4.1 Animal subjects and choice tasks 76
3.4.2 Behavioral analysis 79
3.4.3 Neuronal recordings 81
3.4.4 Neuronal classification within task modality 81
3.4.5 Comparing classification across choice task 84
3.4.6 Selective activity range 86
Chapter 4: Neuronal origins of biases in economic choices under sequential offers 87
4.1 Introduction 88
4.2 Results 93
4.2.1 Choice biases under sequential offers 93
4.2.2 Origins of choice biases: Computational framework 99
4.2.3 Reduced accuracy under sequential offers emerged at the valuation stage 100
4.2.4 The order bias emerged during value comparison (decision stage) 104
4.2.5 The preference bias emerged late in the trial (post-comparison) 111
4.3 Discussion 119
4.3.1 Behavioral values, neuronal values and the origins of choice biases 119
4.3.2 Conclusion 122
4.4 Methods 123
4.4.1 Animal subjects, choice tasks and neuronal recordings 123
4.4.2 Preliminary analyses 125
4.4.3 Data sets 128
4.4.4 Comparing tuning functions across choice tasks 130
4.4.5 Neuronal measures of relative value 131
4.4.6 Activity profiles of chosen juice cells 132

4.5 Supplementary figures 134
Chapter 5: Conclusion 139
References 142

List of Figures

Figure 2.1: High-current stimulation of OFC disrupts valuation……..……..…….…..18

Figure 2.2: Effects of electrical stimulation at different current levels……..…….21

Figure 2.3: Prediction of range-dependent choice bias induced by electrical stimulation…..…24

Figure 2.4: Range-dependent choice bias induced by neuronal facilitation of OFC…..…….25

Figure 2.S1: Exp.2, control for choice frequency……..40

Figure 2.S2: Exp.2, results obtained in paired sessions…….42

Figure 2.S3: Exp.2, analysis of response times (RTs)……...……43

Figure 2.S4: Exp.1, range-dependent choice biases…….…….45

Figure 2.S5: Stimulation in Exp.2 did not systematically alter the sigmoid steepness……...…..46

Figure 2.S6: Exp.1, interpretation of the order bias…….…….47

Figure 3.1: Experimental design and behavioral performance.....……..…….……..56

Figure 3.2: Three example neurons……..…..…….62

Figure 3.3: Comparing classification across tasks, possible results……..……..……64

Figure 3.4: Neuronal classification is consistent across choice tasks……...……...67

Figure 3.5: Significant departures from chance level in OR table reflect correlations between the encoded variables...……...…….……...…….……..69

Figure 3.6: Comparing neuronal classification within and across choice tasks…….…….70

Figure 3.7: Maximum selectivity windows (MSWs) are matched across choice tasks……...74

Figure 4.1: Computational framework…..……..…….....92

Figure 4.2: Experimental design and choice biases……..……..…….....96

Figure 4.3: Order bias and preference bias……...……...98

Figure 4.4: Lower choice accuracy in Task 2 reflects weaker offer value signals…..…..…...102

Figure 4.5: Fluctuations in order bias and fluctuations in the activity of chosen value cells....106

Figure 4.6: Order bias and circuit inhibition…….....……..……...109

Figure 4.7: The preference bias does not reflect differences in the activity of chosen value cells……..……...……..……...113

Figure 4.8: Preference bias and choice probability in chosen juice cells……...…..…..…...117

Figure 4.S1: Comparing tuning functions across choice tasks……...…...…...135

Figure 4.S2: The order bias does not reflect differences in the tuning of offer value cells…….136

Figure 4.S3: The preference bias does not reflect differences in the tuning of offer value cells.……...…...137

List of Tables

Table 2.S1: Exact p values for the statistical tests ran for Fig.2.2……..…….……..48

Table 2.S2: Data set for Exp.1……..……..…….……..49

Table 3.1: Definition of variables in Task 1 and Task 2…….....……..…….……..58

Table 3.2: Neuronal classification in Task 2…….……...……..……...……..59

Table 4.S1: Neuronal encoding of decision variables in the two choice tasks…...…….……138

Acknowledgments

I am deeply grateful to my PhD advisor Camillo Padoa-Schioppa. He has been a great mentor, and teaches and influences me from all aspects in being a scientist and doing research. I am inspired by his optimism and passion in pursuing scientific questions, and I admire his intelligence and great intuition in science. I also very appreciate the opportunity he has provided to me, and the support and advice from him for my future academic career.

I would like to thank my committee members, Todd Braver, Adam Kepecs, Ilya Monosov, Lawrence Snyder and Joni Wallis for their support and advice in my PhD research, and Daniel Moran for his help during the early stage. I appreciate all the professors and peers in the CCSN pathway. They have been extremely helpful and opened my mind to think about neuroscience questions in a broader way.

I would also like to thank all the current and previous members of the Padoa-Schioppa lab. I am grateful to Ahmad Jezzini, Alessandro Livi, Jiaxin Tu and Manning Zhang for being so supportive and friendly. I enjoyed a lot from the intellectual and fun conversation during the lab meetings and lab dinners. Jue Xie was a great mentor when I was first rotating in the lab. Katherine Conen has been and will be the peer I admire. Sebastien Ballesta has been a wonderful colleague to work with, and I am very thankful to have co-authored with him. The biggest thanks go to Heide Schoknecht. She makes the lab feel like family by celebrating everyone's birthday, and she helped train the monkeys in all the experiments.

I feel lucky to have many friends to make my graduate school life brighter. Special gratitude goes to Hao Chen, Zhikai Liu, and Kaining Zhang. I would also like to thank the Neuroscience program directors, and to the program coordinator Sally Vogt.

Finally, I owe my deepest gratitude to my parents for their love and care. They always have faith in me and support me for all the decisions I made without any doubt. I also want to thank my partner, Ty Rhoads. He always cheers me up and shows me his greatest understanding and support. I feel grateful to have him in my life.

This dissertation study was funded by CCSN pre-doctoral fellowship.

Special thanks to the Washington University Graduate School for allowing us to use this dissertation and thesis template as a starting point for the development of this document.

Weikang Shi

Washington University in St. Louis

May 2022

ABSTRACT OF THE DISSERTATION

Causal Function and Bias Correlation of the Orbitofrontal Cortex in Economic Choices

by

Weikang Shi

Doctor of Philosophy in Biology and Biomedical Sciences

Neurosciences

Washington University in St. Louis, 2022

Professor Camillo Padoa-Schioppa, Chair

Economic choices entail two mental processes, value calculation and value comparison (Niehans, 1990). Studies in the last twenty years have shown that neurons in the orbitofrontal cortex (OFC) could support both processes. Namely, in the studies in which monkeys chose between two juice options with various amounts, three functional cell groups had been found in the OFC: offer value cells encode the value of individual juices, chosen juice cells encode the choice in a binary way and chosen value cells encode the value of the chosen juice (Padoa-Schioppa and Assad, 2006). These results suggest a decision circuit within OFC with offer value cells encoding the input and chosen juice cells encoding the output (Padoa-Schioppa, 2011). However, this proposal remains tentative. If OFC is crucial to the economic choices, neural activities in the OFC should 1) causally relate to the decisions and 2) explain the behavioral variabilities. Therefore, in my dissertation studies, I aim to examine these two aspects. In the first study, we use electrical stimulation to establish the causal link between neuronal activity in the OFC and the economic choices. We find that low current micro-stimulation increases the

encoded values and facilitates the choices by inducing a range-dependent bias. On the other hand, high current micro-stimulation disrupts both the valuation and comparison stages, and affects the order bias under sequential offer and reduces the choice accuracy. In the second study, we focus on the neural correlates with behavioral biases under sequential offers. We train the monkeys to perform a task in which trials from simultaneous offers and sequential offers are randomly interleaved. We first confirm that the same neural circuit mechanism is adopted under simultaneous offers and sequential offers. This result provides the basis to examine the neural correlates using a unified decision model we proposed based on simultaneous offers. We then compare the behavioral patterns of simultaneous offers and sequential offers. We find that sequential offers show lower choice accuracy, bias in favor of the preferred juice (preference bias) and bias in favor of the second offer (order bias). Neural correlates of each of the biases reveal that low choice accuracy partly reflects the weaker value signals in sequential offers, order bias is correlated with comparison signals and preference bias emerges late in the comparison stage. Taken together, my dissertation studies fill in some important gaps between the neuronal activity of the OFC and the economic choices.

Chapter 1: Introduction

1.1 Economic choices and the orbitofrontal cortex

1.1.1 Economic choices

Imagining you are in a restaurant and looking at the menu, you have many options, and you need to choose one of them for lunch. Neuroeconomics studies how the brain makes the economic choices in this case. Neuroeconomics is rooted in behavioral economics, which could date back to the eighteenth century. During this classical period, Daniel Bernoulli, Adam Smith and Jeremy Bentham hypothesized that for individuals, economic choices relied on computing and comparing subjective values of options (Kreps, 1990; Niehans, 1990). This proposal inspired many of the following economists. Since then, the concept of subjective values has developed into the idea of expected utilities and has been widely accepted in the field of economics (Kreps, 1990). Expected utility theories with modifications were used to explain many different aspects in the human economic behaviors. With a great number of behavioral studies at hand, starting from late twentieth century, psychologists turned to focus on the cognitive mechanisms behind these behaviors (Kahneman et al., 1982; Kahneman and Tversky, 1979, 2000). Following this line, neuroeconomics was originated, and has been a lively field for decades (Camerer et al., 2005). Over almost two hundred years, this field has experienced a prosperous growth with tremendous details being filled in, however, the core idea has not changed, that is, economic choices entail two mental stages, value computation and comparison. In the era of neuroeconomics, this field aims to understand how the brain processes these two mental stages. Studies have been done and continue to be done to understand which brain areas participate in

the mental stages, and how single neurons, neural populations and neural circuits play the role. With the development of the technology, neuroeconomics study has extended outside of human research. Monkey and rodent models have been well established and continued shedding light upon the field.

Early efforts focused on value computation, and the first step was to define the values. According to the expected utility hypothesis (Kreps, 1990), values were the mathematical expectations of the utilities of options. Therefore, in a risky decision, such as gambling, the value of one option was the money one could gain or lose multiplied by the probability. However, such objective definition lost the subjectiveness of these values. To define the subjective value, people started to focus on the behavioral pattern. Economic choices were all about choosing among options, therefore, instead of calculating the absolute value of one option, it was possible to focus on the preferences revealed by the choices. Hypothetically, economic choices are guided by subjective values, and options with higher values are more likely to be chosen. Therefore, by looking at the choice pattern, one can derive the values that guide the behavior. In this favor, many studies have designed trade-off tasks between goods, and the trade-off pattern would demonstrate the relative subjective values between two goods. For example, one apple might be better than one orange, however, one apple and two oranges might be chosen equally often. It demonstrates that one apple has twice value of one orange. Although the pure value of an apple or an orange may never be identified, such analysis measures the subjective preference over the two options, and if one option is used as the value unit, subjective values can be therefore defined (e.g., the value of an apple is 2 in the unit of orange). However, the definition of relative values has the circularity problem: values are not defined independently from the behaviors. Identifying the physical entities could be a solution, and from the perspective of neuroscience,

the physical entities are neurons. Therefore, after well defining values, the next step in the field of neuroeconomics moves to pursue the value signals within the brain. Typically, multiple variables based on values are defined, such as values of one option or chosen options. These variables will then serve as regressors to correlate with neural activities. Conclusions can be drawn from significant correlations that these neurons encode the variables (Kable and Glimcher, 2007, 2009; Padoa-Schioppa and Assad, 2006; Rangel et al., 2008; Wallis and Rich, 2011). Following this line of analysis, value signals have been found in many brain areas in both human and animal studies (Padoa-Schioppa and Cai, 2011; Padoa-Schioppa and Conen, 2017; Wallis, 2007, 2012), such as orbitofrontal cortex (OFC) and ventromedial prefrontal cortex (vmPFC).These value representations across different brain areas support that neuronal activities are the physical entities of subjective values. After decades of substantial progress, now the field drastically moves to disentangle the mechanism behind value comparison. While solving this question, studies in neuroeconomics have been deeply influenced by related fields such as motor systems and perceptual decisions. Hence, these fields provide different working hypotheses for economic choices, including distributed consensus(Cisek, 2012), attentional drift diffusion model(Krajbich et al., 2010; Krajbich et al., 2012; Krajbich and Rangel, 2011) and accept/reject model (Hayden, 2018).

1.1.2 The orbitofrontal cortex

The focus of OFC in economic choices started from the patient Phineas Gage back in the nineteenth century (Damasio et al., 1994). After recovering from the damage of his left frontal lobe, his behaviors had changed dramatically including complex decision makings (Damasio et al., 1994). Since then, an extensive literature of human patient studies found that damages of OFC are associated with violations in economic choices (Camille et al., 2011; Cavedini et al.,

2006; Fellows, 2011; Fellows and Farah, 2007; Rahman et al., 2001; Rahman et al., 1999; Strauss et al., 2014; Volkow and Li, 2004). In animal studies, results showed that lesions of homologous OFC area in non-human primates and rodents impair goal-directed behaviors (Gallagher et al., 1999; Gardner et al., 2017; Gardner et al., 2020; Gremel and Costa, 2013; Izquierdo and Murray, 2004; Izquierdo et al., 2004; West et al., 2011). Goal-directed behaviors are defined based on reinforcer devaluation (Balleine and Dickinson, 1998; Colwill and Rescorla, 1985; Daw et al., 2005). In these experiments, subjects have first learned the rewards (values) of the options through the mechanism of reinforcement learning. Then before the choice task, subjects are divided into two groups. The experiment groups undergo a devaluation procedure of one of the options, such as selective satiation or association with bitter taste. As the result of devaluation, during the choice task, compared with control groups, the experimental subjects choose significantly less of the devalued options. These results are interpreted as that devaluation has reduced the subjective value of one option. In the OFC lesion studies in animal models, the evidence of impairment in goal-directed behaviors was that subjects were less sensitive to the reinforcer devaluation (Pickens et al., 2003; Rhodes and Murray, 2013; Rudebeck and Murray, 2008, 2011; West et al., 2011). Taken together, these studies showed that OFC played a crucial role in economic choices.

In all these different studies, the definitions and locations of the OFC are slightly different. Commonly, the OFC refers to brain area located at the orbital gyrus, including Brodmann area 11l and 13m/l (Carmichael et al., 1994; Carmichael and Price, 1994; Ongur and Price, 2000). Non-human primates have homologous OFC defined in the same way; in rodents, the homologue is lateral orbital (LO) area (Ongur and Price, 2000). It is the center of the orbital network, which is a heavily interconnected network across many sensory related brain areas (Ongur et al., 1998;

Ongur and Price, 2000; Price, 2007; Way et al., 2007). Anatomically, OFC receives input from sensory areas such as visual, somatosensory, olfactory, gustatory, and insular cortex, as well as areas with higher cognitive functions, such as memory hub hippocampus and emotion center amygdala. These afferent connections make OFC the potential brain area that integrates both external and internal information and then forms the subjective values. Concurrently, OFC sends output to the lateral prefrontal cortex (Petrides and Pandya, 2006; Saleem et al., 2013), which then projects widely to motor and premotor areas (Takahara et al., 2012). Such connection indicates that OFC might finalize the decision and project the output to the downstream to transit into a motor action. From the connectivity pattern, several other brain areas appear seemingly to play the similar function as OFC. First candidate is anterior cingulate cortex (ACC). ACC has little interconnection with OFC (Ongur and Price, 2000); however, its connection pattern is similar with OFC (Ongur et al., 2003; Paus, 2001), putting it at the similar position as a brain area integrating signals from different sources. However, ACC lesions did not affect reinforcer devaluation indicating that ACC may not be the core brain area in economic choices (Kennerley et al., 2006; Rudebeck et al., 2008; Rushworth et al., 2007). Another brain area is ventromedial prefrontal cortex (vmPFC, area 14). Due to its adjacent location to OFC (Ongur and Price, 2000), early lesion studies focused on vmPFC may accidentally damage OFC and misled the researchers to conclude its function in economic choices. Recent studies with more precise lesions and neural activity recordings indicated that vmPFC may not involve in economic choices (Rudebeck and Murray, 2011). What is more, despite its close location to OFC, vmPFC has distinct connection pattern, and OFC and vmPFC have sparse interconnection (Ongur et al., 2003; Ongur and Price, 2000). It is more likely that vmPFC has different functions. Except for OFC, basolateral amygdala (BLA) is another brain area that affects reinforcer devaluation after

lesions (Baxter et al., 2000; Ostlund and Balleine, 2008; Pickens et al., 2003; Rhodes and Murray, 2013; Wellman et al., 2005). BLA and OFC also show strong interconnections (Ongur and Price, 2000). Further work is required to distinguish the function of BLA and OFC in economic choices.

1.2 Value signals in the OFC

Many studies have found that OFC encodes value-related signals. Early work found that neurons in OFC responded to juice quantities modulated by motivational level of the animals and external context such as temporal delay (Roesch and Olson, 2005; Roesch et al., 2006), and responded to potential aspects related to juice values, including juice types (Wallis and Miller, 2003) and delivery probabilities (Raghuraman and Padoa-Schioppa, 2014). The first clearest results came from a task in which monkeys chose between two different juices offered in variable amounts (Padoa-Schioppa and Assad, 2006). The task paradigm provided a quantity/quality trade-off between the two options, and the indifference point of the choice pattern measured the relative value. In this study, three types of neurons have been identified based on their encoding properties: offer value cells encode the value associated with one juice type; chosen juice cells encode the juice type of the chosen option; chosen value cells encode the value of the chosen option regardless of juice type. These results are significant in three ways: First, as mentioned, relative value is a subjective measure, this study confirms the neural correlates of subjective values, indicating that neurons might be the physical entities for the values (Kreps, 1990; Padoa-Schioppa, 2007; Padoa-Schioppa and Cai, 2011). Second, they show that neural representation of values is “good-based”, which means that OFC neurons are associated with one juice option (Padoa-Schioppa, 2011). Third, the properties of the cell types imply a decision network, in

which offer value cells encode the input information and chosen juice cells encode the output of choice and may project the decision to the downstream brain area. Therefore, these results lead to a proposal that decisions might be processed within the OFC, both valuation and comparison (Padoa-Schioppa and Conen, 2017). Many subsequent works have shown converging evidence that "good-based" representation of subjective values appear in OFC under variant conditions. In a recent study with juice bundle task (Pastor-Bernier et al., 2019), in which two juice types bundled together to form options, the researchers found that some OFC neurons encoded the integrated value of one bundle and that some neurons encoded the value associated with one juice. In another study (Ballesta and Padoa-Schioppa, 2019), researchers used a similar juice quantity/quality trade-off task but presented the two options sequentially. In this sequential offer task, researchers successfully replicated the finding of three neuron types in the OFC. These results indicated that "good-based" value encoding might be a universal mechanism and invariant in different types of economic choices.

The variance of economic choices is more than different types of task structures (Padoa-Schioppa, 2013). Even in the simplest task, choosing between two options at the same time, the context may change and lead to different behavioral consequences. If OFC is the neural mechanism behind economic choices, it should be able to adapt to these different behavioral contexts. The first study is about menu invariance (Padoa-Schioppa and Assad, 2008). It is the property that the identities or the values of the other options do not affect the neuronal encoding of the value associated with one particular good, that is, value encoding is invariant to the menu. It was observed in a study (Padoa-Schioppa and Assad, 2008) in which monkeys chose between three juices (A, B and C) offered pairwise, and trials of each pairs (A:B, B:C and C:A) were interleaved. In this task, OFC neurons encoded the values and identities of each juice option

through offer value cells and chosen juice cells, and these encodings did not depend on the other juice offered concurrently, for example, B associated neurons (i.e. offer value B cells and chosen juice B cells) stayed stable in both A:B and B:C conditions.

The second study is about range adaptation. Neuronal adaptation exists ubiquitously in sensory, cognitive, and motor systems. In neuroeconomics and OFC, range adaptation is a property of value encoding neurons, including offer value cells and chosen value cells. For these neurons, their gains are inversely correlated with the value ranges contextually available (Conen and Padoa-Schioppa, 2019; Cox and Kable, 2014; Kobayashi et al., 2010; Padoa-Schioppa, 2009; Saez et al., 2017). For example, range adaptation was found in the study (Padoa-Schioppa, 2009), in which the value offered for each juice varied from trial to trial within a fixed range, and value ranges varied across sessions. The tuning of offer value and chosen value cells was always linear, but their tuning slopes were inversely proportional to the range of values available in any given session. Thus, the same range of firing rates represented different value ranges in different sessions. This range adaptation result shows how value representation can flexibly adapt to changing context (Conen and Padoa-Schioppa, 2019; Rustichini et al., 2017).

The third study is about remapping (Xie and Padoa-Schioppa, 2016). Completely different sets of goods can be provided in different decision contexts, and remapping is the property about how the neuronal representation in OFC adjusts to this aspect of context variability. The major results came from the study where monkeys chose between different pairs of juices in two blocks of trials (A:B and C:D). Different types of neurons (i.e. offer value cells, chosen juice cells and chosen value cells) were identified separately in each trial block. Neurons encoding the identity or the subjective value of particular goods in a given context ‘‘remapped’’ and became

associated with different goods when the context changed. For example, neurons associated with juice A became associated with juice C. Concurrently, the functional role of individual cells and the overall organization of the decision circuit remained stable across contexts. For example, offer value cells remained offer value cells. Therefore, neuronal remapping indicates both the stability (stable circuit) and the flexibility (adaptive remapping) of value representation of OFC neurons. Overall, OFC encodes values in a stable but flexible way, making it very suitable as the neural mechanism behind economic choices.

However, it should be noted that, finding and confirming the value signals in the OFC still cannot guarantee the sufficiency and necessity of the brain area in economics choices. There are several reasons. First, even though these tasks were well designed, the definition of values may still be confused by other factors, such as motivation (Tremblay and Schultz, 1999). Second, the claim that economic decisions are made "as if" subjective values are generated and compared is still a hypothesis. The value signals detected in these experiments may lead to other behaviors rather than economic choices (Wallis and Rich, 2011). Hence, value signals do not imply that these neurons participate in the choice per se. Third, brain is a network, and OFC keeps communicating with other brain areas (Ongur and Price, 2000). Value signals found in the OFC may be generated somewhere else and projected to the OFC. These questions all point to the issue of building the causal relationship between value encoding of OFC and economic choices (Wolff and Olveczky, 2018). The first study presented in this dissertation aims to build such causal relationship, and the details will be discussed in **Chapter 2**.

1.3 Decision mechanism of the OFC

In the recent study in which monkeys chose between two juice options with variant amount(Padoa-Schioppa and Assad, 2006), the researchers found three types of cells encoding offer value associated with one juice type, the type of chosen juice, and the chosen value. These cell groups include both the input (offer value) and output (chosen juice), proposing that decisions might be formed within this area through a local neural circuit. Two lines of evidence support this proposal: first one is the computational modeling; second one is the experimental results linking the neuronal fluctuations with decision variabilities.

Many different computational models support the concept that good-based decisions are generated within the OFC. First, in one study (Rustichini and Padoa-Schioppa, 2015), researchers built a biophysically realistic neural network directly comprised of the three groups of cells identified in OFC (Padoa-Schioppa and Assad, 2006). This model was adapted from a neural network designed for perceptual decisions (Wang, 2002; Wong and Wang, 2006), which obtained biophysically realistic parameters derived from experimental results (Brunel and Wang, 2001). The model successfully generated the binary economic choices. Second, other modelling studies without restricts about the three cell groups still suggest that these cell groups are important and necessary for making value-based choice. For example, in one study (Song et al., 2017), researchers trained a recurrent neural network (RNN) with a variety of decision-making tasks. The network was not specific to any particular tasks and not restricted to have any types of structures. When the researchers trained the RNN with a value-based binary choice task, similar with the task used for monkeys (Padoa-Schioppa and Assad, 2006), they found that after the training, the units in the RNN recapitulated the three types of cells identified from the

experiments, that is units encoding offer value, chosen value and chosen juice. Similar results were also found in other types of neural network (Zhang et al., 2018). These models were based on more liberal assumptions, however, they ultimately converged to the same results, suggesting that the three groups of neurons identified in OFC might be necessary to generate good-based economic decisions.

For experimental evidence, the most important ones come from the analysis between neural activity in the OFC and choice variability. In the context of economic choices, choice variability appears when decisions are split when facing the same options (hard trials), for example animal may sometimes choose 1A or 2B, when the options are 2B:1A. Several results found that the trial-by-trial fluctuations in the activity of different groups of cells in OFC can explain these choice variabilities.

The first study is to analyze the choice probability (CP). CP has been frequently studied for the perceptual decisions (Britten et al., 1992). It is a property of individual neuron. It measures the probability that an imaginary ideal observer would successfully infer the outcome when looking at the activity of this neuron. In perceptual decisions, CP analysis of the sensory input neurons is extremely useful, because it can test whether the brain uses this sensory information to guide the decisions. Therefore, for economic decisions, there were studies focusing on offer value cells, the input units of the OFC decision network (Conen and Padoa-Schioppa, 2015; Padoa-Schioppa, 2013). If CPs of offer value cells are higher than chance level, we could say economic decisions may be guided by the input value information calculated by offer value cells. In the experiments, although the authors found that although the CPs of offer value cells were lower compared than the typical CPs found in the sensory neurons in perceptual decisions (Britten et al., 1992; Britten et al., 1996; Cohen and Newsome, 2009; Nienborg and Cumming, 2006, 2014; Romo et al.,

2002), they were still significantly higher than chance level. Therefore, economic choices may be primarily based on the values encoded by offer value cells.

The second analysis focused on the output units in the OFC decision network, chosen juice cells. Studies has found that the choice hysteresis is correlated with the activity of these output united in the time window before the offer presentation (‘‘predictive activity’’) (Padoa-Schioppa, 2013). Predictive activity of chose juice cells sets the initial state of neural circuit before a new trial starts. When in the new trial, the decision is easy to make, one group of chosen value cells will have dominant activity and exceed the influence from the initial state. However, if the decision is hard, which means the values of the two options are similar, neither group of chosen value cells dominates the activity, in this case, the initial state becomes effective to influence the decisions. Therefore, another way to understand this predictive activity of chosen juice cells is that it is largely the tail activity from the previous trial. Choice hysteresis is a history bias: monkeys tend to choose on any given trial the same juice chosen in the previous trial, especially for the difficult trials (Padoa-Schioppa, 2013). Thus, the correlation between choice hysteresis and predictive activity indicated an underlying neural mechanism for this history bias. To be noted, these findings have been replicated in the modeling work as well (Bonaiuto et al., 2016; Rustichini and Padoa-Schioppa, 2015).

These two sets of analyses showed that both the offer value cells and chosen juice cells are involved to generate economic decisions. The third analysis suggests that chosen value cells also contribute to the decisions. The phenomenon, termed as “activity overshooting”, describes that the activity of chosen value cells is also modulated by the value of the non-chosen option on top of the chosen value (Padoa-Schioppa, 2013): chosen value cells have higher activity when the non-chosen value makes the decision more difficult. In other words, firing rates of chosen value

cells present a transient overshooting reflecting the decision difficulty. This result indicates that activity overshooting may be accounted for if chosen value cells are within the decision circuit. The result is replicated by models as well (Rustichini and Padoa-Schioppa, 2015).

Following the similar lines of analyses, in the **Chapter 3** and **Chapter 4** of my dissertation, we will explore how neural activity in OFC correlates with choice variability and choice bias under the condition of sequential offers.

1.4 Summary

In the modern era of neuroeconomics, the goal is to identify the neural entities of values and reveal the decision mechanisms in the brain at neuronal level. Values that guide economic choices are subjective and integrating both internal and external states. Neural entities of values should reflect these properties. Anatomical connection of OFC provides a premise that neural activity of the OFC functions as the physical entity of values. Lesion studies specified its uniqueness as one of the only two brain areas known so far to affect reinforcer devaluation which shares the spirit of economic choices. Results focused on neural activity showed that OFC encodes integrated subjective values. These value representations show a stable but flexible property, which suit well the traits of economic choices. What's more, OFC has been found encoding both the input and output in economic choices, indicating that a decision circuit might be formed within this brain area. Such idea is further supported by computational modeling and experimental results linking neural activities and choice variability. Taken together, studies from the past decades demonstrate that OFC is the core brain area for both stages of the economic choices: valuation and comparison.

With all these previous understandings in hand, in my dissertation studies presented in the following chapters, we aimed to further explore the link between OFC and economic choices. We specially study the causal function of OFC in economic choices (**Chapter 2**) and the neural correlates of choice variability under the condition of sequential offers (**Chapter 3** and **Chapter 4**).

Chapter 2: Values encoded in orbitofrontal cortex are causally related to economic choices

This chapter is adapted from the following publication with the permission from the co-authors:

Ballesta*, S., Shi*, W., Conen, K. E., & Padoa-Schioppa, C. (2020). Values Encoded in Orbitofrontal Cortex are Causally Related to Economic Choices. Nature, 588(7838), 450-453. (* equal authorship)

Abstract

When agents make economic choices, neurons in the orbitofrontal cortex encode the subjective values of offered and chosen goods. Neuronal activity in this area suggests the formation of a decision, and neural signals capturing the binary choice outcome emerge gradually over time. However, it is unclear whether these neural processes are causally related to choices. More generally, the evidence linking economic choices to value signals in the brain remains correlational. We address this fundamental issue using electrical stimulation in rhesus monkeys. We show that suitable currents bias choices by increasing the value of individual offers. Furthermore, high-current stimulation disrupts both the computation and the comparison of subjective values. These results validate a centuries-old hypothesis and provide new foundation for research in neuroeconomics.

2.1 Introduction

In the 18th century, Daniel Bernoulli, Adam Smith and Jeremy Bentham proposed that economic choices rely on the computation and comparison of subjective values (Niehans, 1990). This hypothesis continues to inform modern economic theory (Kreps, 1990) and research in behavioral economics (Kahneman and Tversky, 2000), but behavioral measures are ultimately not sufficient to prove the proposal (Camerer et al., 2005). Consistent with the hypothesis, when agents make choices, neurons in the orbitofrontal cortex (OFC) encode the subjective value of offered and chosen goods (Padoa-Schioppa and Assad, 2006). Value encoding cells integrate multiple dimensions (Hare et al., 2008; Kennerley et al., 2009; Pastor-Bernier et al., 2019; Roesch and Olson, 2005). Furthermore, variability in the activity of each cell group correlates with variability in choices (Conen and Padoa-Schioppa, 2015; Padoa-Schioppa, 2013), and the population dynamics suggests the formation of a decision (Eldridge et al., 2016). However, it is unclear whether these neural processes are causally related to choices. More generally, the evidence linking economic choices to value signals in the brain (Bartra et al., 2013; Roesch and Olson, 2007; Schultz, 2015) remains correlational (Stalnaker et al., 2015). Here we show that neuronal activity in OFC is causal to economic choices. We conducted two experiments using electrical stimulation in rhesus monkeys. Low-current stimulation increased the subjective value of individual offers and thus predictably biased choices. Conversely, high-current stimulation disrupted both the computation and the comparison of subjective values, and thus increased choice variability. These results demonstrate a causal chain linking subjective values encoded in OFC to valuation and choice.

2.2 Results

In principle, causal links between a neuronal population and a decision process are demonstrated if one can predictably bias choices using electrical stimulation (Cohen and Newsome, 2004; Clark et al., 2011). Thus classic work established the causal role of the middle temporal (MT) area in motion perception by showing that low-current stimulation biases (Salzman et al., 1990) while high-current stimulation disrupts (Murasugi et al., 1993) perceptual decisions. One challenge in using this approach for economic choices is the lack of columnar organization in OFC. Since neurons associated with different goods available for choice are physically intermixed (Conen and Padoa-Schioppa, 2015), one cannot selectively activate neurons associated with one particular good using electrical stimulation. We developed two experimental paradigms to circumvent this challenge.

2.2.1 Experiment 1: high-current stimulation

Exp.1 examined whether perturbing OFC disrupts choices. Monkeys chose between two juices labeled A and B (with A preferred) offered in variable amounts. The two offers were presented sequentially in the center of a computer monitor (**Fig.2.1A**). Trials in which juice A was offered first and trials in which juice B was offered first were referred to as "AB trials" and "BA trials", respectively. The terms "offer1" and "offer2" referred to the first and second offer, independent of the juice type and amount. For each pair of juice quantities, the sequential order of the two offers varied pseudo-randomly. On roughly half of the trials, high-current stimulation (≥100 μA) was delivered in OFC during offer1 or during offer2 presentation (in separate sessions). In each session, trials with and without stimulation were pseudo-randomly interleaved (see **Methods**).

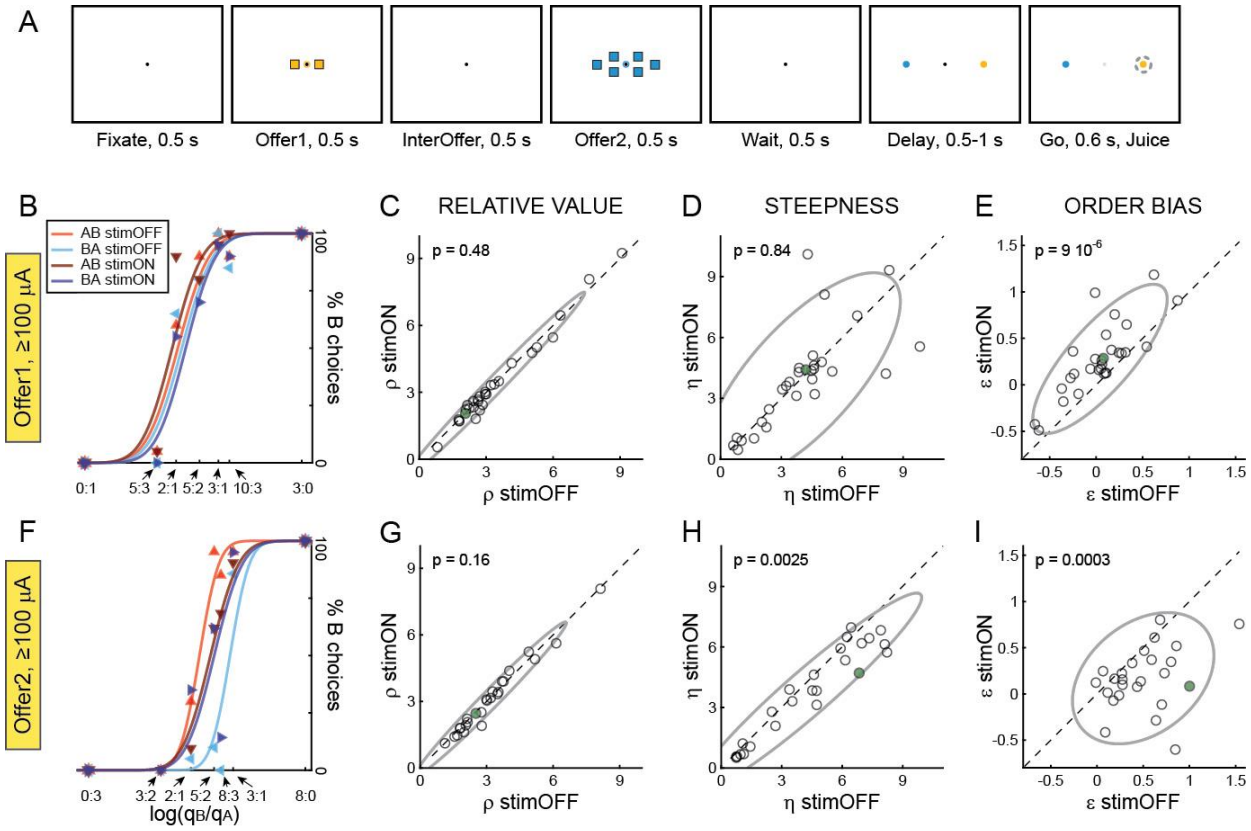

Figure 2.1. High-current stimulation of OFC disrupts valuation. **A.** Experiment 1, design. Offers, represented by sets of squares, appeared centrally and sequentially. In this trial, the animal chose between 2 drops of grape juice and 6 drops of peppermint tea. **B.** Example session 1. In half of the trials, we delivered 125 µA current during offer1. The panel illustrates the choice pattern for AB trials (red) and BA trials (blue), separately for stimOFF trials (light) and stimON trials (dark). Data points are behavioral measures and lines are from probit regressions (Eq.1). In each condition (stimOFF, stimON), the order bias (ε) quantified the distance between the two flex points. In stimOFF trials, a small order bias favored offer2 ($\varepsilon_{stimOFF}$ =0.02). In stimON trials, the order bias increased (ε_{stimON} =0.07). Hence, stimulation biased choices in favor of offer2. **CDE.** Population results for stimulation during offer1 (N=29 sessions, ≥100 µA). Stimulation did not affect relative values (C); it did not consistently affect the sigmoid steepness (D); and it biased choices in favor of offer2 (E). **F.** Example session 2. Here 125 µA current was delivered during offer2. Stimulation induced a bias in favor of offer1 ($\varepsilon_{stimON}<\varepsilon_{stimOFF}$) and increased choice

variability (shallower sigmoids in stimON trials; $\eta_{stimON}<\eta_{stimOFF}$). **GHI.** Population results for stimulation during offer2 (N=25 sessions, ≥100 μA). Stimulation did not affect relative values (G); it reduced the sigmoid steepness (H); and it biased choices in favor of offer1 (I). In panels CDEGHI, green symbols are from sessions shown in B and F; ellipses indicate 90% confidence intervals. All p values are from two-tailed Wilcoxon tests, and very similar results were obtained using t tests.

For each group of trials (stimON, stimOFF), choice patterns were analyzed with a probit regression:

$$\text{choice B} = \Phi(X) \tag{2.1}$$

$$X = a_0 + a_1 \log(q_B/q_A) + a_2 (\delta_{order,AB} - \delta_{order,BA})$$

where choice B = 1 if the animal chose juice B and 0 otherwise, Φ was the cumulative function of the standard normal distribution, q_A and q_B were the quantities of juices A and B offered, $\delta_{order,AB} = 1$ in AB trials and 0 in BA trials, and $\delta_{order,BA} = 1-\delta_{order,AB}$. From the fitted parameters, we derived measures for the relative value $\rho=\exp(-a_0/a_1)$, the sigmoid steepness $\eta=a_1$, and the order bias $\varepsilon=a_2$. Intuitively, ρ was the quantity that made the animal indifferent between 1A and ρB, η was inversely related to choice variability, and ε was a bias favoring the first or second offer. Specifically, $\varepsilon<0$ ($\varepsilon>0$) indicated a bias in favor of offer1 (offer2).

In one representative session, electric current was delivered during offer1. The stimulation induced a choice bias in favor of offer2 (**Fig.2.1B**). This effect was consistent across N=29 sessions: high-current stimulation during offer1 did not systematically alter the relative value or the sigmoid steepness, but it induced a systematic bias in favor of offer2 (**Fig.2.1CDE**). In a different set of N=25 sessions, we delivered ≥100 μA during offer2. In this case, stimulation induced a systematic bias in favor of offer1 (**Fig.2.1FI**). These complementary effects are interpreted as high-current stimulation interfering with or disrupting the ongoing computation of the offer value, resulting in a choice bias for the other offer (see **Methods**). In addition, stimulation during offer2, but not during offer1, significantly increased choice variability (**Fig.2.1FH**). This effect may be interpreted as high-current stimulation disrupting value comparison (i.e., the decision), which took place upon presentation of offer2. A similar effect was observed in mice when OFC was inactivated using optogenetics (Kuwabara et al., 2020).

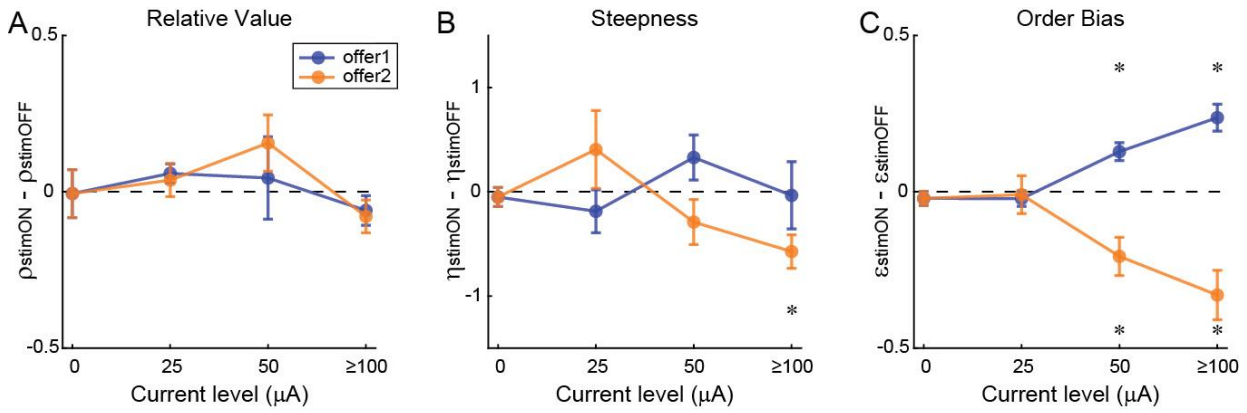

Figure 2.2. Effects of electrical stimulation at different current levels. The whole data set includes N=29/22/29 sessions in which 25/50/≥100 μA were delivered during offer1, N=17/22/25 sessions in which 25/50/≥100 μA were delivered during offer2, and N=50 control sessions (0 μA; 194 sessions total). **A.** Relative value. **B.** Sigmoid steepness. **C.** Order bias. In each panel, blue and yellow refer to stimulation during offer1 and offer2, respectively. Data points are averages across sessions and error bars indicate SEM. Asterisks highlight measures that differed significantly from zero (all $p<0.005$, two-tailed Wilcoxon test). All other measures were statistically indistinguishable from zero (all $p>0.05$, two-tailed Wilcoxon test). **Table 2.S1** provides the exact p values. Statistical analyses based on t tests provided very similar results.

We also examined the effects of stimulation at lower currents. In essence, the effects observed at ≥100 μA diminished and gradually vanished when the electric current was reduced to 50 μA and 25 μA (**Fig.2.2**). In summary, high-current stimulation of OFC disrupted the neural processes underlying economic choice, namely value computation during offer1, and value computation and value comparison during offer2.

2.2.2 Experiment 2: low-current stimulation

The results described so far showed that OFC perturbation can disrupt valuation and choice. We next examined whether subjective values may be increased through physiological facilitation (Wolff and Olveczky, 2018). In Exp.2, we took advantage of the fact that neurons in OFC undergo range adaptation (Kobayashi et al., 2010; Padoa-Schioppa, 2009). **Fig.2.3** illustrates our rationale. In this experiment, monkeys chose between two juices offered simultaneously (**Fig.2.3A**). In these conditions, two groups of cells in OFC encode the offer values of juices A and B (Padoa-Schioppa, 2013; Padoa-Schioppa and Assad, 2006). Importantly, their tuning curves are quasi-linear and the gain is inversely proportional to the value range (range adaptation) (Padoa-Schioppa, 2009; Rustichini et al., 2017). Moreover, cells in each group adapt to their own value range. The effect of low-current stimulation is to increase the firing rate of neurons in proximity of the electrode (Histed et al., 2009; Salzman et al., 1990). In turn, this increase in firing rate is equivalent to a small increase in the offer values. By virtue of range adaptation, for a given current, the increase in value is proportional to the value range (**Fig.2.3BC**). If an equal number of offer value A cells and offer value B cells are close to the electrode tip, then the effect of the electric current is equivalent to increasing both offer values. Crucially, if the two value ranges are unequal, the increases in offer value are also unequal. More

specifically, the offer value of the juice with the larger range increases more. Hence, the net effect on choices is expected as follows: Low-current electrical stimulation should bias choices in favor of the juice offered with the larger value range (**Fig.2.3D; Methods**).

We tested this prediction in two animals. In each session, we selected juice types and quantity ranges such that value ranges (ΔVA, ΔVB) would differ. Electrical stimulation (50 μA) was delivered in OFC for 1 s during offer presentation. Trials with and without stimulation were pseudo-randomly interleaved. In each session, choice patterns were analyzed with a probit regression:

$$\text{choice B} = \Phi(X) \tag{2.2}$$

$$X = a_0 + a_1 \log(q_B/q_A) + a_2 (\delta_{stim,ON} - \delta_{stim,OFF})$$

where $\delta_{stim,ON} = 1$ in stimulation trials and 0 otherwise, and $\delta_{stim,OFF} = 1 - \delta_{stim,ON}$. We computed the relative value for each group of trials and we defined the change in relative value induced by the stimulation as $\delta\rho = \rho_{stimON} - \rho_{stimOFF}$.

In one representative session, value ranges were such that $\Delta V_A < \Delta V_B$. Consistent with our prediction, electrical stimulation induced a bias in favor of juice B ($\delta\rho<0$, **Fig.2.4A**). In another session, where $\Delta V_A > \Delta V_B$, we measured $\delta\rho>0$ (**Fig.2.4B**). A population analysis found that the choice bias $\delta\rho$ and the difference in value range $\Delta V_A - \Delta V_B$ were strongly correlated across sessions. This result held true in each monkey (**Fig.2.4CD**). Control analyses confirmed that range-dependent biases did not reflect simple heuristics (**Fig.2.S1**) and were not dictated by the juice types or the electrode position (**Fig.2.S2**).

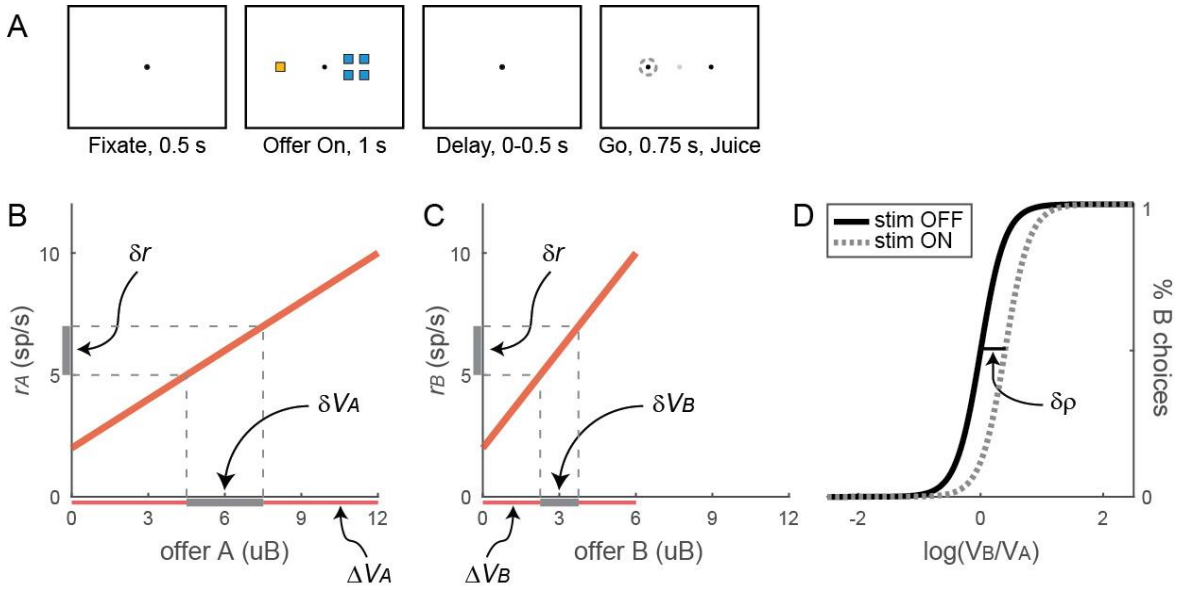

Figure 2.3. Prediction of range-dependent choice bias induced by electrical stimulation (facilitation). **A.** Experiment 2, design. Two offers are presented simultaneously. After a brief delay, the animal indicates its choice with a saccade. Electrical stimulation (50 μA) is delivered throughout offer presentation. **BCD.** Predictions for one example session. In OFC, the encoding of offer values is predominantly positive (higher activity for higher values). Panels B and C represent the (mean) tuning curves for pools of offer value A cells and offer value B cells under adapted conditions. Firing rates (y-axis) are plotted as a function of the offer values (x-axis) expressed in units of juice B (uB). Red horizontal lines represent the two value ranges, with $\Delta V_A > \Delta V_B$. The same firing rate interval δr corresponds to different value intervals, with $\delta V_A > \delta V_B$. Panel D represents choice patterns. Electrical stimulation increases both offer values, but the net effect is a choice bias in favor of juice A ($\delta\rho > 0$). Conversely, in sessions where $\Delta V_A < \Delta V_B$, δr induces $\delta V_A < \delta V_B$, and electrical stimulation biases choices in favor of juice B ($\delta\rho < 0$, not shown). See **Methods**.

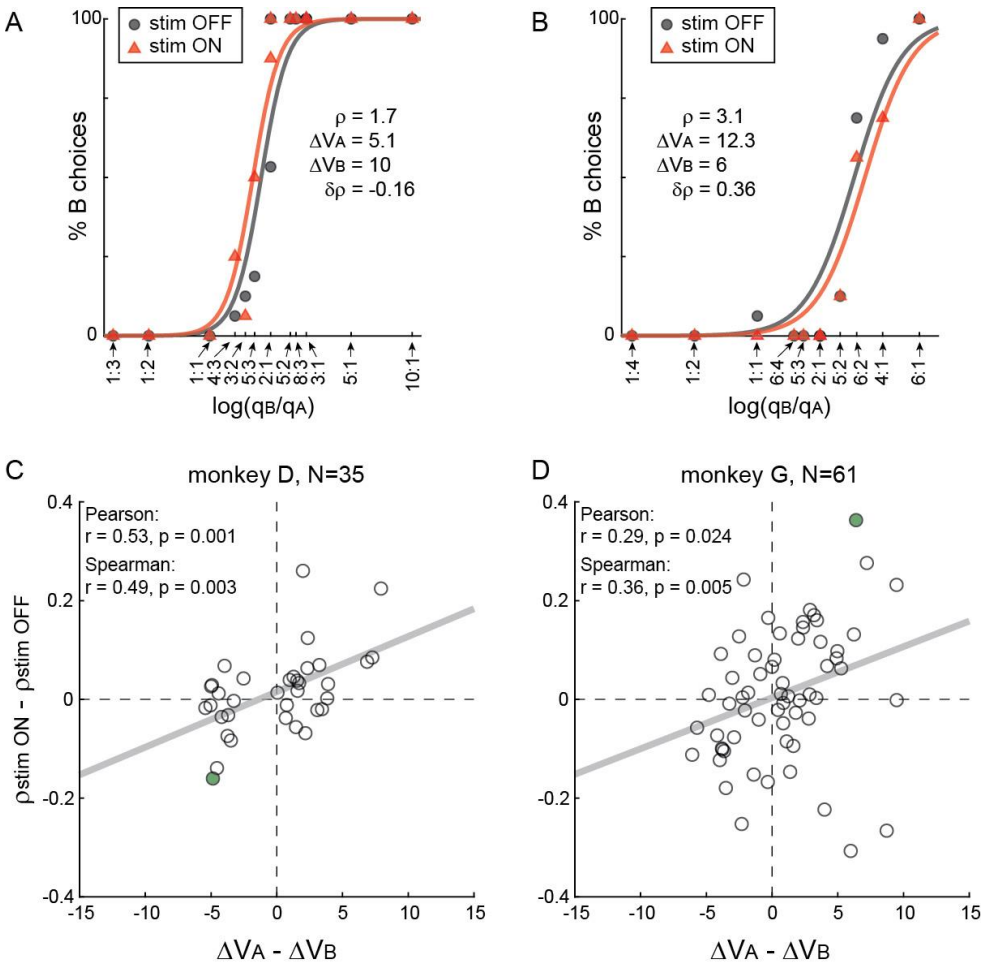

Figure 2.4. Range-dependent choice bias induced by neuronal facilitation of OFC. **A.** Example session 1. In this session, we set $\Delta V_A<\Delta V_B$. Consistent with the prediction, electrical stimulation biased choices in favor of juice B ($\delta\rho<0$). **B.** Example session 2. In this case, we set $\Delta V_A>\Delta V_B$. Electrical stimulation biased choices in favor of juice A ($\delta\rho>0$). **CD.** Population analysis. The two panels refer to the two animals. In each panel, the choice bias ($\delta\rho$, y-axis) is plotted against the difference in value range ($\Delta V_A–\Delta V_B$, x-axis). Each data point represents one session, and the gray line is from a linear regression. Value ranges are expressed in units of juice B (uB). The two measures are significantly correlated in both monkey D (r=0.53, p=0.001, Pearson correlation test; r=0.49, p=0.003, Spearman correlation test) and monkey G (r=0.29, p=0.024, Pearson correlation test; r=0.36, p=0.005, Spearman correlation test). Green data points are from sessions illustrated in panels A and B.

The rationale of Exp.2 rests on the assumption that low-current stimulation increases the value of the two offers (**Fig.2.3**). An analysis of response times (RTs) supported this point. Under normal conditions (stimOFF), RTs decreased as a function of the chosen value. Electrical stimulation generally reduced RTs. Furthermore, linear regressions of RTs onto the chosen value showed that this reduction was driven by lower offsets as opposed to steeper slopes (**Fig.2.S3**). These changes in RTs are as predicted if stimulation increases the subjective value of the chosen goods.

The results of Exp.2 were replicated in a secondary analysis of data from Exp.1. For this analysis, we pooled all trials (AB and BA) and all sessions (stimulation during offer1 or offer2), and we repeated the analysis conducted for Exp.2 (Eq.2.2). We found a significant correlation between the choice bias ($\delta\rho$) and the difference in value range ($\Delta V_A - \Delta V_B$) when stimulation was delivered at 25 μA or 50 μA, but not when it was delivered at ≥100 μA (**Fig.2.S4**). The last observation indicated that the mechanism inducing the range-dependent bias (**Fig.2.3**) was fundamentally different from those inducing the order bias. Interestingly, stimulation at 50 μA induced both biases (see **Methods**).

2.3 Discussion

In the conditions examined here, different groups of neurons in OFC represent individual offer values, the binary choice outcome and the chosen value(Ballesta and Padoa-Schioppa, 2019; Padoa-Schioppa, 2013). Importantly, neurons encoding the binary choice outcome do not adapt to the value range, while chosen value cells adapt to the maximum range independent of the juice type(Conen and Padoa-Schioppa, 2019). Hence, physiological facilitation of these two cell groups should not induce any range-dependent choice bias. Thus range-dependent biases induced by stimulation are mediated by offer value cells (**Fig.2.3**). The order bias observed in Exp.1 is

also understood as an effect on offer value cells. Conversely, the increase in choice variability observed in Exp.1 upon stimulation during offer2 suggests that stimulation currents interfered with value comparison. More work is necessary to ascertain the organization of the decision circuit, including the role of different brain regions(Cisek, 2012; Padoa-Schioppa and Conen, 2017). If values are compared within OFC, the increase in choice variability could be due to the effects of stimulation on the other cell groups. For example, in a neural network model(Rustichini and Padoa-Schioppa, 2015), increasing reverberation increases choice variability(Wong and Wang, 2006).

In conclusion, we have shown that offer values encoded in OFC are causal to economic choices. This result demonstrates a long-held hypothesis and opens new avenues to investigate disorders affecting choices.

2.4 Methods

All experimental procedures conformed to the NIH Guide for the Care and Use of Laboratory Animals and were approved by the Institutional Animal Care and Use Committee (IACUC) at Washington University.

The study was conducted on three male rhesus monkeys (Macaca mulatta): G (age 8, 9.1 kg), J (age 7, 10.0 kg), and D (age 8, 11.5 kg). Before training, we implanted in each monkey a head-restraining device and an oval recording chamber under general anesthesia. The chamber (main axes, 50×30 mm) was centered on stereotaxic coordinates (AP 30, ML 0), with the longer axis parallel to a coronal plane. During the experiments, the animals sat in an electrically insulated enclosure with their head restrained. A computer monitor was placed 57 cm in front the animal. Behavioral tasks were controlled through custom-written software

(http://www.monkeylogic.net/). The gaze direction was monitored by an infrared video camera (Eyelink; SR Research) at 1 kHz.

2.4.1 Choice tasks

In Experiment 1 (Exp.1; monkeys G and J), animals chose between two juices labeled A and B, (with A preferred) offered in variable amounts. The two offers were presented sequentially in the center of a computer monitor (**Fig.2.1A**). Each trial began with the animal fixating a dot (0.35° of visual angle) in the center of the monitor. After 0.5 s, two offers appeared in sequence. Each offer was represented by a set of colored squares (side = 1° of visual angle), where the color indicated the juice type and the number of squares indicated the juice amount. Along with the offer, a small colored circle (0.75° of visual angle) appeared around the fixation dot. The circle indicated to the animal the juice identity in the case of null offer (0 drops; forced choices). The animal maintained center fixation throughout the initial fixation (0.5 s), offer1 time (0.5 s), inter-offer time (0.5 s), offer2 time (0.5 s), wait time (0.5 s), and delay time (0.5-1 s). At the end of the delay, the fixation point was extinguished and the animal indicated its choice with a saccade. It then maintained peripheral fixation for 0.6 s before juice delivery. Center fixation was imposed within 3°. Trials in which juice A was offered first and trials in which juice B was offered first were referred to as "AB trials" and "BA trials", respectively. The terms "offer1" and "offer2" referred to the first and second offer, independent of the juice type and amount. For each pair of juice quantities, the presentation order (AB, BA) and the spatial location of the saccade targets varied pseudo-randomly and were counterbalanced across trials. We designed offer types such that for most values of offer1 the animal split choices between the two offers (Ballesta and Padoa-Schioppa, 2019). Thus the monkey was discouraged from making a decision before

offer2. Sessions typically included ~400 trials and offered quantities varied from trial to trial pseudo-randomly. An "offer type" was defined by two juice quantities in given order (e.g., [1A:3B] or [3B:1A]). Stimulation was delivered in half of non-forced choice trials, pseudo-randomly selected.

In Experiment 2 (Exp.2; monkeys D and G), animals performed a similar task, except that the two juices were offered simultaneously (**Fig.2.3A**). After initial fixation (0.5 s), two offers appeared on the two sides of the fixation point. Offers remained on the monitor for 1 s and then disappeared. After a brief delay (0-0.5 s), the fixation point was extinguished and the animal indicated its choice with a saccade. The chosen juice was delivered after 0.75 s of peripheral fixation. Sessions typically included ~500 trials. Offered quantities and the spatial disposition varied from trial to trial pseudo-randomly. Previous work showed that in very similar conditions offer value cells in OFC undergo range adaptation (Padoa-Schioppa, 2009). Stimulation was delivered in roughly half of the trials, pseudo-randomly selected. We always tried to set the quantity ranges for the two juices such that the two value ranges would differ appreciably. However, we could not fully control the difference in value ranges, because the relative value of the two juices (ρ) ultimately depended on the animal's choices. In some instances, we ran two paired sessions back-to-back. In these cases, we left the stimulating electrode in place and we used the same two juices in both sessions, but we varied the quantity ranges such that the difference in value range $\Delta V_A - \Delta V_B$ would be >0 in one session and <0 in the other session.

The quantity of juice associated with each square (quantum) was set equal to 70-100 μl in Exp.1, and to 75 μl in Exp.2 (the quantum always remained constant within a session). Across sessions, we used a variety of different juices associated with different colors, including lemon Kool-Aid (bright yellow), grape (bright green), cherry (red), peach (rose), fruit punch (magenta), apple

(dark green), cranberry (pink), peppermint tea (bright blue), kiwi punch (dark blue), watermelon (lime) and 0.65 g/L salted water (light gray). This resulted in a large number of juice pairs.

2.4.2 Electrical stimulation

The chamber provided bilateral access to OFC. Structural MRIs (1 mm sections) performed before and after surgery were used to guide electrode penetrations. Prior to the electrical stimulation experiments, we performed extensive neuronal recordings in each monkey using standard procedures (Ballesta and Padoa-Schioppa, 2019). Recordings and stimulation focused on the central orbital gyrus, in a region corresponding to area 13/11. The analysis of neuronal data confirmed that stimulation experiments focused on the same region examined in previous studies (Ballesta and Padoa-Schioppa, 2019; Padoa-Schioppa and Assad, 2006).

During stimulation sessions, low-impedance (100-500 kΩ) tungsten electrodes (100 μm shank diameter; FHC) were advanced using a custom-built motorized micro-drive (step size 2.5 μm) driven remotely. Stimulation trains were generated by a programmable analog output (Power 1401, Cambridge Electronic Design) and triggered through a TTL by the computer running the behavioral task. Monopolar electric currents were generated by an analog stimulus isolator (Model 2200, A-M Systems). The parameters used for electrical stimulation were as follows.

In Exp.1, electric current was delivered during offer1 or during offer2 (in separate sessions). Stimulation started 0-100 ms after offer onset and lasted 300-600 ms. The stimulation train was constituted of biphasic pulses (200 μs each pulse, 100 μs separation between pulses) delivered at 100-333 Hz frequency19,20,33,34. Variability in these parameters was mostly from early sessions in monkey 1, when we were experimenting with different stimulation protocols. Parameters were not titrated within any session. In different sessions, current amplitudes varied

between 25 and 150 μA (in 1 session, 200 μA). Stimulation was performed in both hemispheres of monkey G (left: AP 31:36, ML –7:–12; right: AP 31:36, ML 4:9) and in both hemispheres of monkey J (left: AP 31:35, ML –8:–10; right AP 31:35, ML 6:10). Our data set included a total 144 stimulation sessions and 50 control sessions (see **Table 2.S2**). Electric current was delivered either unilaterally or bilaterally, in separate sessions. For each current level, the two groups of sessions were combined in the analysis. Analysis of the condition for which we had two sizeable data sets (namely, offer1 stimulation) indicated that unilateral and bilateral stimulation had similar effects on choices.

In Exp.2, the stimulation train (biphasic pulses, 200 Hz frequency) was delivered throughout offer presentation, for 1 s. Stimulation was always unilateral, and current amplitude was always set at 50 μA. Stimulation was performed in the left hemisphere of monkey D (AP 31:36, ML -6:–10) and in the left hemisphere of monkey G (AP 31:36, ML –7:–11). Trials with stimulation (stimON) and without stimulation (stimOFF) were pseudo-randomly interleaved. Our data set included 97 sessions.

Electrical stimulation did not systematically alter error rates in either experiment. Errors were always defined as fixation breaks occurring any time prior to trial completion. In Exp.1, error rates were not affected by stimulation in any of the experimental conditions (25 μA, offer1, $p = 0.10$; 25 μA, offer2, $p = 0.68$; 50 μA, offer1, $p = 0.15$; 50 μA, offer2, $p = 0.88$; ≥100 μA, offer1, $p = 0.20$; ≥100 μA, offer2, $p = 0.46$; Wilcoxon test, two animals combined). Similarly, stimulation did not alter error rates in Exp.2 ($p = 0.87$; Wilcoxon test, two animals combined).

2.4.3 Data analysis

All analyses were conducted in Matlab (MathWorks Inc). For the primary analysis of data from Exp.1, choice patterns were analyzed with probit regressions, separately for stimOFF trials and stimON trials (Eq.2.1). For each group of trials, we derived measures for the relative value of the juices (ρ), the sigmoid steepness (η) and the order bias (ε). The effects of electrical stimulation on each parameter were assessed using Wilcoxon signed-rank tests and paired t tests (**Fig.2.1, Fig.2.2**). Very similar results were obtained using alternative definitions of the order bias (referring to Eq.2.1, we tested $\varepsilon = a2/a1$ and $\varepsilon = 2\ \rho\ a2/a1$).

For data from Exp.2, we first ran two independent probit regressions for stimON trials and stimOFF trials. We found that electrical stimulation did not systematically alter the sigmoid steepness (**Fig.2.S5**). Thus we ran a probit regression assuming equal steepness for the two groups of trials (Eq.2.2). Except for **Fig.2.S5**, all the results presented here were obtained from the latter fit. Referring to Eq.2.2, we defined $\rho stimON = \exp(-(a0+a2)/a1)$ and $\rho stimOFF = \exp(-(a0-a2)/a1)$.

At the time of Exp.1, we had not planned to examine range-dependent biases. To examine these effects, we pooled sessions in which stimulation was delivered during offer1 or offer2, and we re-analyzed data using the same procedures used for Exp.2.

In all the analyses, we identified as outliers data points that differed from the mean by >3 STD on either axis, and we removed them from the data set. In the primary analyses of Exp.1, there were no outliers. In the analyses of range-dependent biases, the criterion excluded 1/97 session

from Exp.2 and 6/144 sessions from Exp.1. Including these sessions in the analyses did not substantially alter the results.

2.4.4 Predicting the range-dependent bias

Here we formalize the prediction illustrated in **Fig.2.3**. As a premise, previous work found that the tuning curves of offer value cells in OFC are quasi-linear (Rustichini et al., 2017) and the proportion of neurons presenting positive versus negative encoding is roughly 3:1 (Ballesta and Padoa-Schioppa, 2019; Padoa-Schioppa, 2013). Importantly, cells in each group adapt to their own range, not to the maximum range (Conen and Padoa-Schioppa, 2019). Neurons associated with the two juices (A and B) are physically intermixed (Conen and Padoa-Schioppa, 2015).

For given offers q_A and q_B, r_A and r_B indicate the average firing rates for the two pools of offer value cells. The effect of stimulation (facilitation) is a small increase in these firing rates, such that $r_A \rightarrow r_A + \delta r_A$ and $r_B \rightarrow r_B + \delta r_B$. Since the two neuronal populations are physically intermixed, electrical stimulation affects both of them equally. In other words, $\delta r_A = \delta r_B = \delta r$.

For each population, and for each juice type, a small increase in firing rate (δr) is equivalent to a small increase of offered value (δV_A, δV_B). Since offer value cells undergo range adaptation,

$$\delta V_A = (\delta r/\Delta r)\ \Delta V_A \qquad (2.3)$$

$$\delta V_B = (\delta r/\Delta r)\ \Delta V_B$$

where Δr is the range of firing rates (which is the same for both juices), and ΔVA and ΔVB are the ranges of offered values (Padoa-Schioppa, 2009).

We aim to understand how electrical stimulation will affect choices – that is, how the relative value ρ will change under electrical stimulation. To do so, we write the conditions of choice indifference. We assume linear indifference curves and we indicate with V(J) = uJ the value of one unit (one quantum) of juice J. In the absence of stimulation:

$$V(A) = V(\rho_{stimOFF}\, B) \tag{2.4}$$

$$= \rho_{stimOFF}\, V(B)$$

In the presence of stimulation:

$$V(A) + \delta V_A = V(\rho_{stimON}\, B) + \delta V_B \tag{2.5}$$

$$= \rho_{stimON}\, V(B) + \delta V_B \tag{2.6}$$

$$= (\rho_{stimOFF} + \delta\rho)\, V(B) + \delta V_B \tag{2.7}$$

In the last passage, we defined $\delta\rho = \rho_{stimON} - \rho_{stimOFF}$. Now we substitute Eq.2.4 in Eq7 and we re-arrange:

$$\delta V_A = \delta\rho\, uB + \delta V_B \tag{2.8}$$

$$\delta\rho = (\delta V_A - \delta V_B)/uB \tag{2.9}$$

Finally, we substitute Eq.2.3 in Eq.2.9:

$$\delta\rho = \delta r/\Delta r\, (\Delta V_A - \Delta V_B)/uB \tag{2.10}$$

Eq.2.10 captures the key prediction: If decisions are primarily based on the activity of offer value cells, the net effect of electrical stimulation is to change the relative value of the juices by a quantity proportional to the difference in value ranges. Notably, by pooling sessions in **Fig.2.4**

we effectively assumed that $\delta r/\Delta r$ and uB remain constant across sessions. In practice, this might not be true because of variability in stimulation efficacy and because the subjective value of juice B might vary from session to session. These sources of variability effectively add noise to our measurements. However, the prediction that $\delta\rho$ and $(\Delta V_A - \Delta V_B)$ should have the same sign is not affected by these factors.

2.4.5 Interpretation of the order bias

Here we discuss how high-current stimulation in Exp.1 might induce the order bias. We generally assume that electrical stimulation increases neuronal spiking. In Exp.1, currents varied between 25 μA and 150 μA. Previous studies indicate that when currents increase in this range, the effects of stimulation change in several ways. First, for any given cell and for equal number of pulses, the number of emitted spikes increases with the current(Hussin et al., 2015; Lee et al., 2013). Second, as the current increases, the stimulation affects a larger number of cells(Histed et al., 2009; Stoney et al., 1968; Tolias et al., 2005). Third, a regime transition takes place around 50 μA. At lower currents, electrical stimulation induces spiking only through synaptic transmission; at higher currents, stimulation also induces spiking directly through depolarization of the membrane(Hussin et al., 2015). In Exp.1, the animal is presented offers sequentially. Under normal conditions (stimOFF), only one juice is offered in each time window. However, the effect of stimulation is equivalent to presenting offers for both juices in one time window (because cells associated with the two juices are physically intermixed). We assume that for each juice (A and B) the values presented in the two time windows (1 and 2) are added. The order bias is a bias favoring the juice not present on the monitor during the stimulation. With these premises, high currents may induce the order bias for two reasons.

First, decelerating response functions. During electrical stimulation, the total synaptic current entering an offer value cell (i.e., the cell's input) has two components – the current induced by the offer on the monitor (I_O) and the current induced by the electrical stimulation (I_S). For neurons in cortex, we can assume that the number of spikes emitted in a given time window increases with the total synaptic current entering the cell, and that the response function relating these quantities is decelerating (**Fig.2.S6A**) (Arsiero et al., 2007; La Camera et al., 2008). If so, the increase in firing rate due to I_S decreases as a function of I_O. In other words, other things equal, if the cell's firing rate is already high, the stimulation is less effective. Now consider the two groups of cells associated with the two juices. The effect of stimulation is equivalent to adding value to both juices. However, if tuning curves are linear, the stimulation adds more value to the juice that is not currently offered on the monitor, because I_O for cells associated with this juice is lower. Hence, the stimulation induces an order bias, and this effect is stronger at higher currents.

Second, neural hijacking. Experiments in motor cortex suggest that electrical stimulation at low versus high currents has qualitatively different effects on the neuronal output. At low currents, simultaneous stimulation of two cortical locations has additive effects on the EMG activity(Ethier et al., 2006). In contrast, high-current stimulation cancels and replaces the normal EMG activity – a phenomenon termed neural hijacking(Griffin et al., 2011; Van Acker et al., 2013). This effect is understood based on the idea that high current stimulation induces both orthodromic and antidromic spikes, and that antidromic spikes collide with and cancel natural spikes(Griffin et al., 2011). Other work suggests that neural hijacking reflects a regime transition taking place around 50 μA, with higher current stimulating cells directly through the membrane(Hussin et al., 2015). In Exp.1, offer value cells subject to neural hijacking would have

the same output independent of the juice they encode (A or B) and independent of the offer present on the monitor. It is not clear how hijacked neurons are read out by the decision circuit, but we can assume that the read-out value is equivalent for cells in the two groups.

To illustrate why this phenomenon induces an order bias, we consider the case in which stimulation is delivered (or not delivered) when juice A is offered on the monitor. We examine trials in which the two offer values are V_A and V_B. We indicate with ξ the fraction of offer value cells hijacked by the stimulation (same for the two groups), and V_H is the corresponding read-out value. If the total value of each juice is the sum of the values offered in the two time windows, we can compute the total offer values in each condition:

stimOFF: V_A vs. V_B

stimON: $V_A (1- \xi) + \xi V_H$ vs. $V_B + \xi V_H$

Under stimON, values induced by the stimulation cancel each other, and a bias favoring juice B ensues.

Decelerating response functions and neural hijacking interfere with the computation of value. Of note, these phenomena differ from that underlying the disruption of motion perception upon high-current stimulation of area MT, which presumably was due the stimulation activating cells in other mini-columns and opposite preferred direction (Murasugi et al., 1993).

Interestingly, 50 μA stimulation in Exp.1 induced both the order bias (**Fig.2.2**) and the range-dependent bias (**Fig.2.S4**). The concurrent presence of these effects is consistent with either mechanism discussed above. For example, the order bias induced by decelerating response functions would be independent of the value ranges, and thus take place in addition to the range-

dependent bias. Also, 50 μA currents might hijack only a subset of cells, and simply increase the firing rate of other cells. That said, one might wonder how stimulation in any given session can induce both the order bias and the range-dependent bias. In fact, the two biases affect choices in very different ways (**Fig.2.S6B**). The range-dependent bias shifts the total sigmoid (obtained by pooling AB and BA trials) in the direction of the larger value range. Conversely, the order bias separates the two sigmoids for AB trials and BA trials in the positive or negative direction depending on whether the current is delivered during offer1 or offer2. Referring to Eq.2.1, the range-dependent bias is an effect on ρ; the order bias is an effect on ε.

Notably, 50 μA stimulation in Exp.1 induced range-dependent biases, but it did not alter relative values on average across the population (**Fig.2.2**). This is because sessions with $\Delta V_A > \Delta V_B$ and sessions with $\Delta V_A < \Delta V_B$ were pooled in **Fig.2.2**, and changes in relative value averaged out.

In Exp.1, ≥100 μA stimulation during offer2 also increased choice variability. In principle, high-current stimulation may increase variability in two ways: it may add noise to valuation, or it may add noise to the decision. The fact that choice variability increased only when stimulation was delivered during offer2 (and not during offer1) argued against the former and for the latter. Thus we interpret the effect shown in **Fig.2.1H** as electrical stimulation affecting value comparison.

The fact that we measured the order bias upon stimulation during offer2 (and not only during offer1) might seem in contrast with the hypothesis that values are compared within OFC. If so, the increase in choice variability could be mediated by downstream areas. However, neuronal recordings (Ballesta and Padoa-Schioppa, 2019) revealed that when offers are presented sequentially, working memory of the first offer value is not instantiated by sustained activity in offer value cells, and might rely on synaptic mechanisms or other brain regions. At the same

time, the first offer value affects the baseline activity of chosen juice cells upon presentation of offer2, as if setting the initial conditions of the decision circuit (Ballesta and Padoa-Schioppa, 2019). Thus stimulation during offer2 may not affect the two offer values equally. Hence, the order bias is consistent with decisions taking place in OFC.

2.4.6 Data and code availability

The complete data set and the Matlab code used for the analysis are available at: https://github.com/PadoaSchioppaLab/2020_Ballesta_etal_Nature

2.5 Supplementary figures

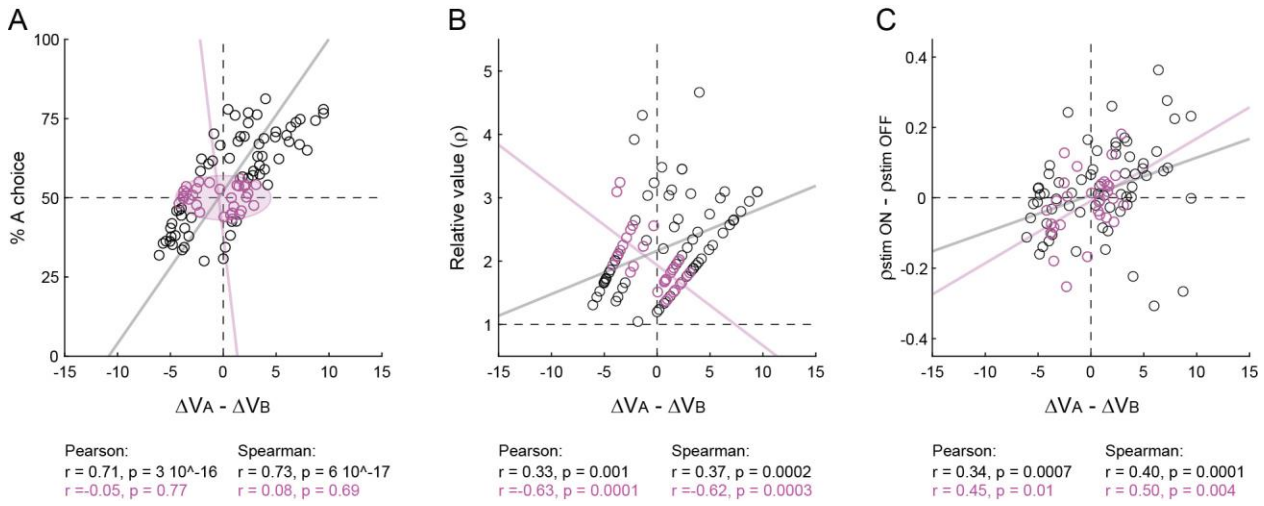

Figure 2.S1. Exp.2, control for choice frequency. We noticed that across sessions the difference in value range (ΔV_A–ΔV_B) was correlated with the fraction of trials in which the animal chose juice A (% A choice) and with the relative value (ρ). In principle, these correlations could represent confounding factors. Indeed, 50 μA stimulation could partly disrupt the valuation process. As a result, the animal might respond by defaulting to the juice type most frequently chosen in that session, or to the preferred juice type. If so, the range-dependent bias would be akin to the order bias (Exp.1), in the sense that it would result from functional disruption as opposed to facilitation. To address this concern, we identified a subset of sessions for which choices between the two juices were split almost evenly. In this subset of sessions, the difference in value range and the fraction of A choices were not correlated. We reasoned that if the range- dependent bias observed for the whole data set was driven by a default to the most frequently chosen option, the bias should disappear when the analysis was restricted to this subset of sessions. However, this was not the case. In fact, the range-dependent bias measured for the selected subset was larger than that measured for the entire population. We concluded that range-dependent biases did not reflect simple heuristics. **A.** Correlation between the difference in value range and the fraction of A choices. Each data point represents one session. Considering the entire data set (black data points, N=96 sessions), the two measures were significantly correlated ($r \geq 0.71$, $p<10^{-15}$, Pearson and Spearman correlation tests). We defined a small ellipse centered on coordinates [0, 50] (axes = [9, 14]). The ellipse

identified a subset of data (pink data points, N=31 sessions) for which the difference in value range and the fraction of A choices were not correlated ($p \geq 0.69$, Pearson and Spearman correlation tests). **B.** Correlation between the difference in value range and the relative value. Considering the entire data set, the two measures were significantly correlated ($r \geq 0.33$, $p \leq 0.001$, Pearson and Spearman correlation tests). However, when the analysis was restricted to the subset of sessions identified in panel A (pink data points), the correlation changed sign. **C.** Range-dependent bias, same data as in **Fig.4CD**. Considering the entire data set, the change in relative value was significantly correlated with the difference in value range ($r \geq 0.34$, $p \leq 0.0007$, Pearson and Spearman correlation tests). The correlation did not dissipate when the analysis was restricted to the subset of sessions identified in panel A (pink data points; $r \geq 0.45$, $p \leq 0.01$, Pearson and Spearman correlation tests). In this figure, data from the two animals are combined. Black and pink lines in the three panels were obtained from Deming regressions.

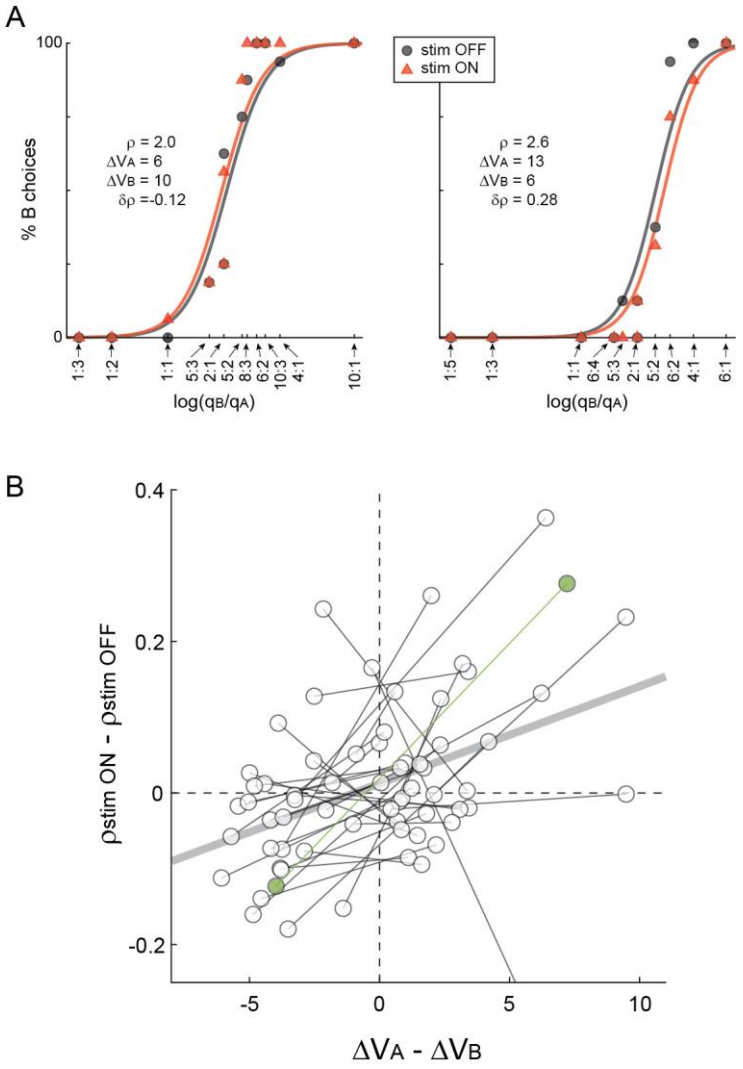

Figure 2.S2. Exp.2, results obtained in paired sessions. In N=33 instances, we ran two back-to-back sessions offering the same two juices and leaving the electrode in place, but changing the quantity ranges such that ΔV_A–ΔV_B would differ. **A.** Example of paired sessions. **B.** Population analysis. Each pair of sessions in the scatter plot is connected by a line, of which we computed the slope. Data points filled in green correspond to sessions in panel A. Data from the two monkeys are pooled. Across the population, slopes were typically >0 (p = 0.007, two-tailed Wilcoxon signed-rank test). Hence, range-dependent biases were not dictated by the juice pair or by the location of the electrode within OFC.

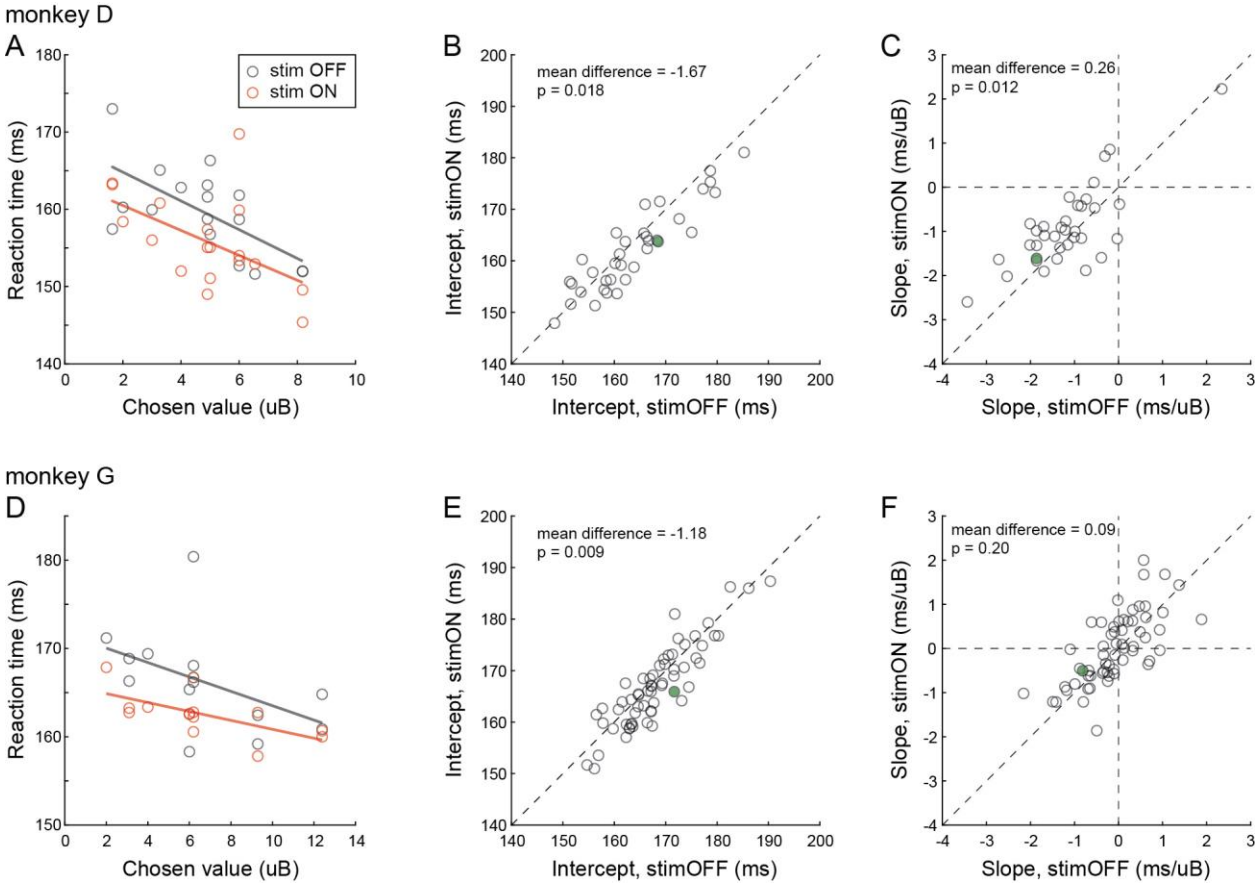

Figure 2.S3. Exp.2, analysis of response times (RTs). **A.** Example session 1. Each data point represents one trial type and the two lines were obtained from linear regressions. Under normal conditions (stimOFF, black), RTs decreased as a function of the chosen value (x-axis). Electrical stimulation (stimON, red) generally reduced RTs. Linear fits reveal that lower RTs were due to a lower intercept, as opposed to a steeper (i.e., more negative) slope. **BC.** Population analysis, monkey D (N=35). For each session, we regressed RTs onto the chosen value, separately for stimOFF and stimON trials. We then compared the intercepts and the slopes at the population level. The picture emerging from panel A was confirmed for the population. In panel B (intercept), each data point represents one session. The population is significantly displaced below the identity line (p=0.018, two-tailed Wilcoxon test). In panel C (slope), it can be noticed that the slope under stimulation was shallower (less negative), probably due to a floor effect. Filled data points correspond to the session shown in panel A. **D.** Example session 2. Same

format as in panel A. **EF.** Population analysis, monkey G (N=61). Same format as in panels BC. Electrical stimulation significantly lowered the intercept but did not significantly alter the slope. Filled data points correspond to the session shown in panel D. In panels BCEF, values indicated in the insert refer to the difference between the stimON measure and the stimOFF measure, averaged across the population. All p values are from two-tailed Wilcoxon tests, and t tests provided very similar results.

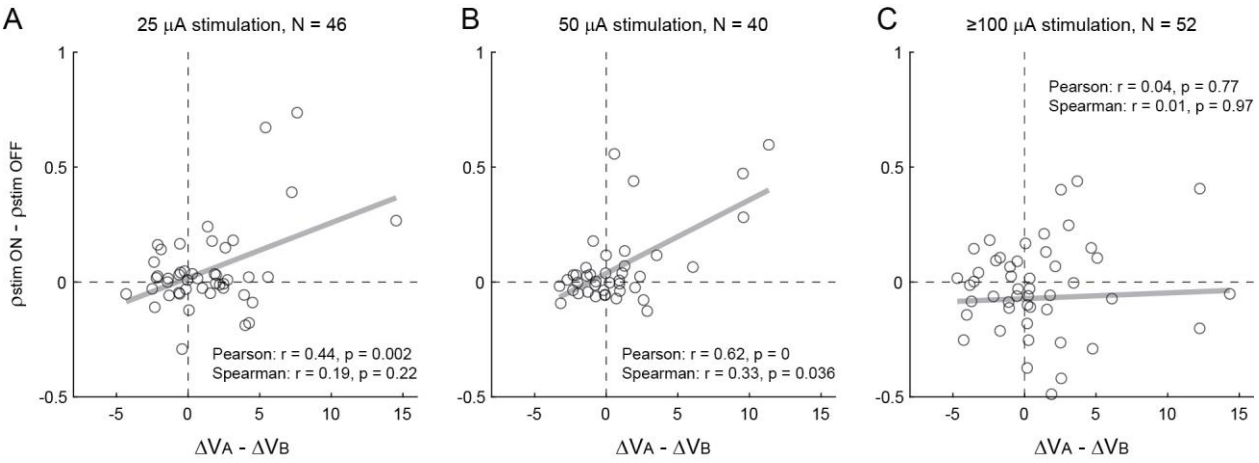

Figure 2.S4. Exp.1, range-dependent choice biases. **ABC.** Results obtained when electric current was delivered at 25 μA, 50 μA and ≥100 μA. In each panel, x- and y-axes represent the difference in value range (in uB) and the difference in relative value, respectively. Each data point represents one session. Sessions from the two animals and with different stimulation times (offer1 or offer2) were pooled. Gray lines were obtained from linear regressions. Each panel indicates the p values obtained from Pearson and Spearman correlation tests. In essence, the choice bias imposed by the stimulation (δρ) was correlated with the difference in value ranges ($\Delta V_A - \Delta V_B$) at low current (25 μA; weakly) and intermediate current (50 μA), but not at high current (≥100 μA).

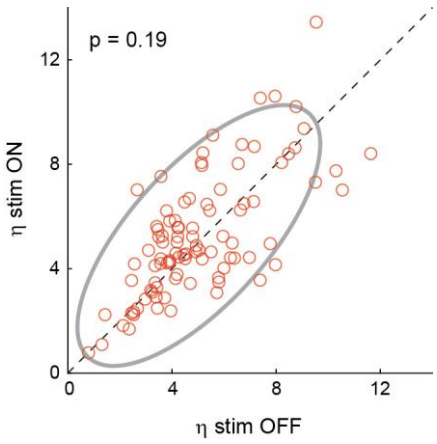

Figure 2.S5. Stimulation in Exp.2 did not systematically alter the sigmoid steepness. For this analysis, the two groups of trials (stimOFF, stimON) were examined separately (see **Methods**). The two axes represent the sigmoid steepness in the two conditions. Sessions from the two animals were pooled (N=95, 2 outliers removed), and each data point represents one session. The gray ellipse represents the 90% confidence interval. The p value is from a Wilcoxon test and similar results were obtained with a t test.

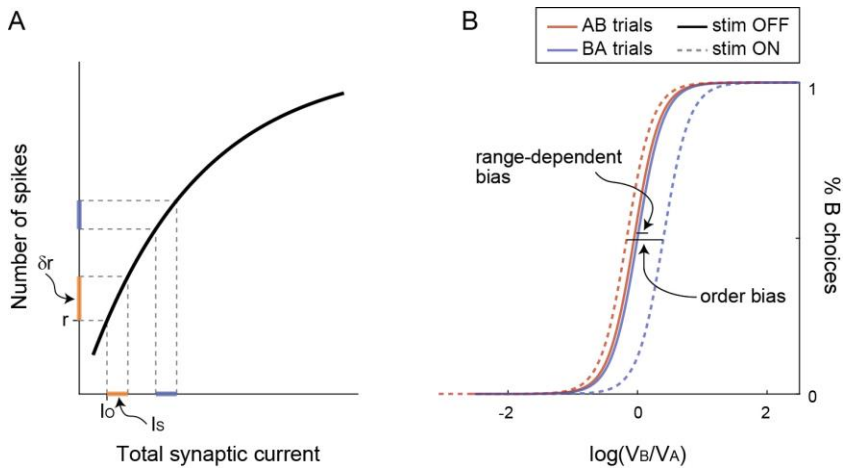

Figure 2.S6. Exp.1, interpretation of the order bias. **A.** Decelerating response function. The black line represents an ideal response function, which relates the number of spikes emitted by a cell in a given time window (y-axis) to the synaptic current entering the cell (x-axis). In the condition highlighted in yellow, I_O is the synaptic current due to the offer on the monitor, r is the corresponding response, I_S is the synaptic current due to the stimulation, and δr is the corresponding increase in the number of spikes. The condition highlighted in blue is similar, except that I_O is larger ($I_{O,blue} > I_{O,yellow}$). Because the response function is decelerating, δr in the blue condition is smaller ($\delta r_{blue} < \delta r_{yellow}$). In Exp.1, only one good was presented at the time. Neurons associated with that good were naturally more active (higher I_O) than neurons associated with the other good. Thus deceleration in the response function induced a bias favoring the good not offered during the stimulation (order bias). For given $I_{O,yellow}$ and $I_{O,blue}$, the difference $\delta r_{yellow} - \delta r_{blue}$ increases with IS. Hence, higher stimulation currents induced larger order biases. **B.** Concurrent presence of order bias and range-dependent bias. The cartoon illustrates an ideal session in Exp.1. We assume that under normal conditions there is no order bias (stimOFF, continuous lines). Thus the two sigmoids for AB trials and BA trials coincide. We also assume that stimulation is delivered during offer1, and that $\Delta V_A - \Delta V_B > 0$. The order bias separates the two sigmoids such that under stimulation the sigmoid for AB trials is on the left of that for BA trials (stimON, dashed lines). The range-dependent bias imposes a shift on the total sigmoid, including both AB and BA trials (not shown), which moves to the right compared to normal conditions. The two choice biases are complementary and independent.

Parameter	Stimulation interval	Current level	P value	P<.005
Relative value	control	0 μA	0.61	
	offer 1	25 μA	0.20	
		50 μA	0.37	
		≥100 μA	0.48	
	offer 2	25 μA	0.83	
		50 μA	0.34	
		≥100 μA	0.16	
Steepness	control	0 μA	0.43	
	offer 1	25 μA	0.47	
		50 μA	0.20	
		≥100 μA	0.84	
	offer 2	25 μA	0.27	
		50 μA	0.10	
		≥100 μA	0.0025	*
Order bias	control	0 μA	0.39	
	offer 1	25 μA	0.46	
		50 μA	$5.5\ 10^{-4}$	*
		≥100 μA	$8.8\ 10^{-6}$	*
	offer 2	25 μA	0.69	
		50 μA	0.0041	*
		≥100 μA	$3.0\ 10^{-4}$	*

Table 2.S1. Exact p values for the statistical tests ran for **Fig.2.2**. All p values are from two-tailed Wilcoxon tests.

Stimulation interval	Current level	Mode	Number of sessions		
			monkey G	monkey J	total
offer 1	≥100 μA	uni	5	8	29
		bi	15	1	
	50 μA	uni	9	7	22
		bi	4	2	
	25 μA	uni	11	4	29
		bi	14	0	
offer 2	≥100 μA	uni	14	6	25
		bi	3	2	
	50 μA	uni	11	11	22
		bi	0	0	
	25 μA	uni	9	6	17
		bi	2	0	
control	0 μA	--	30	20	50
Total	--	--	127	67	194

Table 2.S2. Data set for Exp.1. Labels uni/bi indicate unilateral/bilateral stimulation. For the 54 sessions labeled as ≥100 μA, the current was typically set at 125 μA (47/54 = 87% sessions). In the remaining cases, the current was set at 100 μA (2/54 = 4%), 150 μA (4/54 = 7%) and 200 μA (1/54 = 2%). Removing from the data set sessions at 100, 150 and 200 μA did not substantially alter the results of this study.

Chapter 3: Economic choices under simultaneous or sequential offers rely on the same neural circuit

This chapter is adapted from the following publication with the permission from the co-authors:

Shi, W., Ballesta, S., & Padoa-Schioppa, C. (2021). Economic Choices under Simultaneous or Sequential Offers Rely on the Same Neural Circuit. J Neurosci: in press.

Abstract

A series of studies in which monkeys chose between two juices offered in variable amounts identified in the orbitofrontal cortex (OFC) different groups of neurons encoding the value of individual options (offer value), the binary choice outcome (chosen juice) and the chosen value. These variables capture both the input and the output of the choice process, suggesting that the cell groups identified in OFC constitute the building blocks of a decision circuit. Several lines of evidence support this hypothesis. However, in previous experiments offers were presented simultaneously, raising the question of whether current notions generalize to when goods are presented or are examined in sequence. Recently, Ballesta and Padoa-Schioppa (2019) examined OFC activity under sequential offers. An analysis of neuronal responses across time windows revealed that a small number of cell groups encoded specific sequences of variables. These sequences appeared analogous to the variables identified under simultaneous offers, but the correspondence remained tentative. Thus in the present study we examined the relation between cell groups found under sequential versus simultaneous offers. We recorded from the OFC while monkeys chose between different juices. Trials with simultaneous and sequential offers were

randomly interleaved in each session. We classified cells in each choice modality and we examined the relation between the two classifications. We found a strong correspondence – in other words, the cell groups measured under simultaneous offers and under sequential offers were one and the same. This result indicates that economic choices under simultaneous or sequential offers rely on the same neural circuit.

3.1 Introduction

Neurophysiology experiments where monkeys chose between different juice types identified in the OFC different groups of cells encoding individual offer values, the binary choice outcome (chosen juice) and the chosen value (Padoa-Schioppa and Assad, 2006). Similar results were obtained in monkeys choosing between juice bundles (Pastor-Bernier et al., 2019), in mice (Kuwabara et al., 2020), and in humans using fMRI (Hare et al., 2008; Howard et al., 2015). The variables encoded in OFC capture both the input and the output of the choice process, and the corresponding cell groups are computationally sufficient to generate binary decisions (Rustichini and Padoa-Schioppa, 2015; Song et al., 2017; Zhang et al., 2018). In monkeys, mild electrical stimulation of this area biases choices in predictable ways (Ballesta et al., 2020). Furthermore, lesions in humans (Camille et al., 2011; Yu et al., 2018), high current stimulation in monkeys (Ballesta et al., 2020) or optogenetic inactivation in mice (Gore et al., 2019; Kuwabara et al., 2020) dramatically increases choice variability. The circuit dynamics is consistent with a decision process (Rich and Wallis, 2016), and trial-by-trial fluctuation in the activity of each cell group correlates with choice variability (Padoa-Schioppa, 2013). Taken together, these results suggest that the cell groups identified in OFC constitute the building blocks of a neural circuit in which economic decisions are formed. One caveat is that current notions on this circuit emerge mostly from studies in which two options were presented simultaneously. Yet, in most daily situations, options available for choice appear or are examined in sequence. Moreover, some scholars have argued that choices under sequential or simultaneous offers rely on qualitatively different mechanisms (Hayden and Moreno-Bote, 2018; Hunt et al., 2013; Kacelnik et al., 2011).

To shed light on the mechanisms underlying choices under sequential offers, we recently recorded from the OFC of monkeys choosing between different juices offered sequentially (Ballesta and Padoa-Schioppa, 2019). Consistent with previous observations (Hunt et al., 2018; McGinty et al., 2016), neuronal responses in any time window depended on the presentation order (i.e., on what juice the animal was offered at that time). However, an analysis of neuronal responses across time windows revealed that different groups of cells encoded different patterns of variables, referred to as "sequences". Across a large population of neurons, we identified 8 such sequences. We also noted that these sequences presented analogies with the cell groups previously identified under simultaneous offers. For example, some sequences represented the value of specific juices, while other sequences presented binary responses. These observations suggested that the two sets of cell groups recorded under sequential and under simultaneous offers might in fact be one and the same. If this hypothesis was confirmed, notions on the decision mechanisms acquired under simultaneous offers would apply to a much broader domain of choices than previously recognized.

To test this hypothesis, we recorded the activity of neurons in OFC while monkeys chose between different juices. In each session, choices under simultaneous offers and choices under sequential offers were pseudo-randomly interleaved. In the analysis, we first separated trials with the two choice tasks (modalities) and classified each cell in each choice task. We then considered the whole population and compared the results of the classification obtained for the two choice tasks. We envisioned three possible scenarios: (1) the two choice tasks could engage different neuronal assemblies (different populations); (2) the two tasks might engage the same neuronal population but individual neurons might have different roles in the two tasks (independent classification); or (3) the same groups of neurons might support decisions in the two choice tasks

(corresponding classifications). Statistical analyses provided strong evidence for the last hypothesis. Thus our results indicate that choices under sequential offers and choices under simultaneous offers rely on the same decision circuit.

3.2 Results

Two monkeys chose between different juices offered in variable amounts. Offers were represented by sets of colored squares displayed on a computer monitor, and animals indicated their choice with an eye movement. In each session, trials with two choice modalities were randomly interleaved. In one modality (Task 1), two offers were presented simultaneously (**Fig.3.1A**); in the other modality (Task 2), two offers were presented in sequence (**Fig.3.1B**). A cue presented at the beginning of the trial indicated to the animal the choice modality for that trial. The two juices used in each session were labeled A and B, with A preferred, and we indicated the quantities offered in any given trial with q_A and q_B. For Task 2, trials in which juice A was offered first and trials in which juice B was offered first were referred to as AB trials and BA trials, respectively. The first and second offers were referred to as offer1 and offer2, respectively.

3.2.1 Comparing choices across tasks

Our data set included 306 sessions from two monkeys (115 from J, 191 from G). Sessions included 216-880 trials (mean ± std = 590 ± 160). For each session, we analyzed trials with the two choice tasks separately using probit regressions (see **Methods**). For Task 1 (simultaneous offers), the probit fit provided measures for the relative value ρ_{Task1} and the sigmoid steepness η_{Task1}. For Task 2 (sequential offers), the probit fit provided measures for the relative value ρ_{Task2},

the sigmoid steepness η_{Task2} and the order bias ε (**Fig.3.1C-F**). Intuitively, the relative value was the quantity ratio q_B/q_A that made the animal indifferent between the two juices, the sigmoid steepness was inversely related to choice variability, and the order bias (measured in Task 2) was a bias favoring the first or the second offer. Specifically, $\varepsilon<0$ indicated a bias favoring offer1 and $\varepsilon>0$ indicated a bias favoring offer2.

The experimental design gave us the opportunity to compare choices across tasks. Our analyses revealed several phenomena. First, the relative values measured in the two tasks were very similar and highly correlated across sessions ($r>0.90$; **Fig.3.1D**). At the same time, ρ_{Task1} and ρ_{Task2} presented some differences. Specifically, relative values in Task 2 were generally higher than in Task 1 ($p<10^{-10}$, t test), and this effect increased with the relative value. Second, sigmoids measured in Task 2 were significantly shallower compared to Task 1 ($p<10^{-25}$, t test; **Fig.3.1E**). In other words, presenting offers in sequence substantially increased choice variability. Third, in Task 2, animals showed an order bias favoring offer2 (**Fig.3.1F**). This effect was highly significant ($p<10^{-25}$, t test) but quantitatively modest (mean(ε) = 0.26 uB) compared to relative values, which typically ranged between 1 and 4 uB (mean(ρ) = 2.26 uB).

These three behavioral phenomena – larger choice variability, preference bias and order bias – were likely due to the higher cognitive demands imposed by Task 2 (see **Discussion**). Importantly, these effects were relatively small and essentially orthogonal to the main question addressed in this study, concerning the relation between cell groups recorded in the two choice tasks. Thus for the analyses of neuronal activity presented in the rest of this study, we examined responses of each neuron in each task in relation to variables defined based on the relative value measured in the same task, ignoring the order bias (see **Table 3.2**).

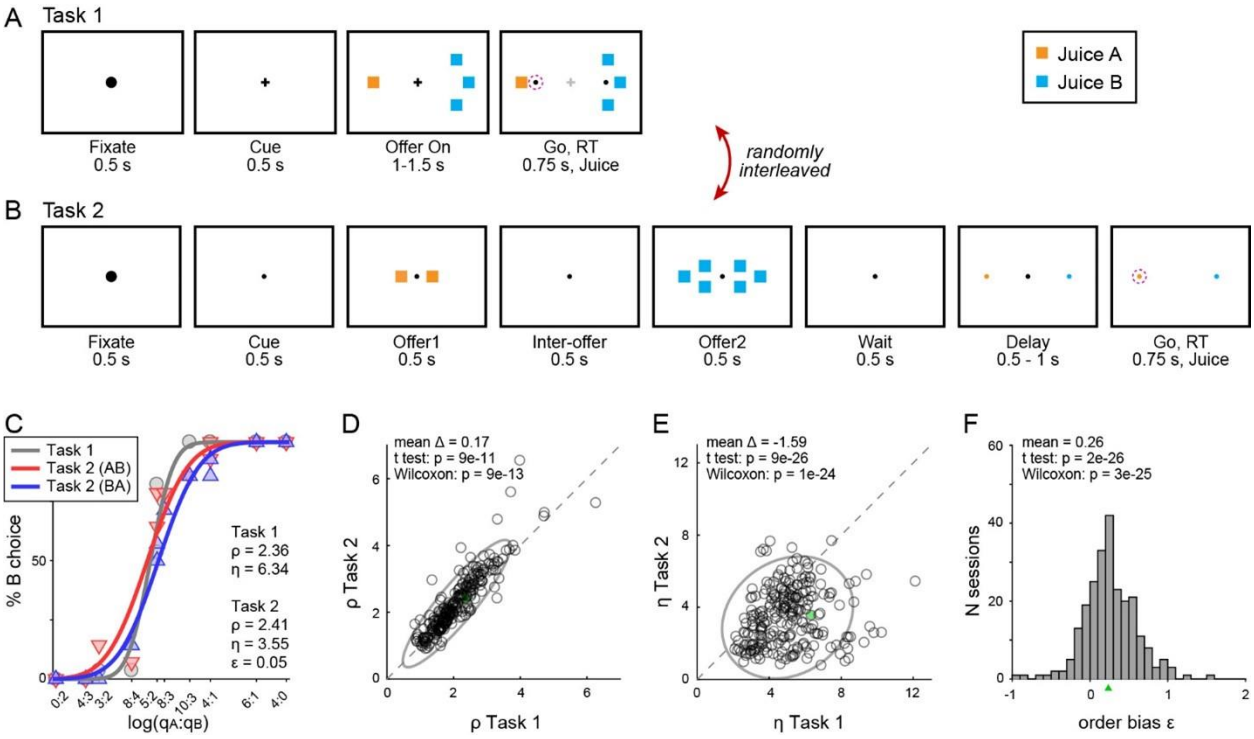

Figure 3.1. Experimental design and behavioral performance. **AB.** Experimental design. In each session, a monkey chose between two juices labeled A and B (A preferred). Trials with two choice modalities, referred to as Task 1 and Task 2, were randomly interleaved. At the beginning of each trial, the animal fixated a large dot in the center of the monitor. After 0.5 s, the fixation point changed to either a small dot or a cross; this cue indicated to the animal the task used in that trial. In Task 1 (simultaneous offers), two offers appeared on the left and right sides of the fixation point. The animal maintained fixation for a randomly variable delay, at the end of which the fixation point was extinguished and two saccade target appeared by the offers (go signal). The animal indicated its choice with a saccade and maintained peripheral fixation until juice delivery. In Task 2 (sequential offers), the two offers were presented in sequence and spaced by an inter-offer delay. Two saccade targets matching the colors of the two offers appeared on the two sides of the fixation point. After a variable delay, the fixation point was extinguished (go signal). The animal indicated its choice with a saccade and maintained peripheral fixation until juice delivery. For each offer, the color indicated the juice type and the number of squares indicated the juice

amounts. Thus in the trials shown here, the animal chose between 1 drop of juice A and 3 drops of juice B. The left/right configuration in Task 1, the presentation order in Task 2 and the left/right position of the saccade targets in Task 2 varied randomly from trial to trial. In both tasks, fixation breaks prior to the go signal lead to trial abortion. The same offer types were used for both tasks. **C.** Example sessions. The percent of B choices (y-axis) is plotted against the log quantity ratio (x-axis). Each panel includes data points for Task 1 (gray circles) and for Task 2 (red and blue triangles for AB trials and BA trials, respectively). Sigmoids were obtained from probit regressions (**Eq.3.1** and **Eq.3.2**). The panel indicates the relative value (ρ) and sigmoid steepness (η) measured in each task, and the order bias (ε) measured in Task 2. A choice bias favoring offer2 ($\varepsilon>0$) corresponds to the blue sigmoid displaced to the right of the red sigmoid. **D.** Comparing the relative value (ρ) across choice tasks. Relative values measured in Task 1 (x-axis) are plotted against those measured in Task 2 (y-axis). Each data point represents one session. Gray ellipses indicate 90% confidence intervals. The two measures were highly correlated. However, relative values were generally higher in Task 2 than in Task 1, and this effect increased with ρ (the main axis of the ellipse is rotated counterclockwise compared to the identity line). **E.** Comparing the sigmoid steepness (η) across choice tasks. Sigmoids in Task 2 were consistently shallower (lower η; higher choice variability) compared to Task 1. **F.** Distribution of order bias measured across sessions. A small triangle indicates the mean. Animals presented a consistent bias favoring offer2. In panels DEF, results from both monkeys were pooled (N = 241 sessions; 65 outliers removed, see **Methods**). Statistical tests and p values are indicated in each panel. The sessions shown in panel C is highlighted in cyan in panels DE.

Task 1		
	Variable	**Definition**
1	offer value A	$\rho\ q_A$
2	offer value B	q_B
3	chosen value	value of chosen offer
4	chosen juice	binary; 1 if A chosen; 0 if B chosen
Task 2		
	Variable	**Definition**
1	AB | BA	binary; 1 in AB trials; 0 in BA trials
2	offer value A | AB	$\rho\ q_A$ in AB trials, 0 in BA trials
3	offer value A | BA	$\rho\ q_A$ in BA trials, 0 in AB trials
4	offer value B | AB	q_B in AB trials, 0 in BA trials
5	offer value B | BA	q_B in BA trials, 0 in AB trials
6	offer value 1	value of offer1
7	offer value 2	value of offer2
8	chosen value	value of chosen offer
9	chosen value A	chosen value if A chosen, 0 otherwise
10	chosen value B	chosen value if B chosen, 0 otherwise
11	chosen juice A	binary; 1 if A chosen; 0 if B chosen
12	chosen juice B	binary; 0 if A chosen; 1 if B chosen

Table 3.1. Definition of variables in Task 1 and Task 2. Values were always defined in units of juice B (uB) based on relative values derived from the probit regressions (**Eqs.3.1-3.2**). Thus, the value of q_B drops of juice B was equal to q_B; the value of q_A drops of juice A was equal to $\rho\ q_A$. Each variable could be encoded with a positive or negative sign. For Task 2, variables chosen juice A and chosen juice B coincided except for the sign (we use this notation for clarity).

Seq #	Time windows		
	post-offer1	**post-offer2**	**post-juice**
#1	offer value A | AB +	offer value A | BA +	chosen value A +
#2	offer value A | AB -	offer value A | BA -	chosen value A -
#3	offer value B | BA +	offer value B | AB +	chosen value B +
#4	offer value B | BA -	offer value B | AB -	chosen value B -
#5	AB | BA +	AB | BA -	chosen juice A
#6	AB | BA -	AB | BA +	chosen juice B
#7	offer value1 +	offer value2 +	chosen value +
#8	offer value1 -	offer value2 -	chosen value -

Table 3.2. Neuronal classification in Task 2. Ballesta and Padoa-Schioppa (2019) found that under sequential offers neurons in OFC encoded different variables in different time windows. However, focusing on three primary time windows, the vast majority of neurons presented one of 8 specific patterns of variables, referred to as variable "sequences". The 8 sequences identified in that study are defined in this table, where + and - indicate the sign of the encoding. These sequences seem roughly analogous to the variables identified under simultaneous offers. For example, seq #1 encodes the value of juice A when the animal is offered that juice (post-offer1 in AB trials; post-offer2 in BA trials). Upon juice delivery, seq #1 encodes the value of juice A conditioned on juice A being chosen. Thus neurons classified as seq #1 seem analogous to offer value A+ neurons found under simultaneous offers. Similarly, cells classified as seq #2, seq #3 and seq #4 seem analogous to offer value A–, offer value B+ and offer value B– cells found under simultaneous offers, respectively. Cells classified as seq #5 or seq #6 encode in a binary way the identity of the juice (A or B) offered to the animal or chosen by the animal. These neurons appear tentatively analogous to chosen juice cells identified under simultaneous offers. Finally, cells classified as seq #7 or seq #8 encode the value of either juice, provided that the animal focuses on it. They appear tentatively analogous to chosen value+ and chosen value- cells identified under simultaneous offers, with the understanding that the value encoded by these neurons is that upon which the animal places its mental focus and not necessarily the chosen one.

3.2.2 Neuronal classification in each choice task

Previous studies of choices under simultaneous offers identified in OFC different groups of cells encoding individual offer values, the binary choice outcome and the chosen value (Padoa-Schioppa and Assad, 2006). Similarly, recent work on choices under sequential offers identified different groups of cells encoding different decision variables (Ballesta and Padoa-Schioppa, 2019). Our goal was to ascertain whether the two sets of cell groups correspond to each other. To do so, we recorded and analyzed the activity of 1,526 cells (672 cells from monkey J and 854 cells from monkey G). In the analysis, our general strategy was to classify cells separately in each task according to the same criteria used in previous work, and to then compare the results of the two classifications at the population level. Thus we divided trials with Task 1 and Task 2 and proceeded in steps.

For Task 1 trials, we defined four 500 ms time windows aligned with the offer presentation (post-offer, late-delay) and the juice delivery (pre-juice and post-juice). A "trial type" was defined by two offers and a choice. For Task 2 trials, we defined three 500 ms time windows aligned with the two offers (post-offer1, post-offer2) and with the juice delivery (post-juice). A "trial type" was defined as two offers in a particular order and a choice. For each task, each trial type and each time window, we averaged spike counts across trials. In each task, a neuronal response was defined as the firing rate of one cell in one time window as a function of the trial type. Neuronal responses were submitted to an ANOVA (factor: trial type). Neurons presenting a significant modulation ($p<0.01$) in at least one task and at least one time window were identified as task-related and included in subsequent analyses. In total, 645/1,526 (42%) cells met this criterion. Further analyses were restricted to this population.

While inspecting individual responses, we made three observations. First, replicating several previous studies, responses in Task 1 appeared to encode one of the variables offer value, chosen juice or chosen value (**Fig.3.2**). Second, confirming the results of our recent study on sequential offers, neurons in Task 2 appeared to encode different variables in different time windows. Across time windows, particular sequences of variables were most frequent. For example, in the three time windows under consideration, the neuron in **Fig.3.2C** encoded variables offer value B | BA, offer value B | AB and chosen value B. These variables define sequence #3 in **Table 3.2**. In the same time windows, the cell in **Fig.3.2F** encoded variables –AB|BA, AB|BA and chosen juice B. These variables define sequence #5. Similarly, the cell in **Fig.3.2I** encoded variables offer value 1, offer value 2 and chosen value, which define sequence #7. Third and most important, there appeared to be a reliable correspondence between neuronal responses recorded in the two tasks. In principle, neurons tuned in one task could be untuned in the other task. That is, different cell assemblies in OFC could support choices in the two tasks. In contrast, neurons were typically tuned in both tasks or not at all. Furthermore, the variable encoded in Task 1 corresponded to specific sequences encoded in Task 2. For example, neurons encoding offer value A in Task 1 typically encoded sequence #1 in Task 2; neurons encoding offer value B in Task 1 typically encoded sequence #3 in Task 2; neurons encoding chosen juice A in Task 1 typically encoded sequence #5 in Task 2; etc. The three example cells in **Fig.3.2** illustrate this point.

For a statistical analysis, we classified neurons in Task 1 and Task 2 following the same procedures of previous studies (Ballesta and Padoa-Schioppa, 2019; Padoa-Schioppa, 2013). For Task 1, we regressed each response against each variable. Each regression provided a slope and the R^2. If the slope differed significantly from zero ($p<0.05$) the variable was said to explain the

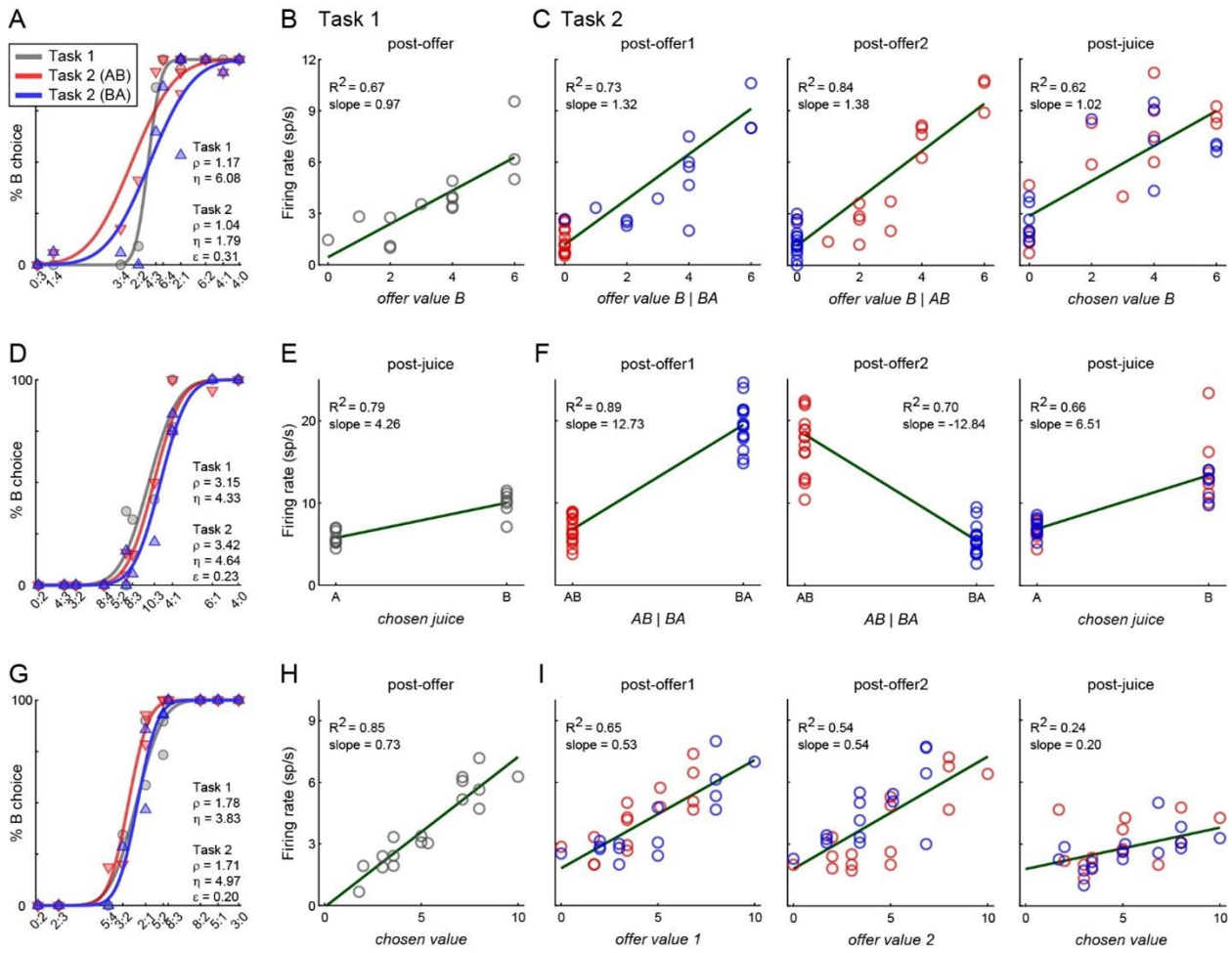

Figure 3.2. Three example neurons. **A-C.** Example 1, offer value B + (seq #3) cell. Panel A illustrates the choice pattern. Panel B illustrates the neuronal response measured in Task 1 (time window: post-offer). Each data point represents one trial type, and the firing rate (y-axis) is plotted against variable offer value B. The gray line is from a linear regression. In C, the three panels illustrate the neuronal responses measured in Task 2 (time windows: post-offer1, post-offer2, post-juice). Each data point represents one trial type, red and blue colors are for AB and BA trials, and gray lines are from linear regressions. In the three time windows, this cell seemed to encode variables offer value B | BA, offer value B | AB, and chosen value B, respectively, all with a positive slope. This pattern of responses corresponds to seq #3 (see **Table 3.2**). **D-F.** Example 2, chosen juice B (seq #6) cell. Same conventions as in example 1. In panel E (Task 1, post-juice time window), firing rates are plotted against the variable chosen juice. In the

three time windows defined for Task 2, the cell seemed to encode variables AB | BA, – AB | BA and chosen juice B, respectively. This pattern of responses corresponds to seq #6 (see **Table 3.2**). **G-I.** Example 3, chosen value + (seq #7) cell. Same conventions as in example 1. In panel H (Task 1, post-offer time window), firing rates are plotted against the variable chosen value. In the three time windows defined for Task 2, the cell seemed to encode variables offer value 1, offer value 2 and chosen value. This pattern of responses corresponds to seq #7 (see **Table 3.2**).

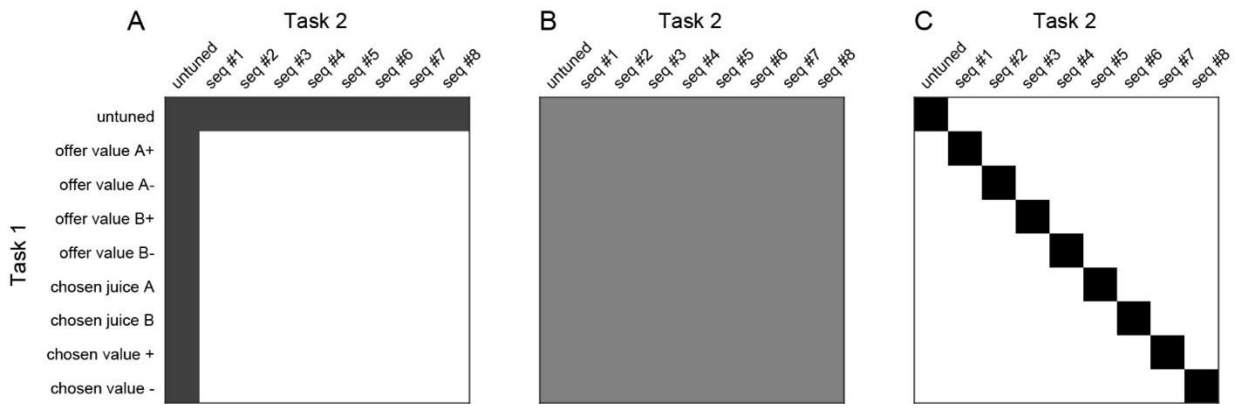

Figure 3.3. Comparing classification across tasks, possible results. In this cartoon, rows and columns represent different cell groups defined for Task 1 and Task 2, respectively. For each entry, the gray shade indicates the number of cells classified according to the corresponding groups in the two tasks (or the corresponding odds ratio). The three panels illustrate three possible scenarios. **A.** Separate populations. Task 1 and Task 2 might recruit different groups of neurons. **B.** Independent classification. The two tasks might recruit the same neurons but the role of any cell in one task might me unrelated to that in the other task. **C.** Consistent classification. Task 1 and Task 2 might recruit the same neurons and each cell might have the same functional role in the two tasks.

response. If the slope was statistically indistinguishable from zero, we set R^2=0. We considered the signed sR^2, where the sign was obtained from the regression slope, summed it over time windows, took the absolute value, and assigned each neuron to the variable providing the maximum |sum(sR^2)| (see **Methods**). Task-related cells not explained by any variable in any time window were labeled "untuned". For Task 2, we used a very similar procedure, except that, for any of the 8 sequences, different variables were examined in different time windows (**Table 3.2**). Again, each neuron was assigned to the sequence providing the maximum |sum(sR^2)|, where sR^2 is the signed R^2 and the sum is across time windows.

3.2.3 Matching classifications across choice tasks

To compare the results across tasks, we constructed a contingency table where rows represented classes in Task 1, columns represented classes in Task 2, and in each entry quantified the cell count. We envisioned three possible scenarios illustrated in **Fig.3.3**. (1) The table might be concentrated on the first row and first column (**Fig.3.3A**), indicating that the two tasks engage different neuronal populations; (2) the table might present a uniform distribution (**Fig.3.3B**), indicating that the two tasks engage the same neuronal population but the role of individual neurons differs across task; or (3) the contingency table might be concentrated on the diagonal (**Fig.3.3C**), indicating that individual neurons have the same role in the two choice tasks.

Fig.3.4A illustrates the cell counts actually measured in the experiments. The vast majority of neurons were either non-task related (881/1,526 = 58%), or tuned in both tasks (490/1,526 = 32%). Importantly, different groups of cells accounted for different numbers of neurons. Thus to compare each cell count to chance level, we computed for each entry the odds ratio (OR; see **Methods**). We thus obtained a table of ORs (**Fig.3.4B**). For each entry, OR=1 was chance level;

conversely, OR>1 or OR<1 indicated that the cell count was above or below that expected by chance, respectively. For each entry, a Fisher's exact test ($p<0.01$) assessed whether departure from chance was statistically significant (**Fig.3.4C**). Inspection of **Fig.3.4B** reveals that cell counts were significantly above chance for all entries on the diagonal. Conversely, the vast majority of off-diagonal entries (69/72) was at or below chance level. In conclusion there was a strong correspondence between the class identified for any given cell in Task 1 and that identified for the same cell in Task 2.

We noted that a few off-diagonal entries in **Fig.3.4B** were significantly above chance. We conducted two analyses to assess the significance of this observation. First, we examined this finding could be explained by the correlation between different variables defined in **Table 3.1**. This correlation and the intrinsic variability of neuronal firing rates likely induced some mis-classification. We thus expected that instances for which $OR_{i,j}$ was significantly >1 would occur only when the variables indexed by i and j were highly correlated with each other. To test our hypothesis, we generated the correlation matrix C, separately for each task. For Task 1, entry $C_{m,n}$ in this matrix was simply the correlation between variables m and n, which did not depend on the time window. For Task 2, since each sequence included different variables in different time windows, we computed the correlation matrix separately in each time window using the relevant variables. We then calculated the mean correlation matrix across time windows. The correlation matrices obtained for the two tasks were similar, and we averaged them to obtain the average correlation matrix, referred to as table Z. Of note, table Z was symmetric by construction (**Fig.3.5A**). Inspection of it reveals that correlations between specific pairs of variables were particularly high. For example, variables offer value A+ and chosen value A were highly correlated ($r = 0.69$). Similarly, variables offer value B+ and chosen value B were highly

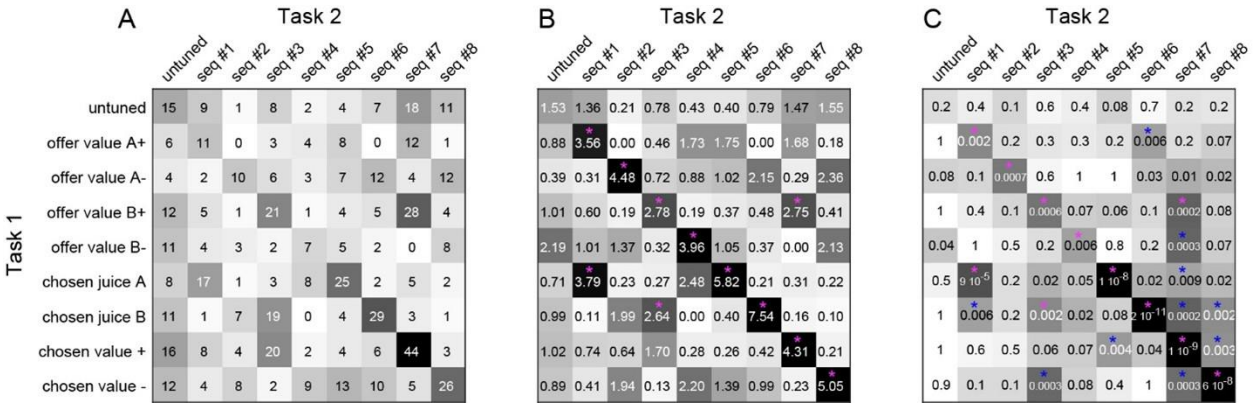

Figure 3.4. Neuronal classification is consistent across choice tasks. **A.** Contingency table (N = 645 cells). Numbers and gray scale indicate cell counts. **B.** Table of odds ratios. For each entry in panel A we computed the odds ratio (OR; see **Methods, Eq.3.4**). ORs are indicated here by numbers and gray scale colors. Chance level corresponds to OR = 1; conversely, OR>1 (OR<1) indicate that the cell count was higher (lower) than expected by chance. Red asterisks (*) indicate that the ORs was significantly >1 ($p<0.01$, Fisher's exact test). For all entries on the main diagonal, OR was significantly >1, indicating that the two choice tasks yielded the same classification results. Of note, cell counts on the first column (untuned in Task 1) and cell counts on the first row (untuned in Task 2) were all at chance level. **C.** Fisher's exact test, p values. Red/blue asterisks (*) indicate that the OR was significantly higher/lower than 1 ($p<0.01$).

correlated (r = 0.63). To assess the relation between OR table and Z table, we plotted them against each other entry by entry (excluding the diagonals; **Fig.3.5B**). The two tables were highly correlated (Pearson: r = 0.75, p = 4 10^{-11}). Furthermore, significant departure from chance level in the OR table ($OR_{i,j}>1$) occurred only when the variable correlation was particularly high ($Z_{i,j}>0.5$).

Second, to compare the results in **Fig.3.4B** to some benchmark, we generated equivalent OR tables separately for each choice task. For Task 1, we divided trials randomly in two sets (set 1 and set 2; see **Methods**). We analyzed the two sets of trials separately and thus obtained two independent classifications. We repeated this operation for each cell in the population, and generated a contingency table (not shown) and a table of ORs (**Fig.3.6A**) where rows and columns corresponded to set 1 trials and set 2 trials, respectively. We repeated this analysis for data from Task 2 and obtained an equivalent OR table (**Fig.3.6B**). Since the two sets of trials were interleaved and the criterion used to separate them was arbitrary, we expected the OR tables to concentrate on the diagonal. Conversely, non-zero off-diagonal entries should capture noise in the classification procedures due to the correlation between encoded variables (**Fig.3.5A**) and to trial-to-trial variability in spike counts. To assess whether the table in **Fig.3.4B** (across tasks) differed significantly from the tables in **Fig.3.6AB** (within task) we used a Breslow-Day test (see **Methods**). **Fig.3.6C** illustrates the results of this analysis. In essence, classifications across tasks were as consistent as classifications within tasks (all $p\geq0.01$).

In all previous analyses, neurons were classified based on the activity recorded in multiple time windows. For a control, we repeated the analysis of **Fig.3.4** using only one time window for each task. We then matched time windows across tasks. Indicating with [x, y] the pair formed by time

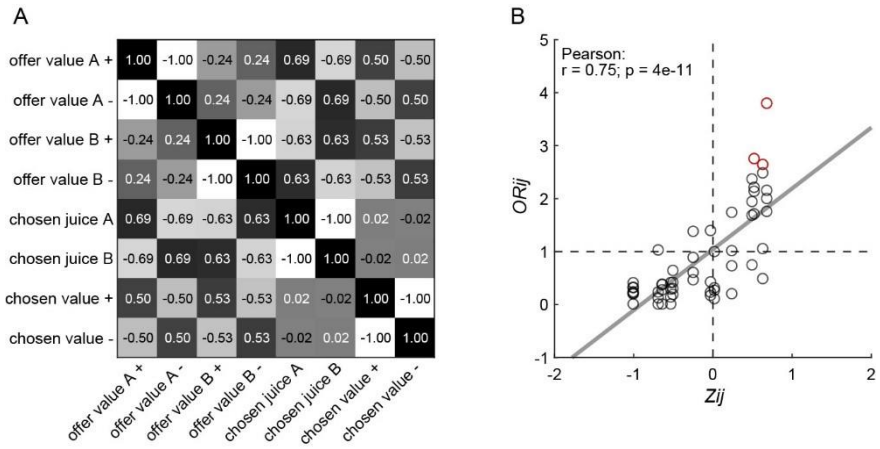

Figure 3.5. Significant departures from chance level in *OR* table reflect correlations between the encoded variables. **A.** Correlation matrix between encoded variables (Z table). Correlations between the encoded variables were first calculated separately for both Task 1 and Task 2. The results were then averaged across tasks and shown here. Green circles highlight entries where correlation was >0.5. **B.** Correlation between *OR* table and Z table. Corresponding entries were plotted against each other. The gray line is from a linear regression, and p values are indicated in the panel. Red data points highlight entries in the *OR* table that were significantly >1. The large correlation measured here (r = 0.75) indicates that significant departures from chance in the *OR* table were likely due to mis-classifications induced by the correlation between encoded variables.

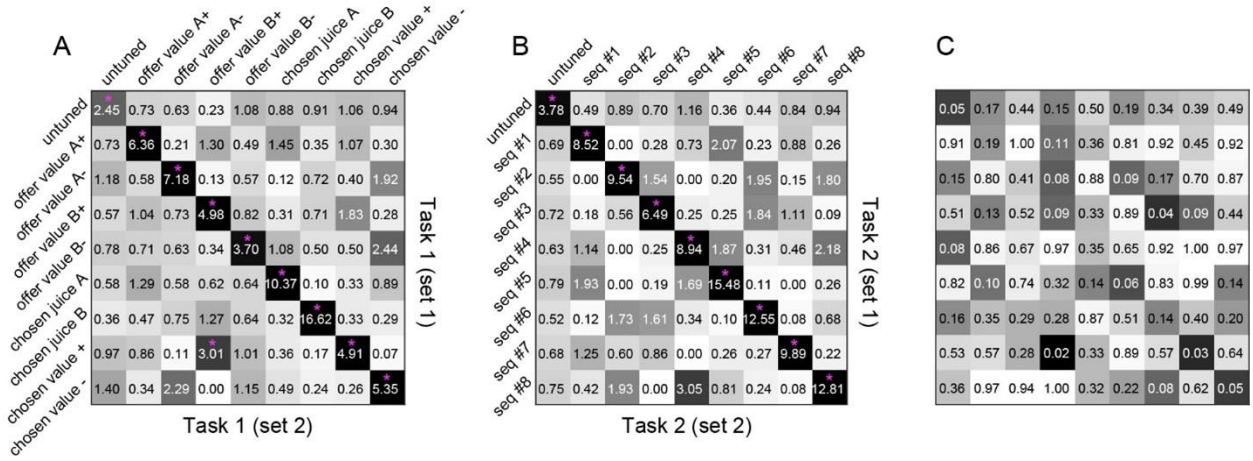

Figure 3.6. Comparing neuronal classification within and across choice tasks. **A.** Odds ratios obtained for Task 1. For each neuron, we divided trials randomly in two sets (set 1 and set 2; see **Methods**). We analyzed the two sets of trials separately and thus obtained two independent classifications. We repeated this operation for each cell in the population, and generated a contingency table (not shown) and a table of ORs, shown here, where rows and columns corresponded to set 1 trials and set 2 trials, respectively. Conventions here are as for **Fig.3.4B**. Since the two sets of trials were interleaved and the criterion used to separate them was arbitrary, the tables of ORs were expected to be concentrated on the diagonal. Indeed, all diagonal entries were significantly above chance ($p<0.01$, Fisher's exact test). Conversely, off-diagonal entries captured the noise in classification procedures. **B.** Odds ratios obtained for Task 2. We repeated this analysis for Task 2 trials and obtained an equivalent table of ORs. Again, all diagonal entries were significantly above chance ($p<0.01$, Fisher's exact test). **C.** Comparing the classification consistency obtained within and across tasks. Each entry in this panel indicates the p value obtained from a Breslow-Day test, and $p<0.01$ would indicate significant differences across OR tables. In practice, we obtained $p>0.01$ for all 81 entries. In other words, the neuronal classification was as consistent across tasks as it was within tasks.

windows x (Task 1) and y (Task 2), we examined the three pairs [post-offer, post-offer1], [post-offer, post-offer2] and [post-juice, post-juice]. In general, the results based on a single time window were similar to those based on multiple windows, albeit noisier. For example, considering the time window pair [post-offer, post-offer1], all the diagonal entries in the OR table were significantly above chance (along with a few off-diagonal entries). The two other pairs of time windows provide similar pictures. These findings confirmed that there was a strong correspondence between the cell classification in the two choice tasks.

Taken together, our results indicated that the cells groups identified under sequential offers are equivalent to those identified under simultaneous offers. Building on this finding, we proceeded with a comprehensive classification based on both choice tasks, by summing the R^2 across all seven time windows (see **Methods**). Henceforth, we may refer to the different groups of cells using the standard nomenclature – offer value, chosen juice and chosen value – independently of the choice task. In total, the final classification resulted in 235 offer value cells, 168 chosen juice cells and 233 chosen value cells.

3.2.4 Matching maximum selectivity windows across choice tasks

To complement the results described above, we examined whether there was some correspondence between the time windows in which any given neuron was most selective in Task 1 and in Task 2. To address this issue, we defined for each cell, each task and each time window the selective activity range (SAR), which captured the strength of the encoding (see **Methods**). For each cell and each task, the maximum selectivity window (MSW) may be defined as the time window for which SAR was maximal. Because neurons often responded similarly in

different time windows (e.g., post-offer1 and post-offer2 in Task 2), we used a soft definition and identified as MSW any time window such that SAR / max(SAR) > 0.6.

To compare the MSWs identified for each cell in the two tasks across the population, we generated a contingency table where rows and columns represented time windows in the two tasks and each entry indicated the number of cells with corresponding MSWs (**Fig.3.7A**). We also computed the corresponding table of odds ratios (**Fig.3.7B**), and the p values obtained from Fisher's exact tests (**Fig.3.7C**). The results indicated that time windows for which neurons were maximally selective in the two tasks were systematically related across the population. Specifically, cells for which MSW = post-offer in Task 1 typically had MSW = post-offer1 and/or MSW = post-offer2 in Task 2. Similarly, cells for which MSW = post-juice in Task 1 typically had MSW = post-juice in Task 2. This finding supports the understanding that individual neurons have similar functions in the two choice tasks.

3.3 Discussion

The past 20 years witnessed enormous progress in the understanding of the cognitive and neural underpinnings of economic choices. An extensive body of work demonstrates beyond reasonable doubt that subjective values are explicitly represented at the neuronal level (Kable and Glimcher, 2009; O'Doherty, 2014; Padoa-Schioppa, 2007; Perkins and Rich, 2021). Furthermore, substantial evidence links economic decisions to neuronal activity in the OFC. Neurons in this area represent different decision variables in a categorical way (Hirokawa et al., 2019; Onken et al., 2019). In particular, when monkeys (or mice) choose between juices, different groups of cells encode individual offer values, the binary choice outcome and the chosen value (Kuwabara et al.,

2020; Padoa-Schioppa and Assad, 2006). These variables capture both the input and the output of the choice process, suggesting that the cell groups identified in OFC might constitute the building blocks of e decision circuit. The population dynamics (Rich and Wallis, 2016), correlations between neuronal and behavioral variability (Padoa-Schioppa, 2013), the effects of lesion (Camille et al., 2011; Yu et al., 2018) or inactivation (Gore et al., 2019; Kuwabara et al., 2020), and computational modeling (Rustichini and Padoa-Schioppa, 2015; Song et al., 2017; Zhang et al., 2018) support this proposal. These and corroborating results set the stage for a detailed understanding of the decision mechanisms. One important caveat is that current notions came primarily from studies in which two offers were presented simultaneously. Yet, in many daily choices, offers appear or are examined sequentially, and some authors suggested that choices under sequential offers may rely on fundamentally different mechanisms (Hayden and Moreno-Bote, 2018; Hunt et al., 2013; Kacelnik et al., 2011). Thus the purpose of this study was to assess whether choices under sequential and simultaneous offers engage the same neural circuit. In a previous study, we recorded from the OFC under sequential offers. Through an analysis of neuronal responses across time windows, we identified different groups of neurons encoding different sequences of decision variables (Ballesta and Padoa-Schioppa, 2019). Importantly, since any choice task engages only a subset of neurons, it remained unclear whether choices under sequential or simultaneous offers rely on the same neuronal population, or whether the functional role of any given cell would be preserved across choice modalities. In the present study, we alternated two choice tasks on a trial-by-trial basis. In a nutshell, we found a strong correspondence between the cell groups previously identified in the two conditions. In other words, choices under sequential or simultaneous offers appear to rely on the same neural circuit.

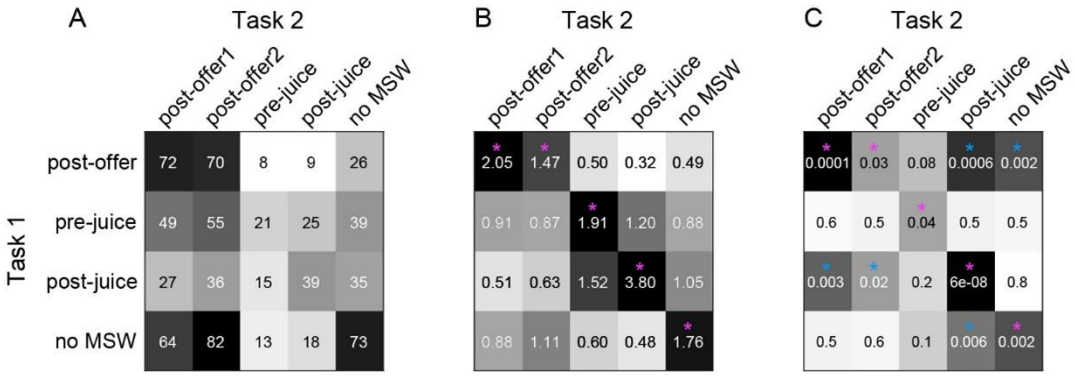

Figure 3.7. Maximum selectivity windows (MSWs) are matched across choice tasks. **A.** Contingency table of MSWs (N = 776 pairs of time windows from 645 cells). Rows and columns indicate time windows in Task1 and Task2, respectively. Numbers and gray scale indicate cell counts. Cells for which SAR=0 were classified as "no MSW". **B.** Table of odds ratios (ORs). Magenta asterisks (*) indicate that OR was significantly >1 ($p<0.05$, Fisher's exact test). **C.** Fisher's exact test, exact p values. Magenta/blue asterisks (*) indicate that OR was significantly higher/lower than 1 ($p<0.05$).

This result indicates that notions emerging from studies of choices under simultaneous offers generalize to a much broader domain of choices than previously recognized.

An interesting question is whether the neuronal populations described here might also subserve foraging choices such as those made by an animal that could continue to exploit the current food patch or leave it in search of better but riskier opportunities. Such choices are sometimes construed as "yes-or-no" and distinguished from binary choices of the sort examined in our experiments (Hayden and Moreno-Bote, 2018; Kolling et al., 2012). However, what appears as a yes-or-no choice could also be construed as a binary choice between two offers – one unambiguous (the current patch) and one more ambiguous (a probability distribution over other possible patches and times necessary to reach them). In economics, the value of the latter offer is often referred to as an opportunity cost. The question of how the brain treats patch-leaving choices – as yes-or-no or binary – remains open. If patch-leaving choices are treated as binary, it seem reasonable to assume that the neuronal populations identified in our studies play the same role when choices are about leaving a food patch. Conversely, if the brain treats patch-leaving choices as qualitatively different, such choices might rely on different neuronal mechanisms. These intriguing questions remain open for future research.

Alternating the two tasks within each session gave us the opportunity to compare choices in a controlled way. We thus discovered three interesting phenomena. Under sequential offers, (a) choices were more variable, (b) relative values were higher (preference bias), and (c) choices were biased in favor of the second offer (order bias). The last observation confirms previous reports (Ballesta and Padoa-Schioppa, 2019; Krajbich et al., 2010; Rustichini et al., 2021). At the cognitive level, these phenomena may be understood as follows. The difference in choice

variability (a) may be interpreted noting that choices under sequential offers were cognitively more demanding because they required holding in working memory the value of offer1, comparing the values of two goods when only offer2 was visible, remembering the chosen juice for an additional delay, and mapping that choice onto the appropriate saccade target. Each of these mental operations could contribute choice variability. Along similar lines, the preference bias (b) may reflect the higher cognitive demands of Task 2. In particular, we note that when the two offer targets appear on the monitor, information about the two values is no longer on display on the monitor. If at that point the animal has not finalized its decision, or if it has failed to retain in working memory the decision outcome, it makes sense to choose the target associated with the more valuable juice (juice A), especially if the value difference between the two juices is large. Finally, the order bias (c) may be interpreted noting that decisions in Task 2 were made shortly after offer2 appeared on the monitor, when that offer was perceptually most salient. Thus a choice bias favoring offer2 is not surprising. The neuronal origins of choice biases including the phenomena documented here remain an important and open question for future work.

3.4 Methods

All the experimental procedures adhered to the NIH Guide for the Care and Use of Laboratory Animals and were approved by the Institutional Animal Care and Use Committee (IACUC) at Washington University.

3.4.1 Animal subjects and choice tasks

Two adult male rhesus monkeys (Macaca mulatta; monkey J, 10.0 kg, 8 years old; monkey G, 9.1 kg, 9 years old) participated in this study. Before training and under general anesthesia, we

implanted on each animal a head restraining device and an oval chamber (axes 50×30 mm). Chambers were centered on stereotaxic coordinates (A30, L0), with the longer axis parallel to coronal planes, allowing bilateral access to OFC with coronal electrode penetrations. Structural MRI scans (1 mm sections) obtained before and after surgery were used to locate OFC and guide neuronal recordings. During the experiments, monkeys sat in an electrically and acoustically insulated enclosure (Crist Instrument Co), with their head fixed and pink noise in the background. A computer monitor was placed in front of the animal at 57 cm distance. The gaze direction was monitored at 1 kHz using an infrared video camera (Eyelink, SR Research). The behavioral task was controlled using custom-written software (https://monkeylogic.nimh.nih.gov) (Hwang et al., 2019) based on Matlab (v2016a; MathWorks Inc).

In each session, the animal chose between two juices labeled A and B (A preferred) offered in variable amounts. Each session included trials with two choice modalities, referred to as Task 1 and Task 2 (**Fig.3.1AB**). The two tasks were nearly identical to those used in previous studies (Ballesta and Padoa-Schioppa, 2019; Padoa-Schioppa and Assad, 2006), and trials with the two tasks were pseudo-randomly interleaved. In both tasks, offers were represented by sets of colored squares displayed on the computer monitor. For each offer, the color indicated the juice type and the number of squares indicated the quantity. Each trial began with the animal fixating a large dot in the center of the monitor. After 0.5 s, the initial fixation point changed to a small dot or a small cross; the new fixation point cued the animal to the choice task used in that trial. In Task 1 (**Fig.3.1A**), cue fixation (0.5 s) was followed by the simultaneous presentation of the two offers. After a randomly variable delay (1-1.5 s), the center fixation disappeared and two saccade targets appeared near the offers (go signal). The animal indicated its choice with an eye movement. It

maintained peripheral fixation for 0.75 s, after which the chosen juice was delivered. In Task 2 (**Fig.3.1B**), cue fixation (0.5 s) was followed by the presentation of one offer (0.5 s), an inter-offer delay (0.5 s), presentation of the other offer (0.5 s), and a wait period (0.5 s). Two colored saccade targets then appeared on the two sides of the fixation point. After a randomly variable delay (0.5-1 s), the center fixation disappeared (go signal). The animal indicated its choice with a saccade, maintained peripheral fixation for 0.75 s, after which the chosen juice was delivered. Central and peripheral fixation were imposed within 4-6 and 5-7 degrees of visual angle, respectively.

For any given trial, q_A and q_B indicate the quantities of juices A and B offered to the animal, respectively. An "offer type" was defined by two quantities [q_A, q_B]. On any given session, we used the same juices and the same sets of offer types for the two tasks. For Task 1, the spatial configuration of the offers (left/right) varied randomly from trial to trial. For Task 2, trials in which juice A was offered first and trials in which juice B was offered first were referred as "AB trials" and "BA trials", respectively. The terms "offer1" and "offer2" indicated, respectively, the first and second offer, independently of the juice type and amount. In Task 2, the presentation order varied pseudo-randomly and was counterbalanced across trials for any offer type. The spatial location (left/right) of saccade targets varied randomly and independently of the presentation order. The juice volume corresponding to one square (quantum) was set equal for the two tasks and remained constant within each session. It varied across sessions (70-100 μl) for both monkeys. The association between the initial cue (small dot, small cross) and the choice modality (Task 1, Task 2) varied across sessions, in blocks.

In Task 2, AB trials and BA trials were analyzed separately (see below). A power analysis indicated that comparing neuronal responses across tasks would be most effective if the number of trials for Task 2 was $\sqrt{2}$ times that for Task 1. Thus in most sessions we set the number of trials for Task 2 equal to 1.5 times that for Task 1.

Prior to this study, monkey J had participated in experiments using Task 2 and had no exposure to Task 1. For the current study, the animal was first trained with Task 1 alone and then with the two tasks randomly interleaved. Monkey G had participated in different experiments using simultaneous offers (Task 1) or sequential offers (Task 2). For the current study, the animal was trained to perform the two choice tasks randomly interleaved.

Across sessions, we used the following juices (colors): lemon Kool-Aid (bright yellow), grape juice (bright green), cherry juice (diluted to 3/4 with water or no dilution, red), peach juice (diluted to 3/4 with water, rose), fruit punch (diluted to 1/3 with water, magenta), apple juice (diluted to 1/2 with water, dark green), cranberry juice (diluted to 1/3 with water, pink), peppermint tea (bright blue), kiwi punch (dark blue), watermelon Kool-Aid (lime) and slightly salted water (0.65 g/l concentration, light gray).

3.4.2 Behavioral analysis

Choices in the two tasks were analyzed separately with probit regressions. For Task 1, we used the following model:

$$\text{choice B} = \Phi(X) \tag{3.1}$$

$$X = a_0 + a_1 \log(q_B/q_A)$$

where choice B = 1 if the animal chose juice B and 0 otherwise, Φ was the cumulative function of the standard normal distribution, and q_A and q_B were the quantities of juices A and B offered. From the fitted parameters, we derived measures for the relative value of the juices $\rho_{Task1} = \exp(-a_0/a_1)$ and the sigmoid steepness $\eta_{Task1} = a_1$.

For Task 2, we used the following probit model:

$$\text{choice B} = \Phi(X) \tag{3.2}$$

$$X = a_2 + a_3 \log(q_B/q_A) + a_4 (\delta_{order,AB} - \delta_{order,BA})$$

where $\delta_{order,AB} = 1$ for AB trials and 0 otherwise, and $\delta_{order,BA} = 1 - \delta_{order,AB}$. Thus AB trials and BA trials were analyzed separately but assuming that the two sigmoids had the same steepness. From the fitted parameters, we derived measures for the relative value $\rho_{Task2} = \exp(-a_2/a_3)$, the sigmoid steepness $\eta_{Task2} = a_3$, and the order bias $\varepsilon = 2\ \rho_{Task2}\ a_4/a_3$. The order bias was defined such that $\varepsilon<0$ ($\varepsilon>0$) indicated a bias in favor of offer1 (offer2). We also defined the relative values specific to AB trials and BA trials as $\rho_{AB} = \exp(-(a_2+a_4)/a_3)$ and $\rho_{BA} = \exp(-(a_2-a_4)/a_3)$. Of note, the order bias was defined such that $\varepsilon \approx \rho_{BA} - \rho_{AB}$.

In some cases, one or both choice patterns presented complete or quasi-complete separation (i.e., the animal split choices for ≤1 offer types). In these cases, the fitted steepness (η) was high and unstable. We identified outlier sessions using an interquartile criterion. Defining IQR as the interquartile range, values below the first quartile minus 1.5*IQR or above the third quartile plus 1.5*IQR were identified as outliers and removed from the behavioral analysis (**Fig.3.1D-F**). This criterion excluded 14/115 sessions for monkey J and 51/191 sessions for monkey G. Including

all sessions in the analysis did not substantially change the results. Importantly, data from all sessions were included in the neuronal analyses.

3.4.3 Neuronal recordings

Neural recordings focused on area 13m in the central orbital gyrus (Ongur and Price, 2000). We recorded from both hemispheres of monkey J (left: AP 31:35, ML –8:–10; right: AP 31:35, ML 6:10) and both hemispheres of monkey G (left: AP 31:36, ML –7:–12; right: AP 31:36, ML 4:9). Tungsten single electrodes (100 µm shank diameter; FHC) were advanced remotely using a custom-built motorized micro-drive (step size 2.5 µm). Typically, one motor advanced two electrodes placed 1 mm apart, and 1-2 such pairs of electrodes were advanced unilaterally or bilaterally in each session. Each electrode would usually record the activity of 1-2 cells (average 1.25 cells/electrode). Amplified signals (gain: 10,000) were filtered (high-pass cutoff: 300 Hz; low-pass cutoff: 6 kHz; Lynx 8, Neuralynx), digitized (frequency: 40 kHz) and saved to disk (Power 1401, Cambridge Electronic Design). Spike sorting was performed off-line (Spike 2 v6, Cambridge Electronic Design). Only cells that appeared well isolated and stable throughout the session were included in the analysis.

3.4.4 Neuronal classification within task modality

For each neuron, trials from Task 1 and Task 2 were first analyzed separately using the procedures developed in previous studies (Ballesta and Padoa-Schioppa, 2019; Padoa-Schioppa and Assad, 2006). For Task 1, we defined four time windows: post-offer (0.5 s after offer onset), late-delay (0.5-1 s after offer onset), pre-juice (0.5 s before juice onset) and post-juice (0.5 s after juice onset). A “trial type” was defined by two offered quantities and a choice. For Task 2, we

defined three time windows: post-offer1 (0.5 s after offer1 onset), post-offer2 (0.5 s after offer2 onset) and post-juice (0.5 s after juice onset). A “trial type” was defined by two offered quantities, their order and a choice. For each task, each trial type and each time window, we averaged spike counts across trials. A “neuronal response” was defined as the firing rate of one cell in one time window as a function of the trial type. Neuronal responses in each task were submitted to an ANOVA (factor: trial type). Neurons passing the $p<0.01$ criterion in at least one time window in either task were identified as “task-related” and included in subsequent analyses.

Following previous work (Padoa-Schioppa, 2013; Padoa-Schioppa and Assad, 2006), neurons in Task 1 were classified in one of four groups offer value A, offer value B, chosen juice or chosen value. Each variable could be encoded with positive or negative sign, leading to a total of 8 cell groups. For the classification, we proceeded as follows. Each neuronal response was regressed against each of the four variables defined in **Table 3.1**. If the regression slope b_1 differed significantly from zero ($p<0.05$), the variable was said to "explain" the response. In this case, we set the signed R^2 as $sR^2 = \text{sign}(b_1)\, R^2$; if the variable did not explain the response, we set $sR^2 = 0$. After repeating the operation for each time window, we computed for each cell the $\text{sum}(sR^2)$ across time windows. Neurons explained by at least one variable in one time window, such that $\text{sum}(sR^2) \neq 0$, were said to be tuned; other neurons were labeled “untuned”. Tuned cells were assigned to the variable and sign providing the maximum $|\text{sum}(sR^2)|$, where $|\cdot|$ indicates the absolute value. Indicating with “+” and “–” the sign of the encoding, each neuron was thus classified in one of 9 groups: offer value A+, offer value A–, offer value B+, offer value B–, chosen juice A, chosen juice B, chosen value+, chosen value– and untuned.

Neuronal classification in Task 2 followed the procedures described by Ballesta and Padoa-Schioppa (2019). Under sequential offers, neuronal responses in OFC were found to encode different variables defined in relation to the presentation order (AB or BA). Specifically, the vast majority of responses were explained by one of 11 variables defined in **Table 3.1**. These included one binary variable capturing the order (AB | BA), six variables representing individual offer values (offer value A | AB, offer value A | BA, offer value B | AB, offer value B | BA, offer value 1, and offer value 2), three variables capturing variants of the chosen value (chosen value, chosen value A, chosen value B) and a binary variable representing the binary choice outcome (chosen juice). Each of these variables could be encoded with a positive or negative sign. Most neurons appeared to encode different variables in different time windows. In principle, considering 11 variables, 2 signs of the encoding and 3 time windows, neurons might present a very large number of variable patterns across time windows. Remarkably, however, the vast majority of OFC neurons presented one of 8 patterns. These patterns are referred to as sequences and defined in **Table 3.2**. Thus we classified each cell as encoding one of these 8 sequences. For each cell and each time window, we regressed the neuronal response against each of the variables predicted by each sequence. If the regression slope b_1 differed significantly from zero ($p<0.05$), the variable was said to explain the response and we set the signed R^2 as $sR^2 = sign(b_1) R^2$; if the variable did not explain the response, we set $sR^2 = 0$. After repeating the operation for each time window, we computed for each cell the sum(sR^2) across time windows for each of the 8 sequences. Neurons such that sum(sR^2) $\neq 0$ for at least one sequence were said to be tuned; other neurons were untuned. Tuned cells were assigned to the sequence that provided the maximum |sum(sR^2)|. As a result, each neuron was classified in one of 9 groups: seq #1, seq #2, seq #3, seq #4, seq #5, seq #6, seq #7, seq #8 and untuned.

3.4.5 Comparing classification across choice task

We aimed to ascertain the relation between the classifications obtained for Task 1 and Task 2. To do so, we used statistical analyses for categorical data (Agresti, 2019). First, we constructed a 9x9 contingency table in which rows and columns represented, respectively, the cell classes defined in Task 1 and Task 2, and each entry indicated the number of neurons with the corresponding classifications. Second, to estimate whether the cell count obtained for any particular pair of classes departed from chance level, we computed a table of odds ratios. For each location (i, j) in the contingency table, $X_{i,j}$ indicated the number of cells classified as class i in Task 1 and as class j in Task 2. We defined:

$$a_{1,1} = X_{i,j} \tag{3.3}$$

$$a_{1,2} = \sum_{n \neq j} X_{i,n}$$

$$a_{2,1} = \sum_{m \neq i} X_{m,j}$$

$$a_{2,2} = \sum_{m \neq i, n \neq j} X_{m,n}$$

The corresponding odd ratio (OR) was defined as:

$$OR_{i,j} = (a_{1,1}/a_{1,2})/(a_{2,1}/a_{2,2}) \tag{3.4}$$

The OR was calculated for each entry of the contingency table. We thus obtained a 9x9 table. For each entry (i, j), $OR_{i,j} = 1$ was the chance level. Conversely, $OR_{i,j} > 1$ ($OR_{i,j} < 1$) indicated that the number of neurons classified as (i, j) was higher (lower) than expected by chance based

on the number of cells in class i and the number of cells in class j. To assess whether departures from chance level were statistically significant, we used the two-tailed Fisher's exact test, separately for each entry.

To compare the across-tasks table to some benchmark, we created two within-task tables. For each choice task and each trial type, we randomly divided trials in two sets (1 and 2). Pooling trial types, we obtained two complete sets of trials (set 1 and set 2). This procedure ensured that each set had the same number of trial types. For Task 1 data, we repeated the cell classification procedure described above separately for each trial set. We thus generated the within-task contingency table and the table of ORs comparing the results obtained for sets 1 and 2. We repeated these operations for Task 2 data. To assess whether the two within-task tables of ORs and the across-tasks table of ORs differed significantly from each other, we used the Breslow-Day test (Breslow and Day, 1980). In essence, this test examines the homogeneity of ORs, with the null hypothesis that different strata are statistically identical. In our case, the null hypothesis was that for each location in the OR table, the three measures (two within-task and one across-task) were statistically identical. The Breslow-Day test is ultimately a Chi-squared test. Its statistic has an asymptotic Chi-squared distribution with k–1 degrees of freedom. Here the test was conducted entry by entry, with d.f. = 2, and $p<0.01$ identified statistical significance.

Following the results presented in this study, we proceeded with a comprehensive ('final') classification based on the activity recorded in both tasks. For each task-related cell, we calculated the sum(sR^2) for the eight variables in Task 1 ($sum(sR^2)_{Task1}$) and eight sequences in Task 2 ($sum(sR^2)_{Task2}$) as described above. We then added the corresponding $sum(sR^2)_{Task1}$ and $sum(sR^2)_{Task2}$ to obtain the $sum(sR^2)_{final}$. Neurons such that $sum(sR^2)_{final} \neq 0$ for at least one class

were said to be tuned; other neurons were untuned. Tuned cells were assigned to the cell class that provided the maximum $|\text{sum}(sR^2)_{final}|$.

3.4.6 Selective activity range

In each task, neurons respond to the encoded variables in multiple time windows. The strength of the encoding, referred to as selectivity, varies across windows and from cell to cell. Thus for each cell and for each task, one might identify the time window with maximum selectivity. We examined whether there was a systematic relationship between the maximum selectivity window measured for any given cell im the two tasks. To do so, we first defined the activity range (AR). For each cell and each time window, we performed the linear regression

$$fr = b_0 + b_1 EV \tag{3.5}$$

where fr was the firing rate, EV was the encoded variable and b_0 and b_1 were the fitted parameters. Indicating the minimum and maximum of EV respectively as EV_{min} and EV_{max}, we computed $\Delta EV = EV_{max} - EV_{min}$. The activity range was defined as $AR = |b_1 \Delta EV|$, where $|\cdot|$ indicates the absolute value. We also defined the selective activity range as:

$$SAR = P \times N \times AR \tag{3.6}$$

where P = 1 if the response passed the ANOVA criterion and 0 otherwise and N = 1 if the slope of the encoded variable differed significantly from zero and 0 otherwise.

Chapter 4: Neuronal origins of biases in economic choices under sequential offers

This chapter is adapted from the following publication with the permission from the co-authors:

Shi, W., Ballesta, S., & Padoa-Schioppa, C. (2021). Neuronal Origins of Biases in Economic Choices under Sequential Offers. bioRxiv.

Abstract

Economic choices are characterized by a variety of biases. Understanding their origins is a long-term goal for neuroeconomics, but progress on this front has been modest. Here we examined choice biases observed when two goods are offered sequentially. In the experiments, monkeys chose between different juices offered simultaneously or in sequence. Choices under sequential offers were less accurate (higher variability). They were also biased in favor of the second offer (order bias) and in favor of the preferred juice (preference bias). Analysis of neuronal activity in orbitofrontal cortex revealed that these phenomena emerged at different computational stages. Specifically, the lower choice accuracy reflected weaker offer value signals (valuation stage); the order bias emerged during value comparison (decision stage); the preference bias emerged late in the trial (post-comparison). The approach developed here, taking advantage of recent discoveries on the decision circuit, may shed light on other aspects of economic behavior.

4.1 Introduction

Some of the most mysterious aspects of economic behavior are choice biases documented in behavioral economics. Standard economic theory fails to account for these effects, and one of the long-term goals of neuroeconomics is to shed light on their origins (Camerer et al., 2005; Glimcher and Rustichini, 2004). Progress on this front has been relatively modest, largely because the neural underpinnings of (even simple) economic choices remained poorly understood until recently. However, the last 15 years have witnessed substantial advances. An important turning point for the field was the development of experimental protocols in which subjects choose between different goods and relative subjective values are inferred from choices. Decision variables defined based on these values are then used to interpret neural activity (Kable and Glimcher, 2007; Padoa-Schioppa and Assad, 2006; Plassmann et al., 2007). Numerous studies using this paradigm have shown that neurons in multiple brain regions explicitly represent the values of offered and chosen goods (Amemori and Graybiel, 2012; Cai et al., 2011; Cai and Padoa-Schioppa, 2012; Hosokawa et al., 2013; Jezzini and Padoa-Schioppa, 2020; Kim et al., 2008; Lak et al., 2014; Levy et al., 2010; Louie and Glimcher, 2010; Padoa-Schioppa and Assad, 2006; Pastor-Bernier et al., 2019; Shenhav and Greene, 2010). Furthermore, experiments using electrical stimulation showed that offer values encoded in the orbitofrontal cortex (OFC) are causally linked to choices (Ballesta et al., 2020). These results are of great significance for three reasons.

First, the identification in OFC and other brain regions of distinct groups of neurons encoding different decision variables is essential to ultimately understand the neural circuit and the mechanisms through which economic decisions are formed.

Second, in a more conceptual sense, the results summarized above provide a long-sought validation for the construct of value. The proposal that choices entail computing and comparing subjective values was put forth by early economists such as Bernoulli and Bentham (Niehans, 1990). Although this idea has remained influential, values defined at the behavioral level suffer from a fundamental problem of circularity. On the one hand, choices supposedly maximize values; on the other hand, values cannot be measured behaviorally independent of choices (Samuelson, 1938). Because of this problem, the construct of value gradually lost centrality in economic theory. Thus in the standard neoclassic formulation choices are "as if" driven by values, but there is no commitment to the idea that values are actually computed (Samuelson, 1947). In this perspective, the fact that neuronal firing rates in any brain region are linearly related to values defined at the behavioral level constitutes powerful evidence that choices indeed entail the computation of values (Camerer, 2008).

Third and less frequently discussed, the identification of neurons encoding offer values and other decision variables, together with some rudimentary understanding of the decision circuit, provides the opportunity to break the circularity problem described above. To appreciate this point, consider the fact that economic choices are often affected by seemingly idiosyncratic biases. For example, while choosing between two options offered sequentially, people and monkeys typically show a bias favoring the second option (Ballesta and Padoa-Schioppa, 2019; Krajbich et al., 2010; Rustichini et al., 2021). This order bias might occur for at least two reasons. (1) Subjects might assign a higher value to any given good if that good is offered second. (2) Alternatively, subjects might assign identical values independent of the presentation order, and the bias might emerge downstream of valuation, for example during value comparison. In the latter scenario, by introducing the order bias, the decision process would

actually fail to maximize the value obtained by the agent. Due to the circularity problem described above, these two hypotheses are ultimately not distinguishable based on behavior alone. However, access to a credible neural measure for the offer values makes it possible, at least in principle, to disambiguate between them. The results presented in this study build on this fundamental idea.

In a recent experiment, monkeys chose between two juices offered in variable amounts. In each session, we randomly interleaved two types of trials referred to as two tasks. In Task 1, offers were presented simultaneously; in Task 2, offers were presented in sequence (Shi et al., 2021). Probit regressions provided behavioral measures for the relative values of the two juices. Comparing choices across tasks, we observed three interesting phenomena. (1) Monkeys were substantially less accurate (higher choice variability) in Task 2 (sequential offers) compared to Task 1 (simultaneous offers). (2) Choices in Task 2 were biased in favor of the second offer (order bias). (3) Choices in Task 2 were biased in favor of the preferred juice (preference bias). These phenomena are especially interesting because in most daily situations offers available for choice appear or are examined sequentially. In the present study, we investigated the neuronal origins of these phenomena, collectively referred to as choice biases.

Neuronal recordings focused on the OFC. Earlier work on choices under simultaneous offers identified in this area different groups of cells encoding individual offer values, the binary choice outcome (chosen juice), and the chosen value (Padoa-Schioppa, 2013; Padoa-Schioppa and Assad, 2006). Furthermore, previous analyses of the present data set indicated that choices under sequential offers engage the same neuronal populations (Ballesta and Padoa-Schioppa, 2019; Shi et al., 2021). In other words, the cell groups labeled offer value, chosen juice and chosen value

can be identified in either choice task and appear to preserve their functional role. In first approximation, the variables encoded in OFC capture both the input (offer values) and the output (chosen juice, chosen value) of the choice process, suggesting that the cell groups identified in this area constitute the building blocks of a decision circuit (Padoa-Schioppa and Conen, 2017). A series of experimental (Ballesta et al., 2020; Camille et al., 2011; Rich and Wallis, 2016) and theoretical(Friedrich and Lengyel, 2016; Rustichini and Padoa-Schioppa, 2015; Solway and Botvinick, 2012; Song et al., 2017; Zhang et al., 2018) results support this view. In this study, we put forth a more articulated computational framework (**Fig.4.1**). In our account, different groups of OFC neurons participate in value computation and value comparison, and these processes are embedded in an ensemble of mental operations taking place before, during and after the decision itself. In this view, sensory information, memory traces and internal states are processed upstream of OFC and integrated in the activity of offer value cells. These neurons provide the primary input to a circuit formed by chosen juice cells and chosen value cells, where values are compared. The output of this circuit feeds brain regions involved in working memory and the construction of action plans.

This framework guided a series of analyses relating the activity of each cell group to the behavioral phenomena described above. Our results revealed that different biases emerged at different computational stages. The lower choice accuracy observed under sequential offers reflected weaker offer value signals (valuation stage). Conversely, the order bias did not have neural correlates at the valuation stage, but rather emerged during value comparison (decision stage). Finally, the preference bias did not have neural correlates at the valuation stage or during value comparison; it emerged late in the trial, shortly before the motor response.

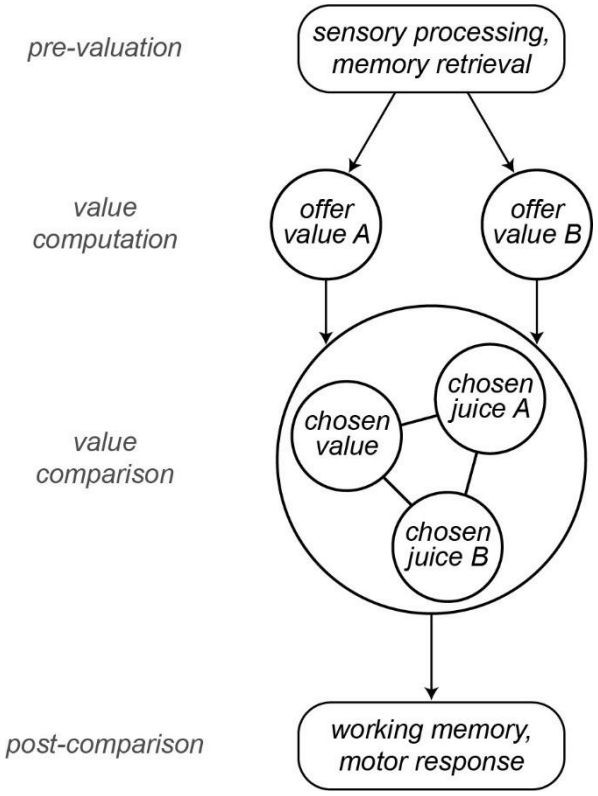

Figure 4.1. Computational framework. Information about sensory input, stored memory and the motivational state is integrated in the computation of offer values. In OFC, offer value cells provide the primary input to a decision circuit composed of chosen juice cells and chosen value cells. The detailed structure of the decision circuit is poorly understood, but previous work indicates that decisions under sequential offers rely on mechanisms of circuit inhibition. In essence, the value of good offered first (offer1) imposes a negative onset on the activity of chosen juice cells associated with the other offer (offer2). Notably this circuit might also subserve working memory. The decision output, captured by the activity of chosen juice cells, informs other brain regions that maintain it in working memory and transform it into a suitable action plan. Choice measured behaviorally is ultimately defined by the motor response. This framework highlights the fact that choice biases and/or noise might emerge at multiple computational stages. Of note, the arrows indicated here capture only the primary connections.

4.2 Results

4.2.1 Choice biases under sequential offers

Two monkeys participated in the experiments. In each session, they chose between two juices labeled A and B, with A preferred. Offers were represented by sets of colored squares on a monitor, and animals indicated their choice with a saccade. In each session, two choice tasks were randomly interleaved. In Task 1, offers were presented simultaneously (**Fig.4.2A**); in Task 2, offers were presented in sequence (**Fig.4.2B**). A cue displayed at the beginning of the trial revealed to the animal the task for that trial. Offers varied from trial to trial, and we indicate the quantities offered in any given trial with q_A and q_B. An "offer type" was defined by two quantities [q_A, q_B], and the same set of offer types was used for the two tasks in each session. For Task 2, trials in which juice A was offered first and trials in which juice B was offered first are referred to as "AB trials" and "BA trials", respectively. The first and second offers are referred to as "offer1" and "offer2", respectively.

The data set included 241 sessions (101 from monkey J, 140 from monkey G; see **Methods**). Sessions lasted for 217-880 trials (mean ± std = 589 ± 160). For each session, we analyzed choices in the two tasks separately using probit regressions. For Task 1 (simultaneous offers), we used the following model:

$$\text{choice B} = \Phi(X) \qquad (4.1)$$

$$X = a_0 + a_1 \log(q_B/q_A)$$

where choice B = 1 if the animal chose juice B and 0 otherwise, Φ was the cumulative function of the standard normal distribution, and q_A and q_B were the quantities of juices offered on any given trial. From the fitted parameters a_0 and a_1, we derived measures for the relative value of the two juices $\rho_{Task1} = \exp(-a_0/a_1)$ and for the sigmoid steepness $\eta_{Task1} = a_1$. Intuitively, the relative value was the quantity ratio q_B/q_A that made the animal indifferent between the two juices, and the sigmoid steepness was inversely related to choice variability.

For Task 2 (sequential offers), we used the following probit model:

$$\text{choice B} = \Phi(X) \tag{4.2}$$

$$X = a_2 + a_3 \log(q_B/q_A) + a_4 (\delta_{order,AB} - \delta_{order,BA})$$

where $\delta_{order,AB} = 1$ for AB trials and 0 otherwise, and $\delta_{order,BA} = 1 - \delta_{order,AB}$. In essence, AB trials and BA trials were analyzed separately but assuming that the two sigmoids had the same steepness. From the fitted parameters a_2, a_3 and a_4, we derived measures for the relative value of the two juices $\rho_{Task2} = \exp(-a_2/a_3)$, for the sigmoid steepness $\eta_{Task2} = a_3$, and for the order bias $\varepsilon = 2\,\rho_{Task2}\,a_4/a_3$. Intuitively, the order bias was a bias favoring the first or the second offer. Specifically, $\varepsilon<0$ indicated a bias favoring offer1; $\varepsilon>0$ indicated a bias favoring offer2. We also defined relative values specific to AB trials and BA trials as $\rho_{AB} = \exp(-(a_2+a_4)/a_3)$ and $\rho_{BA} = \exp(-(a_2-a_4)/a_3)$. Of note, the order bias was defined such that

$$\varepsilon \approx \rho_{BA} - \rho_{AB} \tag{4.3}$$

The experimental design gave us the opportunity to compare choices across tasks independently of factors such as satiation or changes in the internal state. The relative values measured in the two tasks were highly correlated (**Fig.4.2EF**). At the same time, our analyses revealed three

interesting phenomena. First, for both animals, sigmoids measured in Task 2 were significantly shallower compared to Task 1 (**Fig.4.2GH**). In other words, presenting offers in sequence substantially reduced choice accuracy. Second, in Task 2, both animals showed a consistent order bias favoring offer2 (**Fig.4.2IJ**). Third, in both animals, relative values in Task 2 were significantly higher than in Task 1 ($\rho_{Task2}>\rho_{Task1}$), and this effect increased with the relative value (**Fig.4.2EF**). In other words, the ellipse marking the 90% confidence interval for the joint distribution of relative values lay above the identity line and was rotated counterclockwise compared to the identity line.

To further investigate the differences in relative values measured across tasks, we quantified them separately in AB trials and BA trials in each monkey. We thus examined the relation between ρ_{Task1} and $\rho_{Task2,AB}$ and, separately, that between ρ_{Task1} and $\rho_{Task2,BA}$ (**Fig.4.3**). In both animals and in both sets of trials, the ellipse marking the 90% confidence interval was rotated counterclockwise compared to the identity line. Furthermore, the ellipse measured for BA trials was higher than that for AB trials. We quantified these observations with an analysis of covariance (ANCOVA) using the presentation order (AB, BA) as a covariate and imposing parallel lines (**Fig.4.3CF**). In both animals, the two regression lines were significantly distinct (difference in intercept >0, $p \leq 0.002$ in each animal). This result confirmed the presence of an order bias favoring offer2 in Task 2. Concurrently, in both animals the regression slope was significantly >1 ($p \leq 0.04$ in each animal; ellipse rotation). This result indicated that the animal had an additional bias favoring juice A in Task 2, and that this bias increased as a function of the relative value ρ. We refer to this phenomenon as the preference bias.

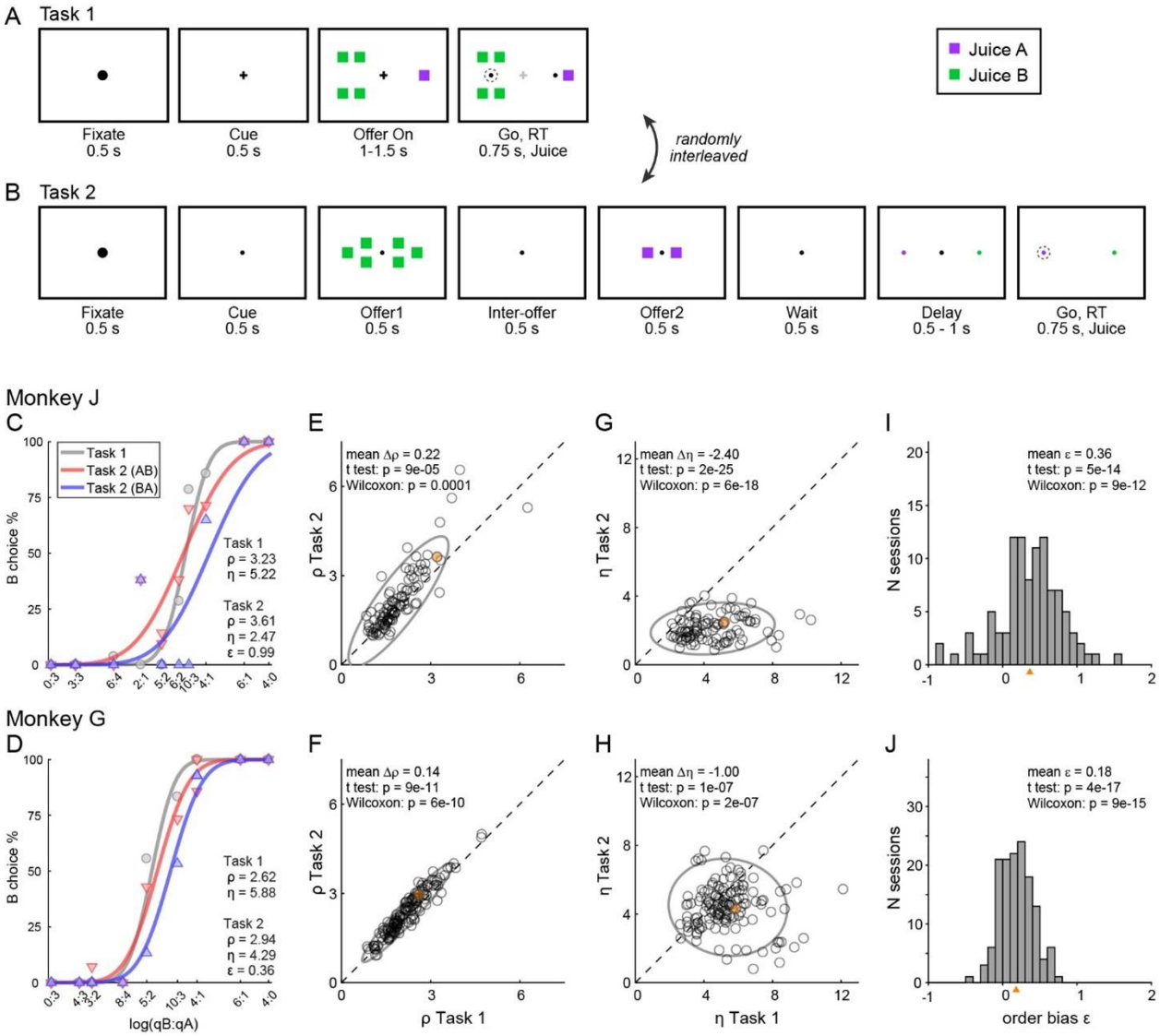

Figure 4.2. Experimental design and choice biases. **AB.** Experimental design. Animals chose between two juices offered in variable amounts. Offers were represented by sets of color squares. For each offer, the color indicated the juice type and the number of squares indicated the juice amount. In each session, trials with Task 1 and Task 2 were randomly interleaved. In Task 1, two offers appeared simultaneously on the left and right sides of the fixation point. In Task 2, offers were presented sequentially, spaced by an inter-offer delay. After a wait period, two saccade targets matching the colors of the offers appeared on the two sides of the fixation point. The left/right configuration in Task 1, the presentation order in Task 2 and the left/right position of the saccade targets in Task 2 varied randomly from trial to trial. In any

session, the same set of offer types was used for both tasks. **C.** Example session 1. The percent of B choices (y-axis) is plotted against the log quantity ratio (x-axis). Each data point indicates one offer type in Task 1 (gray circles) or Task 2 (red and blue triangles for AB trials and BA trials, respectively). Sigmoids were obtained from probit regressions. The relative value (ρ) and sigmoid steepness (η) measured in each task and the order bias (ε) measured in Task 2 are indicated. In this session, the animal presented all three biases. Compared to Task 1, choices in Task 2 were less accurate ($\eta_{Task2} < \eta_{Task1}$) and biased in favor of juice A ($\rho_{Task2} > \rho_{Task1}$; preference bias). Furthermore, choices in Task 2 were biased in favor of offer2 ($\varepsilon > 0$; order bias). **D.** Example session 2. Same format as panel C. **EF.** Comparing relative value across choice tasks. Each data point represents one session and gray ellipses indicate 90% confidence intervals. For both monkeys, relative values in Task 2 (y-axis) were significantly higher than in Task 1 (x-axis). Furthermore, the main axis of each ellipse was rotated counterclockwise compared to the identity line. **GH.** Comparing the sigmoid steepness across choice tasks. For both monkeys, sigmoids were consistently shallower (smaller η) in Task 2 compared to Task 1. **IJ.** Order bias, distribution across sessions. Both monkeys presented a consistent bias favoring offer2 (mean(ε)>0). Panels CEGI are from monkey J (N = 101 sessions); panels DFHJ are from monkey G (N = 140 sessions). Sessions shown in panels CD are highlighted in yellow in panels EFGH. Triangles in panels IJ indicate the mean. Statistical tests and exact p values are indicated in each panel.

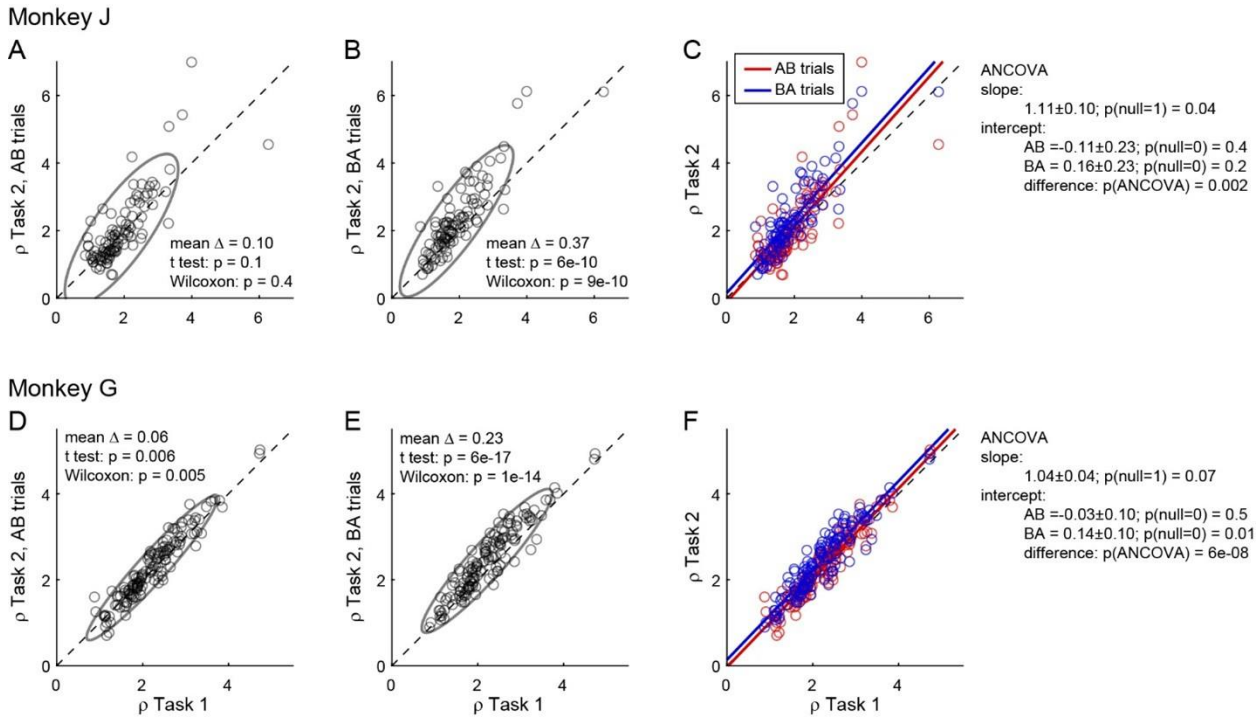

Figure 4.3. Order bias and preference bias. **ABC.** Monkey J (N = 101 sessions). In panels A and B, $\rho_{Task2,AB}$ and $\rho_{Task2,BA}$ (y-axis) are plotted against ρ_{Task1} (x-axis). Each data point represents one session and gray ellipses indicate 90% confidence intervals. The main axis of both ellipses is rotated counterclockwise compared to the identity line (preference bias). In addition, the ellipse in panel B is displaced upwards compared to that in panel A (order bias). In panel C, the same data are pooled and color coded. The two lines are from an ANCOVA (covariate: order; parallel lines). The regression slope is significantly >1 (preference bias) and the two intercepts differ significantly from each other (order bias). **DEF.** Monkey G (N = 140 sessions). Same format. The results closely resemble those for monkey J but the preference bias is weaker.

4.2.2 Origins of choice biases: Computational framework

The following sections present a series of results on the neuronal origins of these biases. We begin by discussing the computational framework for these analyses.

Economic choice is thought to entail two stages: values are assigned to the available offers and a decision is made by comparing values. Importantly, in our tasks and in most circumstances, choices elicit an ensemble of mental operations taking place before, during and after the computation and comparison of offer values. Upstream of valuation, choices examined here entail the sensory processing of visual stimuli and the retrieval from memory of relevant information (e.g., the association between color and juice type). Downstream of value comparison, the decision outcome must guide a suitable motor response. In addition, performance in Task 2 requires holding in working memory the value of offer1 until offer2, remembering the decision outcome for an additional delay, and mapping that outcome onto the appropriate saccade target (**Fig.4.2B**). In principle, choice biases could emerge at any of these computational stages. Likewise, each of these mental operations could be noisy and thus contribute to choice variability.

Neuronal activity in OFC does not capture all of these processes. However, previous work indicates that neurons in this area participate both in value computation and value comparison. In the framework proposed here (**Fig.4.1**), sensory and limbic areas feed offer value cells, where values are integrated. In turn, offer value cells provide the primary input to a neural circuit constituted by chosen juice cells and chosen value cells, where decisions are formed. Finally, the decision circuit is connected with downstream areas, such as lateral prefrontal cortex, engaged in working memory and in transforming choice outcomes into suitable action plans. This scheme

reflects the anatomical connectivity of OFC and other prefrontal regions (Carmichael and Price, 1995a, b; Petrides and Pandya, 2006; Saleem et al., 2013; Takahara et al., 2012); it is motivated by neurophysiology results from OFC (Ballesta et al., 2020; Rich and Wallis, 2016) and connected areas (Cai and Padoa-Schioppa, 2014; Sasikumar et al., 2018); and it is consistent with computational models of economic decisions (Friedrich and Lengyel, 2016; Rustichini and Padoa-Schioppa, 2015; Solway and Botvinick, 2012; Song et al., 2017; Yim et al., 2019; Zhang et al., 2018).

Of note, both offer value and chosen value cells encode subjective values. However, in the framework of **Fig.4.1**, offer value cells express a pre-decision value, while chosen value cells express a value emerging during the decision process. Conversely, the activity of chosen juice cells captures the evolving commitment to a particular choice outcome. In this framework, suitable analyses of neuronal activity may reveal whether particular choice biases emerge at the valuation stage, at the decision stage, or in subsequent computational stages.

4.2.3 Reduced accuracy under sequential offers emerged at the valuation stage

Other things equal, choices under sequential offers (Task 2) were significantly less accurate than choices under simultaneous offers (Task 1; **Fig.4.2**). We first investigated the neural origins of this phenomenon.

The primary data set examined in this study included 183 offer value cells, 160 chosen juice cells and 174 chosen value cells (see **Methods**). Comparing neuronal responses across tasks, we noted that offer value signals in Task 2 were significantly weaker than in Task 1. **Fig.4.4AC** illustrates

one example cell. In both tasks, this neuron encoded the offer value B. However, the activity range (see **Methods**) measured in Task 2 was smaller than that measured in Task 1. This effect was also observed at the population level. For this analysis, we pooled offer value cells associated with juices A and B, and with positive or negative encoding (see **Methods**). For Task 1, we focused on the post-offer time window; for Task 2, we focused on post-offer1 and post-offer2 time windows, pooling trial types from both windows. For each cell, we imposed that the response be significantly tuned in these time windows in each task, and we quantified the mean activity and the activity range (Δr, see **Methods**). At the population level, the mean activity did not differ significantly across tasks ($p = 0.6$, t test; $p = 0.4$, Wilcoxon test **Fig.4.4D**). In contrast, the activity range was significantly lower in Task 2 compared to Task 1 ($\Delta r_{Task2} < \Delta r_{Task1}$; $p = 0.06$, t test; $p = 0.02$, Wilcoxon test **Fig.4.4E**). In other words, offer value signals were weaker in Task 2 compared to Task 1.

The activity of offer value cells is causally related to choices (Ballesta et al., 2020). Furthermore, for given value range and mean activity, the activity range determines the neuronal signal-to-noise ratio. Indeed, we previously found that decreases in the encoding slope of offer value cells due to range adaptation reduce choice accuracy (Conen and Padoa-Schioppa, 2019; Rustichini et al., 2017). Along similar lines, we inquired whether the difference in choice accuracy measured across tasks (**Fig.4.2GH**) might be explained, at last partly, by differences in neuronal activity range (**Fig.4.4E**). We thus examined the relation between the difference in sigmoid steepness ($\Delta\eta = \eta_{Task2} - \eta_{Task1}$) and the difference in activity range ($\Delta\Delta r = \Delta r_{Task2} - \Delta r_{Task1}$). The two measures were positively correlated (Spearman $r = 0.2$, $p = 0.01$; Pearson $r = 0.3$, $p = 0.003$; **Fig.4.4F**). In other words, the drop in choice accuracy observed in Task 2 compared to Task 1

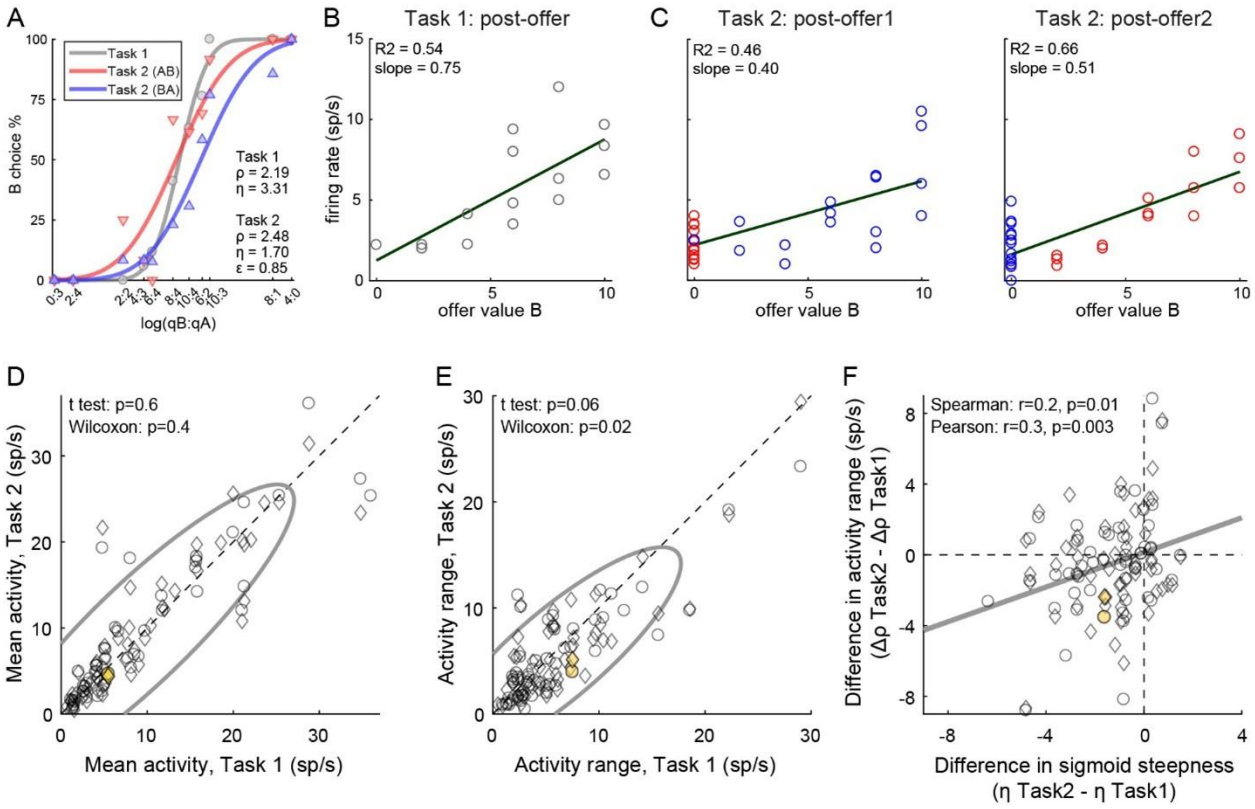

Figure 4.4. Lower choice accuracy in Task 2 reflects weaker offer value signals. **A-C.** Weaker offer value signals in Task 2, example cell. Panel A illustrates the choice pattern. Panel B illustrates the neuronal response measured in Task 1 (post-offer time window). Each data point represents one trial type. In C, two panels illustrate the neuronal responses measured in Task 2 (post-offer1 and post-offer2 time windows). Each data point represents one trial type; red and blue colors are for AB and BA trials, respectively. In panels B and C, firing rates (y-axis) are plotted against variable offer value B and gray lines are from linear regressions. Notably, the cell has lower activity range in Task 2 than in Task 1. **DE.** Weaker offer value signals in Task 2, population analysis (N = 109 offer value cells). The two panels illustrate the results for the mean activity and the activity range, respectively. In each panel, x-axis and y-axis represent measures obtained in Task 1 and Task 2, respectively. Each data point represents one cell. For each cell, we examined one time window (post-offer) in Task 1 and two time windows (post-offer1 and post-offer2) in Task 2. Circles and diamonds refer to post-offer1 and post-offer2 time windows,

respectively. Measures of mean activity measured in the two tasks (panel D) were statistically indistinguishable. In contrast, activity ranges (panel E) were significantly reduced in Task 2 compared to Task 1. Statistical tests and exact p values are indicated in each panel. The example cell shown in panels A-C is highlighted in orange in panels DE. **F.** Offer value signals and choice accuracy (N = 109 cells). For each offer value cell, we computed the activity range Δr in each task (see **Methods**). Here the difference in activity range $\Delta\Delta r = \Delta r_{Task2} - \Delta r_{Task1}$ (y-axis) is plotted against the difference in sigmoid steepness $\Delta\eta = \eta_{Task2} - \eta_{Task1}$ measured in the same session (x-axis). The two measures were significantly correlated across the population. The gray line in panel F is from a linear regression. This analysis was restricted to 53 cells significantly tuned in the post offer time window (Task 1) and post offer1 time window (Task 2), and 56 cells significantly tuned in the post offer time window (Task 1) and post offer2 time window (Task 2).

correlated with weaker offer value signals. Of note, similar analyses on chosen value cells and chosen juice cells yielded negative results (**Fig.4.S1**).

In conclusion, the lower choice accuracy measured in Task 2 compared to Task 1 correlated with weaker offer value signals in OFC. Thus this behavioral phenomenon emerged, at least partly, during valuation.

4.2.4 The order bias emerged during value comparison (decision stage)

The next series of analyses focused on the neural origins of the order bias. Since this phenomenon pertains only to choices under sequential offers, we included in the analyses an additional data set recorded in the same animals performing only Task 2 (see **Methods**).

In the framework of **Fig.4.1**, we first inquired whether the order bias emerged during valuation. If this was the case, for any given good, offer value cells should encode a higher value when the good is presented as offer2. To test this hypothesis, we pooled offer value cells associated with the two juices. For each neuron, 'E' indicated the juice encoded by the cell and 'O' indicated the other juice. We thus refer to EO trials and OE trials. For any given cell, we compared the response recorded in EO trials (post-offer1 time window) with the response recorded in OE trials (post-offer2 time window). If the order bias emerged during valuation, the tuning intercept and/or the tuning slope should be higher for the latter (**Fig.4.S2A**). Contrary to this prediction, across a population of 128 cells, we did not find any systematic difference in intercept or slope (**Fig.4.S2BC**). Furthermore, the difference between the intercepts and slopes measured in OE and EO trials did not correlate with the order bias (**Fig.4.S2D**). In conclusion, assigned values did not depend on the presentation order.

We next examined whether the order bias emerged during value comparison. If so, the bias should be reflected in the activity of both chosen juice and chosen value cells (**Fig.4.1**). For chosen value cells, the hypothesis might be tested noting that in post-offer1 and post-offer2 time windows these neurons encoded the value currently offered independently of the juice type (**Table 4.S1**). Thus the activity measured in these time windows in AB and BA trials provided neuronal measures for the relative values of the two juices. More specifically, for each chosen value cell, we derived the two measures $\rho^{neuronal}_{AB}$ and $\rho^{neuronal}_{BA}$ for AB trials and BA trials, respectively (**Fig.4.5A**; see **Methods**). We also defined the difference $\Delta\rho^{neuronal} = \rho^{neuronal}_{BA} - \rho^{neuronal}_{AB}$. We recall that the order bias was essentially equal to the difference between the relative values measured behaviorally in BA and AB trials ($\varepsilon \approx \rho_{BA} - \rho_{AB}$; **Eq.4.3**). Thus assessing whether the activity of chosen value cells reflected the order bias amounts to testing the relation between $\Delta\rho^{neuronal}$ and ε.

A population analysis of 96 chosen value cells lead to three observations. First, confirming previous results (Padoa-Schioppa and Assad, 2006), neuronal and behavioral measures of relative value were highly correlated and statistically indistinguishable. Second, the two neuronal measures or relative value, $\rho^{neuronal}_{AB}$ and $\rho^{neuronal}_{BA}$, did not differ significantly from each other (**Fig.4.5B**). Third, the difference $\Delta\rho^{neuronal}$ and the order bias ε were significantly correlated across the population (Spearman $r = 0.3$, $p = 0.007$; Pearson $r = 0.2$, $p = 0.02$; **Fig.4.5C**). In conclusion, session-to-session fluctuations in the activity of chosen value cells correlated with fluctuations in the order bias.

Further insights on the order bias came from the analysis of chosen juice cells. Again, for each neuron, E and O indicated the juice encoded by the cell and the other juice, respectively. A

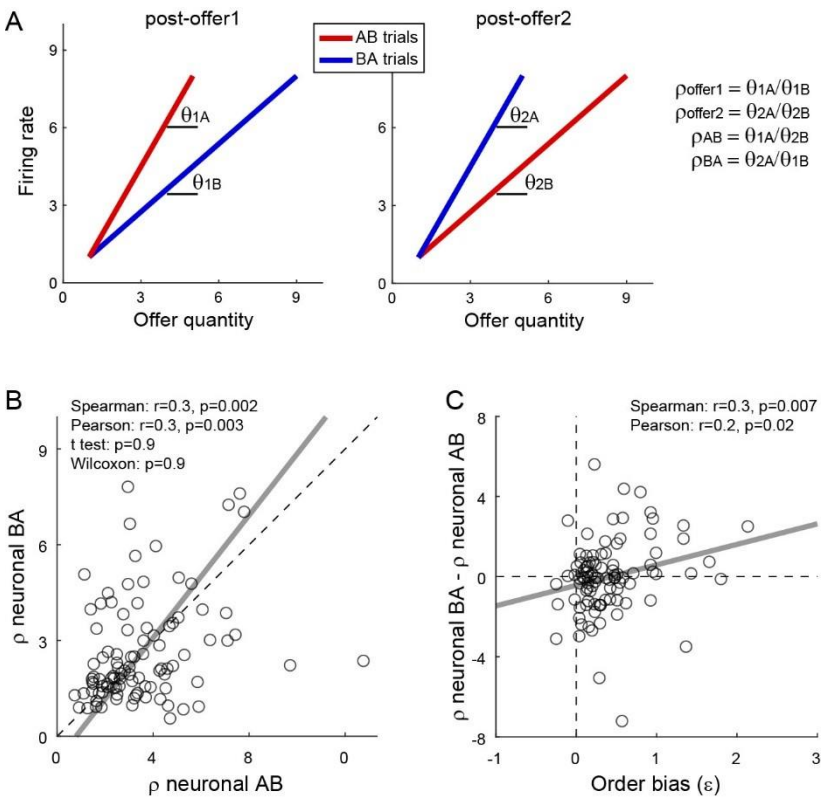

Figure 4.5. Fluctuations in order bias and fluctuations in the activity of chosen value cells. **A.** Neuronal measures of relative value. The two panels represent in cartoon format the response of a chosen value cell in the post-offer1 and post-offer2 time window (Task 2). In each of these time windows, chosen value cells encode the value of the offer on display. Here the two axes correspond to the firing rate (y-axis) and to the offered juice quantity (x-axis). The two colors correspond to the two orders (AB, BA). In each time window, two linear regressions provide two slopes, proportional to the value of the two juices. From the four measures θ_{1A} (left panel, red), θ_{1B} (left panel, blue), θ_{2A} (right panel, blue) and θ_{2B} (right panel, red), we derive four neuronal measures of relative value (**Methods, Eqs.4.9-4.12**). **B.** Neuronal measures of relative value in AB trials and BA trials (N = 96 cells). The x- and y-axis correspond to $\rho^{neuronal}_{AB}$ and $\rho^{neuronal}_{BA}$, respectively. Each data point represents one cell. The two measures are strongly correlated. The gray line is from a Deming regression. **C.** Fluctuations of relative value and fluctuations in order bias (N = 96 cells). For each chosen value cell, we quantified the difference in the neuronal measure of relative

value $\Delta\rho^{neuronal} = \rho^{neuronal}_{AB} - \rho^{neuronal}_{BA}$. Here, the x-axis is the order bias (ε), the y-axis is $\Delta\rho^{neuronal}$, and each data point corresponds to one cell. Although $\Delta\rho^{neuronal}$ was on average close to 0 (panel B), fluctuations of $\Delta\rho^{neuronal}$ correlated with fluctuations of ε across the population. The gray line is from a linear regression. Statistical tests and exact p values are indicated in each panel. This analysis was restricted to 96 cells that had significant θ_{1A}, θ_{1B}, θ_{2A} and θ_{2B}.

previous study found that the baseline activity of chosen juice cells recorded in OE trials immediately before offer2 was negatively correlated with the value of offer1 (i.e., the value of the other juice) – a phenomenon termed circuit inhibition (Ballesta and Padoa-Schioppa, 2019). If the decision is conceptualized as the evolution of a dynamic system (Rustichini and Padoa-Schioppa, 2015; Wang, 2002), circuit inhibition sets the system's initial conditions and is thus integral to value comparison. In this account, the evolving decision is essentially captured by the activity of chosen juice cells in OE trials, which reflects a competition between the negative offset set by the value of offer1 (initial condition) and the incoming signal encoding the value of offer2. If so, the intensity of circuit inhibition should be negatively correlated with the order bias.

We tested this prediction as follows. First, we replicated previous findings and confirmed the presence of circuit inhibition in our primary data set (**Fig.4.6A**). Second, we focused on a 300 ms time window starting 250 ms before offer2 onset. For each chosen juice cell, we regressed the firing rate against the normalized offer1 value (see **Methods**). Thus the regression slope c_1 quantified circuit inhibition for individual cells. Across a population of 295 chosen juice cells, mean(c_1) was significantly <0 ($p = 5\ 10^{-6}$, t test; $p = 9\ 10^{-8}$, Wilcoxon test; **Fig.4.6B**). Third, we examined the relation between circuit inhibition (c_1) and the order bias (ε). Confirming the prediction, the two measures were significantly correlated across the population (Spearman r = 0.1, p = 0.02; Pearson r = 0.1, p = 0.02; **Fig.4.6C**). In other words, stronger circuit inhibition (more negative c_1) corresponded to a weaker order bias (smaller ε).

In conclusion, the order bias did not originate before or during valuation. Conversely, analysis of chosen juice cells and chosen value cells indicated that the order bias emerged during value comparison (decision stage).

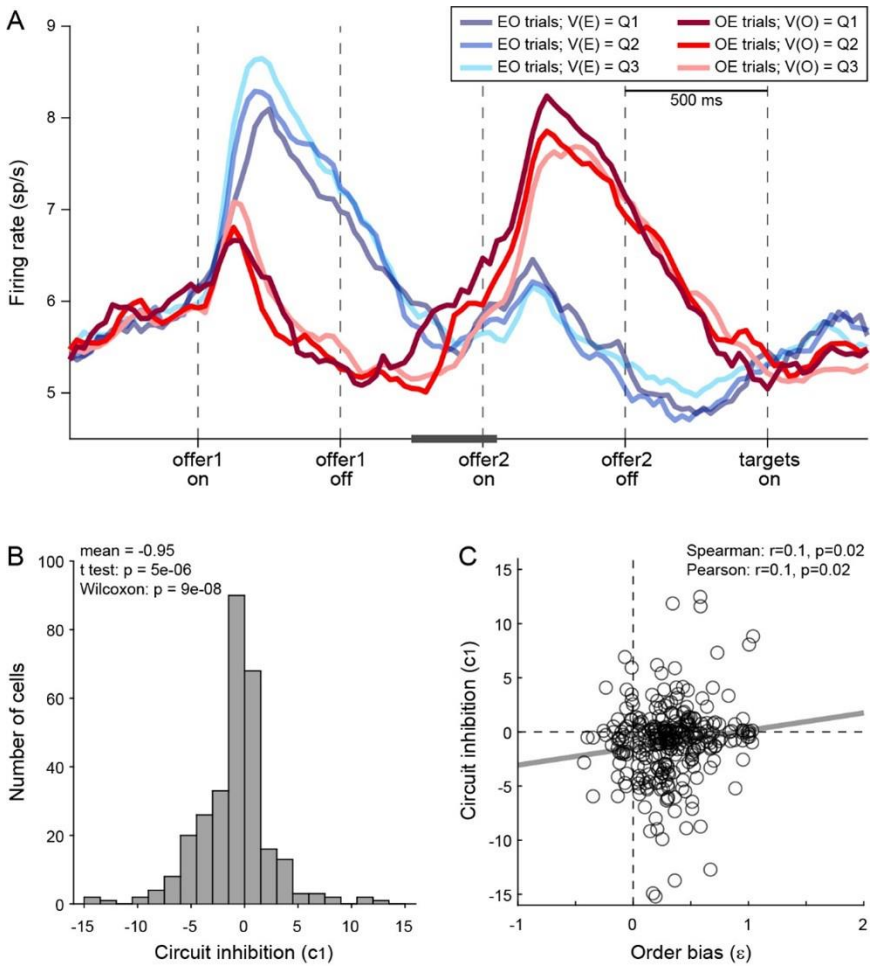

Figure 4.6. Order bias and circuit inhibition. **A.** Circuit inhibition in chosen juice cells (primary data set, N = 160 cells). For each chosen juice cell E and O indicated the encoded juice and the other juice, respectively. We separated EO and OE trials, and divided each group of trials in tertiles based on the value of offer1. For EO trials, this corresponded to V(E); for OE trials, it corresponded to V(O). In this panel, Q1, Q2 and Q3 indicate low, medium and high values of offer1. In OE trials, shortly before offer2, the activity of chosen juice cells was negatively correlated with V(O) – a phenomenon termed circuit inhibition. For a quantitative analysis of circuit inhibition, we focused on 300 ms time window starting 250 ms before offer2 onset (black line). **B.** Circuit inhibition for individual cells (N = 295 cells). For each chosen juice cell, we regressed the firing rate against the normalized V(O) (see **Methods**). The histogram illustrates the distribution of regression slopes (c_1), which quantify circuit inhibition for individual cells.

The effect was statistically significant across the population (mean = -0.95). **C.** Correlation between order bias and circuit inhibition (N = 295 cells). Here the x-axis is the order bias (ε), the y-axis is circuit inhibition (regression slope c_1) and each data point represents one cell. The two measures were significantly correlated across the population. Panel A includes only the primary data set; thus circuit inhibition shown here replicates previous findings (Ballesta and Padoa-Schioppa, 2019). Panels BC include both the primary and the additional data sets (see **Methods**). In panels BC, 47 cells were excluded from the analysis because measures of order bias (ε) or circuit inhibition (c_1) were detected as outliers by the interquartile criterion. Including these cells in the analysis did not substantially alter the results. Statistical tests and exact p values are indicated in panels BC.

4.2.5 The preference bias emerged late in the trial (post-comparison)

When offers were presented sequentially (Task 2), both monkeys showed an additional preference bias that favored juice A and was more pronounced when the relative value of the two juices was larger (**Fig.4.3**). Our last series of analyses focused on the origins of this bias.

First, we inquired whether the preference bias emerged during valuation. If this was the case, one or both of the following should be true: (a) offer value A cells encoded higher values in Task 2 than in Task 1 and/or (b) offer value B cells encoded lower values in Task 2 than in Task 1. Furthermore, these putative effects should increase as a function of the relative value. To test these predictions, we examined the tuning functions of offer value cells. For each cell group (offer value A, offer value B), we pooled neurons with positive and negative encoding. For Task 1, we focused on the post-offer time window; for Task 2, we focused on post-offer1 and post-offer2 time windows, pooling trial types from both windows. Indicating with b_0 and b_1 the tuning intercept and tuning slope (**Eq.4.4**), we computed the difference in intercept $\Delta b_0 = b_{0,Task2} - b_{0,Task1}$ and the difference in slope $\Delta b_1 = b_{1,Task2} - b_{1,Task1}$ for each cell. We then examined the relation between these measures and the relative value ρ across the population, separately for each cell group. Contrary to the prediction, we did not find any correlation between neuronal measures (Δb_0, Δb_1) and the behavioral measure (ρ) for either offer value A or offer value B cells (**Fig.4.S3**). Thus the preference bias did not seem to emerge at the valuation stage.

We next examined chosen value cells. As discussed above, their activity provided a neuronal measure for the relative value ($\rho^{neuronal}$), which reflected the internal subjective values of the juices emerging during value comparison. In principle, $\rho^{neuronal}$ might differ from the relative value derived from choices through the probit regression ($\rho^{behavioral}$) because choices might be

affected by systematic biases originating downstream of value comparison (**Fig.4.1**). In the light of this consideration, we examined the relation between the neuronal measure of relative value in Task 2 ($\rho^{neuronal}_{Task2}$, see **Methods**) and the behavioral measures obtained in the two tasks ($\rho^{behavioral}_{Task1}$, $\rho^{behavioral}_{Task2}$). We envisioned two possible scenarios (**Fig.4.7A**). In scenario 1, the preference bias reflected a difference in values across tasks. In other words, the subjective values of the juices in the two tasks were different and such that the relative value of juice A was higher in Task 2 than in Task 1. If so, $\rho^{neuronal}_{Task2}$ should be statistically indistinguishable from $\rho^{behavioral}_{Task2}$ and systematically larger than $\rho^{behavioral}_{Task1}$. In scenario 2, the subjective values of the juices were the same in both tasks and the preference bias reflected some neuronal process taking place downstream of value comparison. If so, $\rho^{neuronal}_{Task2}$ should be statistically indistinguishable from $\rho^{behavioral}_{Task1}$ and systematically smaller than $\rho^{behavioral}_{Task2}$.

The results of our analysis clearly conformed to scenario 2 (**Fig.4.7B**). For each chosen value cell, we computed $\rho^{neuronal}_{Task1}$ in the post-offer time window and $\rho^{neuronal}_{Task2}$ in the post-offer2 time window. Across the population, the two measures were statistically indistinguishable ($p = 0.3$, t test; not shown). We then regressed $\rho^{neuronal}_{Task2}$ onto $\rho^{behavioral}_{Task1}$. The linear relation between these measures was statistically indistinguishable from identity. Separately, we regressed $\rho^{neuronal}_{Task2}$ onto $\rho^{behavioral}_{Task2}$. In this case, the regression slope was significantly <1 ($p = 0.02$). This result is quite remarkable. It shows that the chosen value represented in the brain in Task 2 was equal to that inferred from choices in Task 1, and significantly different from that inferred from choices in Task 2. This fact implies that the preference bias was costly for the monkey, as it reduced the value obtained on average at the end of each trial.

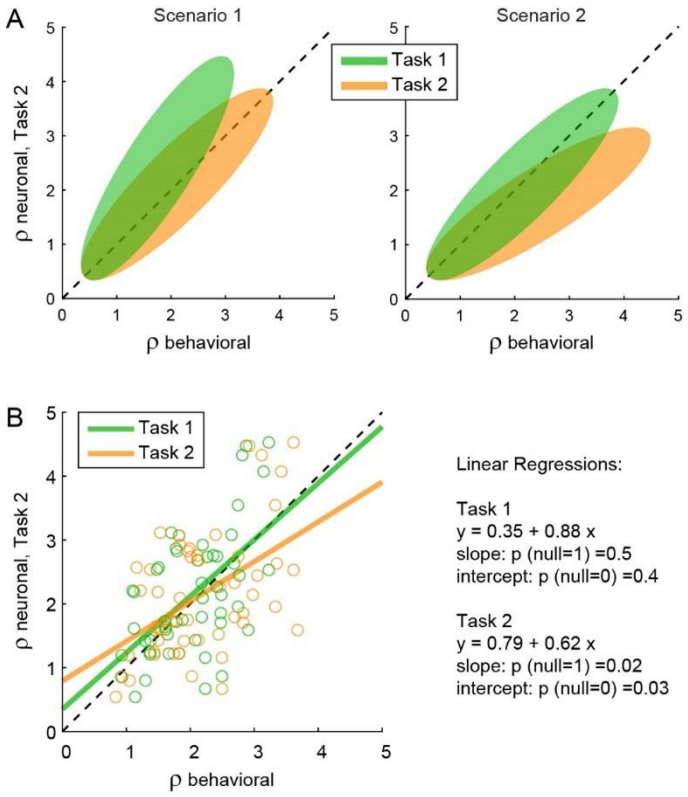

Figure 4.7. The preference bias does not reflect differences in the activity of chosen value cells. **A.** Hypothetical scenarios. The two panels represent in cartoon format two possible scenarios envisioned at the outset of this analysis. In both panels, the x-axis represents behavioral measures from either Task 1 (green) or Task 2 (yellow); the y-axis represents the neuronal measure from Task 2. In scenario 1, the animal assigned higher relative value to juice A in Task 2. Thus, neuronal measures of relative value derived from the activity of chosen value cells in Task 2 ($\rho^{neuronal}_{Task2}$) would align with behavioral measures from the same task ($\rho^{behavioral}_{Task2}$) and be systematically higher than behavioral measures from Task 1 ($\rho^{behavioral}_{Task1}$). In scenario 2, the animal assigned the same relative values to the juices in both tasks. Thus, neuronal measures of relative value in Task 2 ($\rho^{neuronal}_{Task2}$) would be systematically lower than behavioral measures from the same task ($\rho^{behavioral}_{Task2}$) and would align with behavioral measures from Task 1 ($\rho^{behavioral}_{Task1}$). **B.** Empirical results (N = 52 cells). Neuronal measures derived from Task 2 ($\rho^{neuronal}_{Task2}$) are plotted against behavioral measures obtained in Task 1 ($\rho^{behavioral}_{Task1}$, green) or Task 2 ($\rho^{behavioral}_{Task2}$, yellow. Lines are from linear regressions. In essence, $\rho^{neuronal}_{Task2}$ was statistically

indistinguishable from $\rho^{behavioral}_{Task1}$ and systematically lower than $\rho^{behavioral}_{Task2}$. Details on the statistics and exact p values are indicated in the figure. The analysis was restricted to 52 cells that had significant θ_{1A}, θ_{1B}, θ_{2A} and θ_{2B}. For this analysis, $\rho^{neuronal}_{Task2}$ was taken as equal to $\rho^{neuronal}_{offer2}$ (**Eq.4.10**). Other definitions provided similar results (data not shown).

In summary, the preference bias did not reflect differences in the values assigned to individual offers (offer values). Furthermore, insofar as the activity of chosen value cells reflects the decision process (**Fig.4.1**), the preference bias did not seem to emerge during value comparison. So how can one make sense of this behavioral phenomenon? At the cognitive level, the preference bias might be interpreted as due to the higher demands of Task 2. When the two saccade targets appeared on the monitor, information about values was no longer on display (**Fig.4.2B**). If at that point the animal had not finalized its decision, or if it had failed to retain in working memory the decision outcome, the animal might have selected the target associated with the better juice (juice A). Such bias would have been especially strong when the value difference between the two juices was large. In this view, the preference bias would reflect a "second thought" occurring after value comparison, in some trials.

To test this intuition, we turned to the activity of chosen juice cells. As noted above, in Task 2, the evolving decision was captured by the activity of these neurons recorded in OE trials immediately before and after offer2 onset (**Fig.4.8A**). More specifically, the state of the ongoing decision was captured by the distance between the two traces corresponding to the two possible choice outcomes (E chosen, O chosen). For any neuron, we quantified this distance with an ROC analysis, which provided a choice probability (CP). In essence, CP can be interpreted as the probability with which an ideal observed may guess the eventual choice outcome based on the activity of the cell. For each chosen juice cell, we computed the CP at different times in the trial. Across the population, mean(CP) exceeded chance level starting shortly before offer2, consistent with the above discussion on circuit inhibition. We then proceeded to investigate the origins of the preference bias.

We reasoned that, at the net of noise in measurements and cell-to-cell variability, CPs ultimately quantify the animal's commitment to any choice outcome. If the preference bias emerged late in the trial – perhaps after target presentation, if animals had not previously finalized their decision – the intensity of the preference bias should be inversely related to the animals' commitment to any choice outcome measured earlier in the trial. In other words, there should be a negative correlation between the preference bias and CPs computed at the time when decisions normally take place (shortly before or after offer2 onset). Our analyses supported this prediction. To quantify the preference bias intensity independent of the juice pair, we defined the preference bias index PBI = 2 ($\rho_{Task2} - \rho_{Task1}$) / ($\rho_{Task2} + \rho_{Task1}$). We then focused on four 250 ms time windows before offer1 (control window), before and after offer2 onset, and before juice delivery (**Fig.4.8B-E**). Confirming our predictions, CP and PBI were significantly anti-correlated immediately before and during offer2 presentation, but not in the control time window or late in the trial (**Fig.4.8F-I**).

In conclusion, our results indicated that the preference bias did not emerge during valuation or during value comparison. Indeed, the preference bias effectively reduced the value monkeys obtained on average on any given trial. Furthermore, the analysis of chosen juice cells suggests that the preference bias emerged late in the trial, as a "second thought" process that guided choices when decisions were not finalized based on offer values alone.

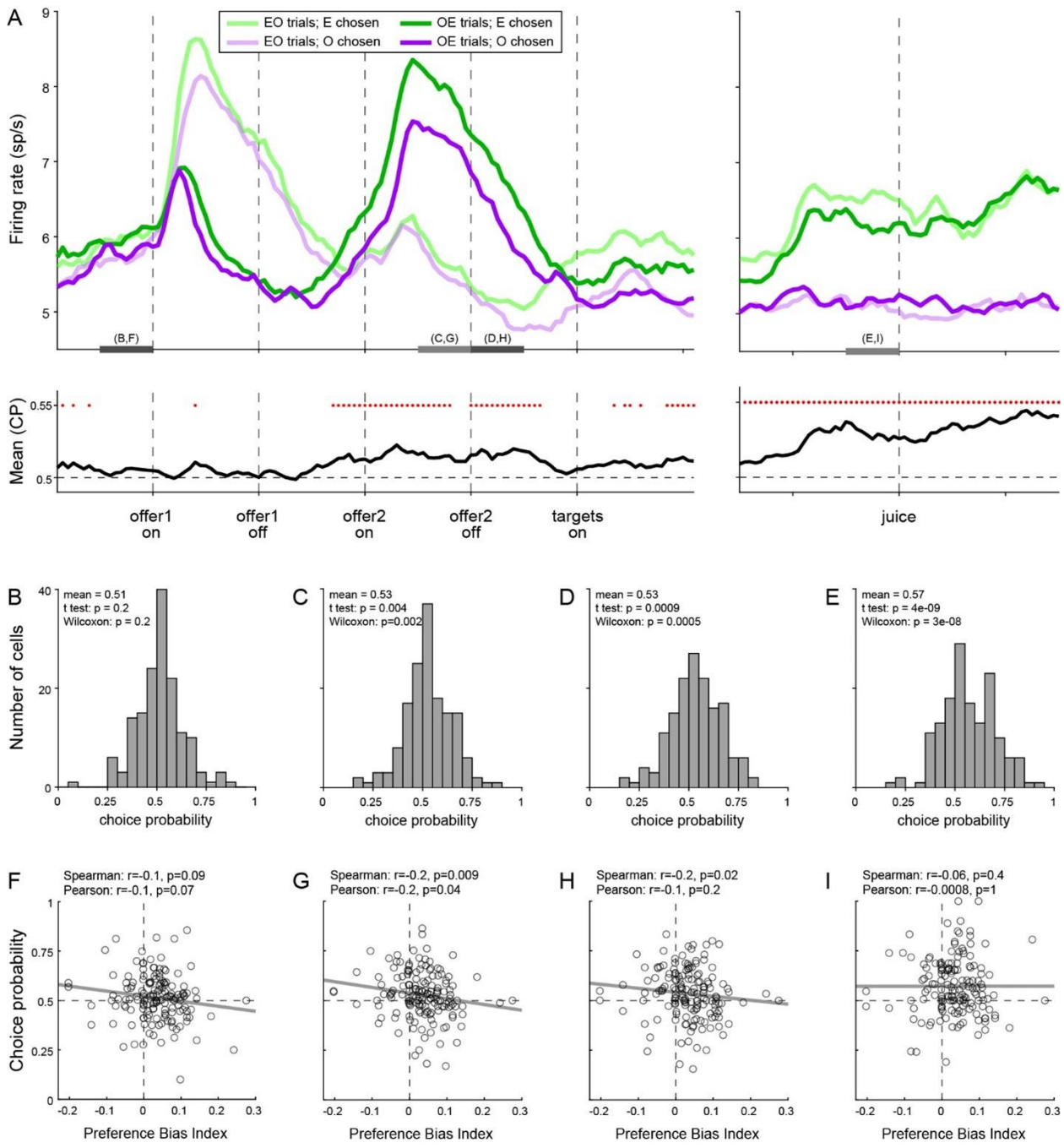

Figure 4.8. Preference bias and choice probability in *chosen juice* cells. **A.** Profiles of activity and choice probability (N = 160 cells). On the top, separate traces are activity profiles for EO trials (dark colors) and OE trials (light colors), separately for E chosen (blue) and O chosen. On the bottom the trace is the mean(CP) computed for OE trials in 100 ms sliding time windows (25 ms steps). Red dots indicate that

mean(CP) was significantly >0.5 ($p<0.001$; t test). Value comparison typically takes place shortly after the onset of offer2. **B-E.** Distribution of CP in four 250 ms time windows. The time windows used for this analysis are indicated in panel A. **F-I.** Correlation between CP and preference bias index. Each panel corresponds to the histogram immediately above it. CPs are plotted against the preference bias index (PBI), which quantifies the preference bias independently of the juice types. Each symbol represents one cell and the line is from a linear regression. CP and PBI were negatively correlated immediately before and after offer2 onset, but not later in the trial. This pattern suggests that the preference bias emerged late in the trial, when decisions were not finalized shortly after offer2 presentation. In panel B-I, 6 cells were excluded because the Matlab function *perfcurve.m* failed to converge.

4.3 Discussion

4.3.1 Behavioral values, neuronal values and the origins of choice biases

Early economists proposed that choices between goods entail the computation and comparison of subjective values. However, the concept of value is somewhat slippery, because values relevant to choices cannot be measured behaviorally other than from choices themselves. This circularity problem hunted generations of scholars, dominating academic debates in the 19th and 20th century. In the end, neoclassic economic theory came to reject (cardinal) values and to rely only on (ordinal) preferences (Niehans, 1990; Samuelson, 1947). In other words, standard economics is agnostic as to whether subjective values are computed at all. The construction of standard economic theory was a historic success, but it came at a cost: the theory cannot explain a variety of biases observed in human choices. In this perspective, neuroscience results showing that neuronal activity in multiple brain regions is linearly related to values defined behaviorally (Bartra et al., 2013; Padoa-Schioppa, 2011; Schultz, 2015), constitute a significant breakthrough. They validate the concept of value and effectively break the circularity surrounding it. Indeed, a neuronal population whose activity is reliably correlated with values measured from choices (behavioral values) may be used to derive independent measures of subjective values (neuronal values). In most circumstances, neuronal values and behavioral values should be (and are) indistinguishable. However, in specific choice contexts, the two measures might differ somewhat. When observed, such discrepancies indicate that choices are partly determined by processes that escape the maximization of offer values. If so, suitable analyses of neuronal activity may be used to assess the origins of particular choice biases.

These considerations motivated the analyses conducted in this study. In our experiments, monkeys chose between two juices offered simultaneously or sequentially. Choices under sequential offers were less accurate, biased in favor of the second offer (order bias), and biased in favor of the preferred juice (preference bias) (Shi et al., 2021). Earlier work had identified in OFC three groups of neurons encoding individual offer values, the chosen juice and the chosen value. Furthermore, experimental findings and computational models suggested that these cell groups constitute the building blocks of a decision circuit (Padoa-Schioppa and Conen, 2017). In this view, offer value cells provide the primary input to a circuit formed by chosen juice cells and chosen value cells, where decisions are formed. Different cell groups in OFC may thus be associated with different computational stages: offer value cells instantiate the valuation stage; chosen value cells reflect values possibly modified by the decision process; and chosen juice cells capture the evolving commitment to a particular choice outcome. In this framework, we examined the activity of each cell group in relation to each behavioral phenomenon.

Our results may be summarized as follows. (1) Other things equal, neuronal signals encoding the offer values were weaker (smaller activity range) under sequential offers than under simultaneous offers. The reason for this discrepancy is unclear, but this neuronal effect was correlated with the difference in choice accuracy measured at the behavioral level. In other words, the drop in choice accuracy observed under sequential offers originated, at least partly, at the valuation stage. (2) The order bias did not correlate with any measure in the activity of offer value cells. However, the order bias was negatively correlated with circuit inhibition in chosen juice cells – a phenomenon seen as key to value comparison (Ballesta and Padoa-Schioppa, 2019). Furthermore, fluctuations in the order bias correlated with fluctuations in the neuronal measure of relative value derived from chosen value cells. These findings indicate that the order

bias emerged during value comparison. (3) The preference bias did not have any correlate in the activity of offer value cells or chosen value cells. Moreover, the preference bias was inversely related to a measure derived from chosen juice cells and quantifying the degree to which the decision was finalized in the "normal" decision window (i.e., following presentation of the second offer). These findings indicate that the preference bias emerged late in the trial, after value comparison.

Two findings are particularly relevant to the distinction between behavioral values and neuronal values. (1) The activity of offer value cells did not present any difference associated with the presentation order or with the juice preference. (2) Relative value derived from chosen value cells under sequential offers differed significantly from behavioral measures obtained in the same task, and were indistinguishable from behavioral measures obtained in the other task (simultaneous offers). Thus the order bias and the preference bias highlighted significant differences between neuronal and behavioral measures of value. These observations imply that the order bias and the preference bias emerged downstream of valuation. Importantly, they also imply that the two choice biases imposed a cost to the animals, in the sense that they reduced the (neuronal) value obtained on average in any given trial. Notably, it would be impossible to draw such conclusion based on choices alone.

While this is the first study to investigate the origins of choice biases building on the distinction between behavioral values and neuronal values, some of our results are not unprecedented. Earlier work showed that human and animal choices are affected by a bias favoring, on any given trial, the same good chosen in the previous trial (Alos-Ferrer et al., 2016; Goodwin, 1977; Padoa-Schioppa, 2013; Schoemann and Scherbaum, 2019; Senftleben et al., 2021). The origins

of this phenomenon, termed choice hysteresis, are hard to pinpoint based on behavioral evidence alone. However, previous analysis of neuronal activity in OFC revealed that choice hysteresis is not reflected in the encoding of offer values (Padoa-Schioppa, 2013). Conversely, choice hysteresis correlates with fluctuations in the baseline activity of chosen juice cells, which is partly influenced by the previous trial's outcome. Thus, similar to the order bias, choice hysteresis appears to emerge at the decision stage.

4.3.2 Conclusion

The past two decades have witnessed a lively interest for the neural underpinnings of choice behavior. In this effort, a significant breakthrough came from the adoption of behavioral paradigms inspired by the economics literature, in which subjective values derived from choices are used to interpret neural activity (Padoa-Schioppa, 2011). Without renouncing this approach, here we took a further step, recognizing that the decision process might sometimes fall short of selecting the maximum offer value, and that choices might sometimes be affected by processes taking place downstream of value comparison. Equivalently, behavioral values and neuronal values might sometimes differ. These ideas may appear uncontroversial, but they have deep implications for economic theory and beyond. Looking forward, the framework developed here, in which the computation and comparison of offer values are central, but choices can also be affected by other processes accessible through neuronal measures, might help unravel other choice biases.

4.4 Methods

All the experimental procedures adhered to the NIH Guide for the Care and Use of Laboratory Animals and were approved by the Institutional Animal Care and Use Committee (IACUC) at Washington University.

4.4.1 Animal subjects, choice tasks and neuronal recordings

This study presents new analyses of published data. Experimental procedures for surgery, behavioral control and neuronal recordings have been described in detail (Shi et al., 2021). Briefly, two male monkeys (Macaca mulatta; monkey J, 10.0 kg, 8 years old; monkey G, 9.1 kg, 9 years old) participated in the study. Under general anesthesia, we implanted on each animal a head restraining device and an oval chamber (axes 50×30 mm) allowing bilateral access to OFC. During the experiments, monkeys sat in an electrically insulated environment with their head fixed and a computer monitor placed at 57 cm distance. The gaze direction was monitored at 1 kHz using an infrared video camera (Eyelink, SR Research). Behavioral tasks were controlled through custom written software (https://monkeylogic.nimh.nih.gov) (Hwang et al., 2019) based on Matlab (v2016a; MathWorks Inc).

In each session, the animal chose between two juices labeled A and B (A preferred) offered in variable amounts. Trials with two choice tasks, referred to as Task 1 and Task 2, were pseudo-randomly interleaved. In both tasks, offers were represented by sets of colored squares displayed on the monitor. For each offer, the color indicated the juice type and the number of squares indicated the quantity. Each trial began with the animal fixating a large dot. After 0.5 s, the initial fixation point changed to a small dot or a small cross; the new fixation point cued the

animal to the choice task used in that trial. In Task 1 (**Fig.4.2A**), cue fixation (0.5 s) was followed by the simultaneous presentation of the two offers. After a randomly variable delay (1-1.5 s), the center fixation point disappeared and two saccade targets appeared near the offers (go signal). The animal indicated its choice with an eye movement. It maintained peripheral fixation for 0.75 s, after which the chosen juice was delivered. In Task 2 (**Fig.4.2B**), cue fixation (0.5 s) was followed by the presentation of one offer (0.5 s), an inter-offer delay (0.5 s), presentation of the other offer (0.5 s), and a wait period (0.5 s). Two colored saccade targets then appeared on the two sides of the fixation point. After a randomly variable delay (0.5-1 s), the center fixation point disappeared (go signal). The animal indicated its choice with a saccade, maintained peripheral fixation for 0.75 s, after which the chosen juice was delivered. Central and peripheral fixation were imposed within 4-6 and 5-7 degrees of visual angle, respectively. Aside from the initial cue, the choice tasks were nearly identical to those used in previous studies (Ballesta and Padoa-Schioppa, 2019; Padoa-Schioppa and Assad, 2006).

For any given trial, q_A and q_B indicate the quantities of juices A and B offered to the animal, respectively. An "offer type" was defined by two quantities [q_A q_B]. On any given session, we used the same juices and the same sets of offer types for the two tasks. For Task 1, the spatial configuration of the offers varied randomly from trial to trial. For Task 2, the presentation order varied pseudo-randomly and was counterbalanced across trials for any offer type. The terms "offer1" and "offer2" indicated, respectively, the first and second offer, independently of the juice type and amount. Trials in which juice A was offered first and trials in which juice B was offered first were referred as "AB trials" and "BA trials", respectively. The spatial location (left/right) of saccade targets varied randomly. The juice volume corresponding to one square (quantum) was set equal for the two choice tasks and remained constant within each session. It

varied across sessions between 70 and 100 µl for both monkeys. The association between the initial cue (small dot, small cross) and the choice task varied across sessions in blocks. Across sessions, we used 12 different juices (and colors) and 45 different juice pairs. Based on a power analysis, in most sessions the number of trials for Task 2 was set equal to 1.5 times that for Task 1.

Neuronal recordings were guided by structural MRI scans (1 mm sections) obtained before and after surgery and targeted area 13m (Ongur and Price, 2000). We recorded from both hemispheres in both monkeys. Tungsten single electrodes (100 µm shank diameter; FHC) were advanced remotely using a custom-built motorized micro-drive. Typically, one motor advanced two electrodes placed 1 mm apart, and 1-2 such pairs of electrodes were advanced unilaterally or bilaterally in each session. Neural signals were amplified (gain: 10,000) band-pass filtered (300 Hz - 6 kHz; Lynx 8, Neuralynx), digitized (frequency: 40 kHz) and saved to disk (Power 1401, Cambridge Electronic Design). Spike sorting was performed off-line (Spike2, v6, Cambridge Electronic Design). Only cells that appeared well isolated and stable throughout the session were included in the analysis.

4.4.2 Preliminary analyses

The present analyses build on the results of a previous study showing that both choice tasks engage the same groups of neurons in OFC (Shi et al., 2021). Here we briefly summarize those findings.

The original data set included 1,526 neurons (672 from monkey J, 854 from monkey G) recorded in 306 sessions (115 from monkey J, 191 from monkey G). In each session, choice patterns were

analyzed using probit regressions as described in the main text (**Eq.4.1** and **Eq.4.2**). For Task 1 (simultaneous offers), the probit fit provided measures for the relative value ρ_{Task1} and the sigmoid steepness η_{Task1}. For Task 2 (sequential offers), the probit fit provided measures for the relative value ρ_{Task2}, the sigmoid steepness η_{Task2} and the order bias ε. For each neuron, trials from Task 1 and Task 2 were first analyzed separately using the procedures developed in previous studies (Ballesta and Padoa-Schioppa, 2019; Padoa-Schioppa and Assad, 2006). For Task 1, we defined four time windows: post-offer (0.5 s after offer onset), late-delay (0.5-1 s after offer onset), pre-juice (0.5 s before juice onset) and post-juice (0.5 s after juice onset). A "trial type" was defined by two offered quantities and a choice. For Task 2, we defined three time windows: post-offer1 (0.5 s after offer1 onset), post-offer2 (0.5 s after offer2 onset) and post-juice (0.5 s after juice onset). A "trial type" was defined by two offered quantities, their order and a choice. For each task, each trial type and each time window, we averaged spike counts across trials. A "neuronal response" was defined as the firing rate of one cell in one time window as a function of the trial type. Neuronal responses in each task were submitted to an ANOVA (factor: trial type). Neurons passing the $p<0.01$ criterion in ≥ 1 time window in either task were identified as "task-related" and included in subsequent analyses.

Following earlier work (Padoa-Schioppa, 2013), neurons in Task 1 were classified in one of four groups offer value A, offer value B, chosen juice or chosen value. Each variable could be encoded with positive or negative sign, leading to a total of 8 cell groups. Each neuronal response was regressed against each of the four variables. If the regression slope b_1 differed significantly from zero ($p<0.05$), the variable was said to "explain" the response. In this case, we set the signed R^2 as $sR^2 = \text{sign}(b_1)\, R^2$; if the variable did not explain the response, we set $sR^2 = 0$. After repeating the operation for each time window, we computed for each cell the sum(sR^2)

across time windows. Neurons explained by at least one variable in one time window, such that $\text{sum}(sR^2) \neq 0$, were said to be tuned; other neurons were labeled "untuned". Tuned cells were assigned to the variable and sign providing the maximum $|\text{sum}(sR^2)|$, where $|\cdot|$ indicates the absolute value. Thus indicating with "+" and "–" the sign of the encoding, each neuron was classified in one of 9 groups: offer value A+, offer value A–, offer value B+, offer value B–, chosen juice A, chosen juice B, chosen value+, chosen value– and untuned.

Neuronal classification in Task 2 followed the procedures described by Ballesta and Padoa-Schioppa (2019). Under sequential offers, neuronal responses in OFC were found to encode different variables defined in relation to the presentation order (AB or BA). Specifically, the vast majority of responses were explained by one of 11 variables including one binary variable capturing the presentation order (AB | BA), six variables representing individual offer values (offer value A | AB, offer value A | BA, offer value B | AB, offer value B | BA, offer value 1, and offer value 2), three variables capturing variants of the chosen value (chosen value, chosen value A, chosen value B) and a binary variable representing the binary choice outcome (chosen juice). Each of these variables could be encoded with a positive or negative sign. Most neurons encoded different variables in different time windows. In principle, considering 11 variables, 2 signs of the encoding and 3 time windows, neurons might present a very large number of variable patterns across time windows. However, the vast majority of neurons presented one of 8 patterns referred to as "sequences". Classification proceeded as follows. For each cell and each time window, we regressed the neuronal response against each of the variables predicted by each sequence. If the regression slope b_1 differed significantly from zero ($p<0.05$), the variable was said to explain the response and we set the signed R^2 as $sR^2 = \text{sign}(b_1)\ R^2$; if the variable did not explain the response, we set $sR^2 = 0$. After repeating the operation for each time window, we

computed for each cell the sum(sR^2) across time windows for each of the 8 sequences. Neurons such that sum(sR^2) ≠ 0 for at least one sequence were said to be tuned; other neurons were untuned. Tuned cells were assigned to the sequence that provided the maximum |sum(sR^2)|. As a result, each neuron was classified in one of 9 groups: seq #1, seq #2, seq #3, seq #4, seq #5, seq #6, seq #7, seq #8 and untuned (**Table 4.S1**).

The results of the two classifications procedures were compared using analyses for categorical data. In essence, we found a strong correspondence between the cell classes identified in the two choice tasks (Shi et al., 2021). Hence, we may refer to the different groups of cells using the standard nomenclature – offer value, chosen juice and chosen value – independently of the choice task. Based on this result, we proceeded with a comprehensive classification based on the activity recorded in both choice tasks. For each task-related cell, we calculated the sum(sR^2) for the eight variables in Task 1 (sum(sR^2)$_{Task1}$) and eight sequences in Task 2 (sum(sR^2)$_{Task2}$) as described above. We then added the corresponding sum(sR^2)$_{Task1}$ and sum(sR^2)$_{Task2}$ to obtain the final sum(sR^2)$_{final}$. Neurons such that sum(sR^2)$_{final}$ ≠ 0 for at least one class were said to be tuned; other neurons were untuned. Tuned cells were assigned to the cell class that provided the maximum |sum(sR^2)$_{final}$|.

4.4.3 Data sets

In some sessions, one or both choice patterns presented complete or quasi-complete separation – i.e., the animal split choices for <2 offer types in Task 1 and/or in Task 2. In these cases, the probit regression did not converge, the resulting steepness η was high and unstable, and the relative value was (often) not well defined. This issue affected the classification analyses described above only marginally, but for the present study it was critical that behavioral

measures be accurate and precise. We thus restricted our analyses to stable sessions by imposing an interquartile criterion on the sigmoid steepness (Tukey, 1977). Defining IQR as the interquartile range, values below the first quartile minus 1.5*IQR or above the third quartile plus 1.5*IQR were identified as outliers and excluded. Thus our entire data set included 1,204 neurons (577 from monkey J, 627 from monkey G) recorded in 241 sessions (101 from monkey J, 140 from monkey G). In this population, the classification procedures identified 183 offer value cells, 160 chosen juice cells and 174 chosen value cells. These neurons constitute the primary data set for this study.

Most of our analyses compared choices and neuronal activity across tasks and were restricted to the primary data set. However, some analyses included only trials from Task 2 and quantified the effects due to the presentation order (AB vs. BA). In these analyses we included an additional data set recorded previously from the same two animals performing only Task 2 (Ballesta and Padoa-Schioppa, 2019). All the procedures for behavioral control and neuronal recording were essentially identical to those described above. Furthermore, behavioral analyses and inclusion criteria were identical to those used for the primary data set. The resulting data set included 1,205 neurons (414 from monkey J, 791 from monkey G) recorded in 196 sessions (51 from monkey J, 145 from monkey G). In this population, the classification procedures identified 243 offer value cells, 182 chosen juice cells and 187 chosen value cells. We refer to these neurons as the additional data set. Importantly, the order bias was also observed in these sessions (Ballesta and Padoa-Schioppa, 2019).

The interquartile criterion was also used to identify outliers in all the analyses conducted throughout this study. In practice, this criterion became relevant only for the analyses shown in **Fig.4.6** and **Fig.4.S2**, as indicated in the respective figure legends.

4.4.4 Comparing tuning functions across choice tasks

Several analyses compared the tuning functions recorded in the two tasks (**Fig.4.4**, **Fig.4.S1-3**). Tuning functions were defined by the linear regression of the firing rate r onto the encoded variable S:

$$r = b_0 + b_1 S \tag{4.4}$$

Regression coefficients b_0 and b_1 were referred to as tuning intercept and tuning slope, respectively. Positive and negative encoding corresponded to $b_1>0$ and $b_1<0$, respectively. We also defined the mean activity and the activity range as follows. Indicating with $[S_{min}, S_{max}]$ the interval of variability for S, $\Delta S = S_{max} - S_{min}$ was the range of S. The mean activity was defined as $r_{mean} = b_0 + b_1 (S_{max}+S_{min})/2$. The activity range was defined as $\Delta r = |b_1 \Delta S|$, where $|\cdot|$ indicates the absolute value.

For any neuronal response, the tuning was considered significant if b_1 differed significantly from zero ($p<0.05$) and if the sign of the encoding was consistent with the cell class (e.g., $b_1>0$ for offer value A + cells). All the analyses comparing tuning functions across tasks were restricted to neuronal responses with significant tuning.

4.4.5 Neuronal measures of relative value

Several analyses relied on neuronal measures for the relative value of the juices ($\rho^{neuronal}$) derived from the activity of chosen value cells. In Task 1, these neurons encode the chosen value independently of the juice type. For each neuronal response, we performed a bilinear regression:

$$r = \theta_0 + \theta_A \, q_A \, \delta_{choice,A} + \theta_B \, q_B \, \delta_{choice,B} \quad (4.5)$$

where θ_0, θ_A and θ_B were the regression coefficients, $\delta_{choice,J} = 1$ if the animal chose juice J and 0 otherwise, and J = A or B. If the response encodes the chosen value, θ_A should be proportional to the value of a quantum of juice A (uA), θ_B should be proportional to the value of a quantum of juice B (uB), and the ratio θ_A/θ_B should equal the value ratio – i.e., the relative value of the two juices. We thus defined

$$\rho^{neuronal} = \theta_A / \theta_B \quad (4.6)$$

Previous studies showed that this measure is statistically indistinguishable from the behavioral measure $\rho^{behavioral}$ derived from the probit analysis of choice patterns (Padoa-Schioppa and Assad, 2006).

In Task 2, in the post-offer1 and post-offer2 time windows, chosen value cells encoded the value of the current offer, independent of the juice type (**Table 4.S1**). For each neuron, we thus performed a bi-linear regression for each of the two time windows:

$$r_1 = \theta_{10} + \theta_{1A} \, q_A \, \delta_{order,AB} + \theta_{1B} \, q_B \, \delta_{order,BA} \quad (4.7)$$

$$r_2 = \theta_{20} + \theta_{2A} \, q_A \, \delta_{order,BA} + \theta_{2B} \, q_B \, \delta_{order,AB} \quad (4.8)$$

where r_1 and r_2 were their responses recorded in the post-offer1 and post-offer2 time windows, respectively, and θ_{10}, θ_{1A}, θ_{1B}, θ_{20}, θ_{2A} and θ_{2B} were regression coefficients. These coefficients provided four neuronal measures of relative value:

$$\rho^{neuronal}_{offer1} = \theta_{1A} / \theta_{1B} \quad (4.9)$$

$$\rho^{neuronal}_{offer2} = \theta_{2A} / \theta_{2B} \quad (4.10)$$

$$\rho^{neuronal}_{AB} = \theta_{1A} / \theta_{2B} \quad (4.11)$$

$$\rho^{neuronal}_{BA} = \theta_{2A} / \theta_{1B} \quad (4.12)$$

In essence, these four measures corresponded to the two time windows (post-offer1 and post-offer2) and to the two presentation orders (AB and BA). Importantly, all these measures were computed conditioned on θ_{1A}, θ_{1B}, θ_{2A} and θ_{2B} differing significantly from zero ($p<0.05$). The analyses illustrated in **Fig.4.5** and **Fig.4.7** were restricted to neurons satisfying this criterion.

In terms of notation, we often omit the superscript in $\rho^{behavioral}$ and we indicate behavioral measures simply as ρ (with the relevant subscripts). We use the superscript "behavioral" only when we explicitly compare behavioral and neuronal measures, for clarity. In contrast, for neuronal measures of relative value we always use the superscript "neuronal".

4.4.6 Activity profiles of chosen juice cells

To conduct population analyses, we pooled all chosen juice cells. The juice eliciting higher firing rates was labeled "E" (encoded) and other juice was labeled "O". In Task 2, we thus referred to EO trials and OE trials, depending on the presentation order.

To illustrate the activity profiles of chosen juice cells in Task 2, we aligned spike trains at offer1 and, separately, at juice delivery. For each trial, the spike train was smoothed using a kernel that mimicked the post-synaptic potential by exerting influence only forward in time (decay time constant = 20 ms) (So and Stuphorn, 2010). In **Fig.4.6A** and **Fig.4.8A** we used moving averages of 100 ms with 25 ms steps for display purposes.

Under sequential offers, chosen juice cells encode different variables in different time windows (see **Table 4.S1**). During offer1 and offer2 presentation, these cells encode in a binary way the juice type currently on display. Later, as the decision develops, these neurons gradually come to encode the binary choice outcome (i.e., the chosen juice). We previously showed that the activity of these neurons recorded in OE trials shortly before offer2 is inversely related to the value of offer1 (Ballesta and Padoa-Schioppa, 2019). This phenomenon, termed circuit inhibition, resembles the setting of a dynamic system's initial conditions and is regarded as an integral part of the decision process (Ballesta and Padoa-Schioppa, 2019).

For a quantitative analysis of circuit inhibition, we focused on a 300 ms time window starting 250 ms before offer2 onset. We excluded forced choice trials, for which one of the two offers was null. For each neuron, we examined OE trials and we regressed the firing rates against the normalized value of offer1:

$$r = c_0 + c_1 V(O)/\Delta V_O \qquad (4.13)$$

where ΔV_O was the value range for juice O. The normalization allowed to pool neurons recorded with different value ranges. The regression slope c_1 quantified circuit inhibition for individual cells, and we studied this parameter at the population level.

The activity of chosen juice cells in OE trials captures the momentary state of the decision and thus the evolving commitment to a particular choice outcome. To quantify the momentary decision state, we conducted a receiver operating characteristic (ROC) analysis (Green and Swets, 1966) on the activity recorded during OE trials. This analysis was conducted on raw spike counts, without kernel smoothing, time averaging or baseline correction. We restricted the analysis to offer types for which the animal split choices between the two juices and we excluded trial types with <2 trials. For each offer type, we divided trials depending on the chosen juice (E or O) and we compared the two distributions. The ROC analysis provided an area under the curve (AUC). For each neuron, we averaged the AUC across offer types to obtain the overall choice probability (CP) (Kang and Maunsell, 2012). The ROC analysis was performed in 100 ms time windows shifted by 25 ms. We also conducted the same analysis on four 250 ms time windows, namely pre-offer1 (–250 to 0 ms from offer1 onset), late offer2 (–250 to 0 ms from offer1 offset), early wait (0 ms to 250 ms after offer2 offset) and pre-juice (–250 to 0 ms before juice delivery) (**Fig.4.8**).

4.5 Supplementary figures

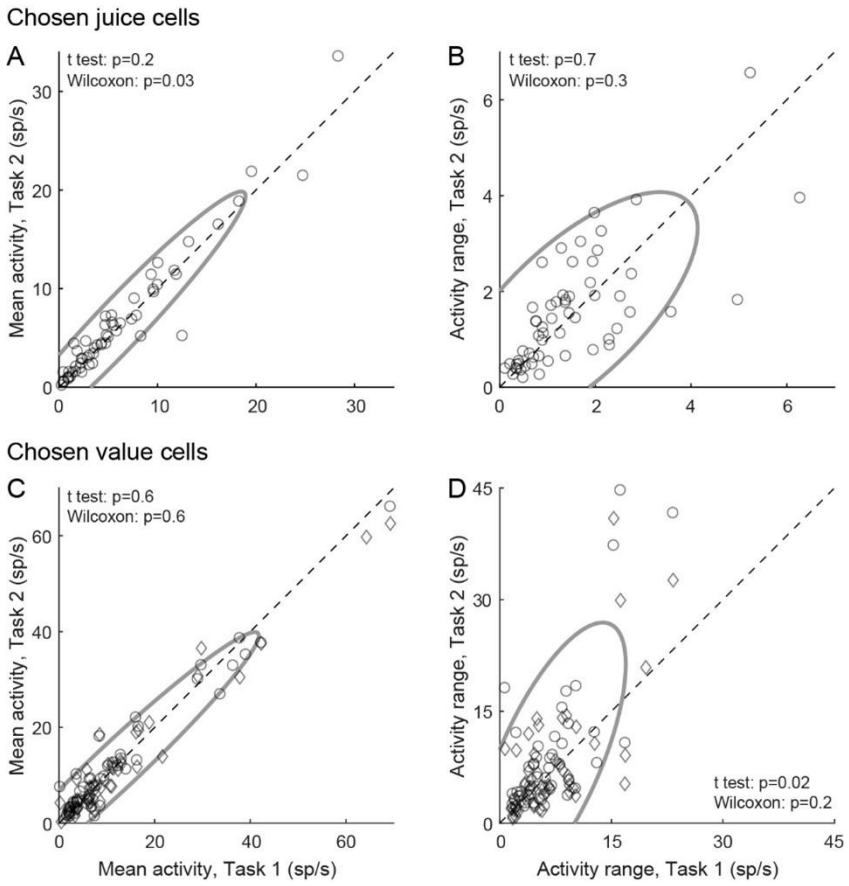

Figure 4.S1. Comparing tuning functions across choice tasks. **AB.** Chosen juice cells (N = 58). Same format as in **Fig.4.4AB**. For each cell, we examined the same time window (post-juice) in both tasks. Both the mean activity and the activity range were statistically indistinguishable across choice tasks. **CD.** Chosen value cells (N = 104). For each cell, we examined one time window (post-offer) in Task 1 and two time windows (post-offer1 and post-offer2) in Task 2. Both the mean activity and the activity range were statistically indistinguishable across tasks. In panels B-G, legends report the results of statistical tests. For both cell groups, fluctuations in activity range were not correlated with fluctuations in choice variability across the population (in both analyses, $|r| < 0.1$, $p > 0.4$; not shown). Only cells presenting significant tuning in the relevant time windows were included in each panel (see **Methods**).

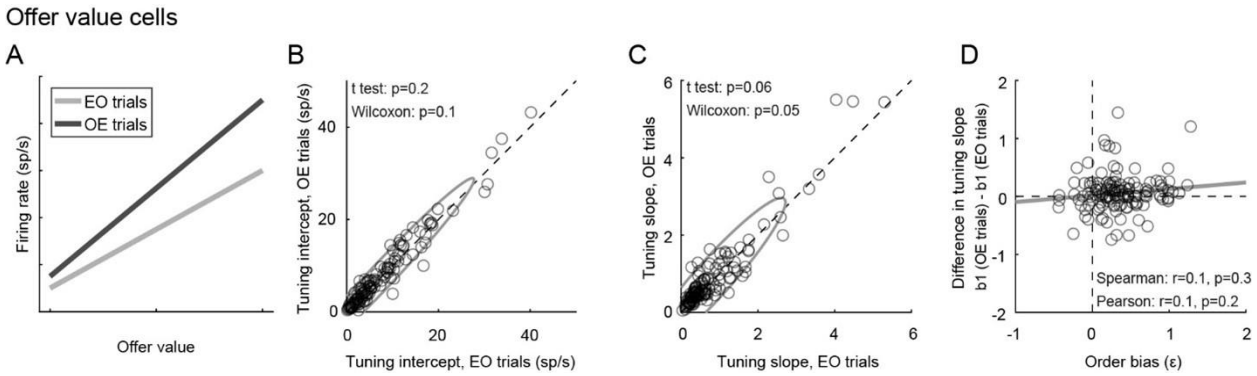

Figure 4.S2. The order bias does not reflect differences in the tuning of offer value cells. **A.** Rationale for the analysis. The two lines represent in cartoon format the hypothetical tuning functions of an offer value cell in the post-offer1 time window (EO trials) and in the post-offer2 time window (OE trials). The order bias would be explained if offer value cells encoded, other things equal, higher values in OE trials than in EO trials. This would be the case if the tuning intercept and/or the tuning slope were higher in OE trials, as depicted here. **B.** Comparison of tuning intercepts. X- and y- axes represent the tuning intercept measured in post-offer1 (EO trials) and post-offer2 (OE trials) time windows, respectively. Each data point represents one cell. The two measures were statistically indistinguishable across the population. **C.** Comparison of tuning slopes. Same format as panel B. The two measures were statistically indistinguishable across the population. **D.** Lack of correlation between differences in tuning slope and order bias. Across the population, we did not find any correlation between the difference in tuning slope (y-axis) and the order bias. Exact p values are indicated in each panel. For this figure, we pooled neurons associated with A and B, and neurons with positive and negative encoding (N = 128 cells total). This analysis was restricted to cells significantly tuned in post-offer1 and post-offer2 time windows (Task 2). An additional 11 cells were removed because measures of order bias were detected as outliers by the interquartile criterion (see **Methods**). Including these cells in the analysis did not substantially alter the results. A similar analysis conducted on chosen value cells yielded similar negative results (not shown).

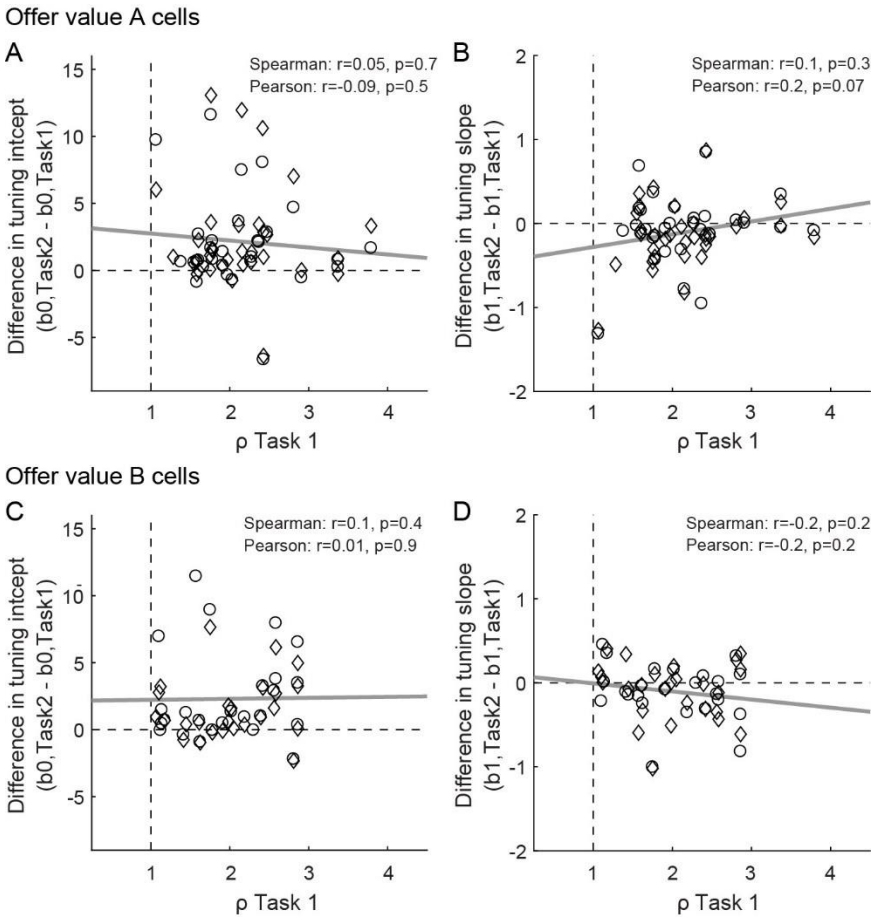

Figure 4.S3. The preference bias does not reflect differences in the tuning of offer value cells. **AB.** Offer value A cells (N = 63 cells). **CD.** Offer value B cells (N = 51 cells). Panels A and C illustrate the relation between differences in tuning intercept (y-axis) and the relative value ρ_{Task1} (x-axis); panels B and D illustrate the relation between differences in tuning slope (y-axis) and ρ_{Task1} (x-axis). For each offer value cell, we examined one time window (post-offer) in Task 1 and two time windows (post-offer1 and post-offer2) in Task 2. In each panel, circles and diamonds refer to post-offer1 and post-offer2 time windows, respectively. Only cells presenting significant tuning in the relevant time windows were included in the analysis (see **Methods**). Exact p values are indicated in each panel and gray lines are from linear regressions. These analyses did not reveal any significant correlation.

Task 1		Task 2		
		post-offer1	**post-offer2**	**post-juice**
offer value A +		offer value A | AB +	offer value A | BA +	chosen value A +
offer value A -		offer value A | AB -	offer value A | BA -	chosen value A -
offer value B +		offer value B | BA +	offer value B | AB +	chosen value B +
offer value B -		offer value B | BA -	offer value B | AB -	chosen value B -
chosen juice A		AB | BA +	AB | BA -	chosen juice A
chosen juice B		AB | BA -	AB | BA +	chosen juice B
chosen value +		offer value1 +	offer value2 +	chosen value +
chosen value -		offer value1 -	offer value2 -	chosen value -

Table 4.S1. Neuronal encoding of decision variables in the two choice tasks. The table summarizes the results of a previous report (Shi et al., 2021). Under simultaneous offers, different groups of OFC neurons encode different decision variables, each with positive or negative sign (indicated here with + and -). In first approximation, each cell encodes the same variable across time windows. Under sequential offers, OFC neurons encode different variables in different time windows. However, the vast majority of them present one of 8 specific patterns of variables, referred to as variable "sequences" and detailed here. Furthermore, there is a clear correspondence between neurons encoding a particular variable in Task 1 and neurons encoding a particular sequence in Task 2. Hence, we can refer to different cell groups in OFC using the standard nomenclature originally defined for Task 1.

Chapter 5: Conclusion

My dissertation focused on two important questions linking the neural activity in the OFC and the economic choices. In the first study, we used micro-stimulation to build the casual link between OFC and economic choices. Monkeys participated in the tasks in which two juice options, offer A and offer B, with various amounts were provided. In the first task paradigm, the two juices were presented sequentially as offer 1 first and then offer 2. High currents injected when offer 1 was presented disrupted the valuation of offer 1 and thus biased the choice in favor of offer 2. Opposite results were observed when stimulating during the offer 2 presentation. Additionally, only the high currents that were injected during the offer 2 presentation, in which comparison between the two juices could be finalized, decreased the choice accuracy (i.e., noisier decisions). These results indicated that high current micro-stimulation in the OFC could disrupt the valuation and potentially the comparison of economic choices and thus induced different behavioral consequences. In the second task paradigm, the two juices were presented simultaneously, and low currents were injected during the presentation of offers. We took advantage of the phenomenon of range adaptation in offer value cells that adapt their linear tuning curves to the value range in one session (Conen and Padoa-Schioppa, 2018; Padoa-Schioppa, 2009). Henceforth, if offer A had higher value range than offer B, neurons associated with offer A (offer value A cells) would have lower tuning slopes. Since low currents increased the firing rates and both A and B cells were affected similarly, lower tuning slopes would induce a higher increase in the value representation, and thus biased the choice in favor of offer A. Opposite results were observed when offer B had higher value range. These results indicated that low current micro-stimulation could facilitate the economic choices through valuation process.

In the second study, we studied the neural correlates of behavioral variabilities and biases under sequential offers. Monkeys participated in a task in which trials under simultaneous offers and sequential offers were randomly interleaved. We first confirmed that the three cell groups as described earlier existed in both task modalities and these cell groups were consistent across task modalities. The result demonstrated that there was only one and the same decision circuit in the OFC that supported both simultaneous offers and sequential offers. With this result in hand, we next examined the neural correlates of behavioral variabilities. Alternating the two modalities allowed us to use the behaviors in simultaneous offers as the baselines and to study the behavioral variabilities specific to sequential offers. We thus found sequential offers had 1) smaller steepness (noisier decisions/lower choice accuracy) compared with simultaneous offers, 2) order bias in favor of offer 2, and 3) higher relative values and this difference increased with the increase of relative values (bias in favor of the preferred juice/preference bias). Each of these phenomena correlated with different neural activities. We found offer value cells had smaller tuning slopes under sequential offers and the difference correlated with steepness difference. This result indicated that weaker valuation under sequential offers correlated with the noisier decisions. On the other hand, both order bias and preference bias correlated with the activity of chosen juice cells in the late time windows, indicating that comparison process related to the two biases. Altogether, these results showed that valuation and comparison could contribute to the behavioral variabilities under sequential offers differently through different groups of cells.

The results from my dissertation provide important and necessary evidence to support the good-based decision model within OFC and its crucial and causal function in economic choices. The analyses discussed in this thesis also provide great insights and pave the way for future studies. First, results in Chapter 2 showed that high current stimulation in offer2 time window affected

both the order bias and steepness, and we interpreted as the disruption of both valuation and comparison stage. However, high current stimulation may also affect passing fibers adjacent to the OFC, therefore, we cannot rule out the possibility that the reduced steepness was due to the disruption of transmission between other brain areas (Jensen and Durand, 2009). Ideally, one would expect the situation in which stimulating OFC only affects comparison stage and decreases the steepness. In a recent unpublished study, we found that stimulation during offer2 time window with very low current level only affects steepness, not the order bias. This result is evidential for the disruption at the comparison stage and the potential reason is that OFC neurons in each stage may have different physical identities and thus have different sensitivities to the electrical stimulation. Therefore, the second important future direction is to understand whether the cell groups identified from activity analysis have physical basis. For example, one can examine whether these groups belonged to different cell types, such as interneurons or pyramidal neurons, or whether they are in different cortical layers. In addition to OFC, BLA seems to have similar functions in the economic choices (Jezzini and Padoa-Schioppa, 2020), therefore, further work should also focus on whether other brain areas, especially BLA, causally contribute to economic choices as well. Our micro-stimulation study provides the paradigm to study other brain areas in a similar way. Besides, it is also important to examine how the connections between OFC and other brain areas relate to economic choices. For example, a recent study showed that communication between OFC and hippocampus was crucial in the value-based learning (Knudsen and Wallis, 2020). Finally, current understandings about economic choices are largely based on simultaneous juice choice tasks. In real life, economic choices could be very complex. Further work should adopt more complex task designs, which will cover more phenomena in the real-life decisions.

References

Agresti, A. (2019). An introduction to categorical data analysis, Third edition. edn (Hoboken, NJ: Wiley).

Alos-Ferrer, C., Hugelschafer, S., and Li, J. (2016). Inertia and decision making. Front Psychol *7*, 169.

Amemori, K., and Graybiel, A.M. (2012). Localized microstimulation of primate pregenual cingulate cortex induces negative decision-making. Nat Neurosci *15*, 776-785.

Arsiero, M., Luscher, H.R., Lundstrom, B.N., and Giugliano, M. (2007). The impact of input fluctuations on the frequency-current relationships of layer 5 pyramidal neurons in the rat medial prefrontal cortex. J Neurosci *27*, 3274-3284.

Balleine, B.W., and Dickinson, A. (1998). Goal-directed instrumental action: contingency and incentive learning and their cortical substrates. Neuropharmacology *37*, 407-419.

Ballesta, S., and Padoa-Schioppa, C. (2019). Economic Decisions through Circuit Inhibition. Curr Biol *29*, 3814-3824 e3815.

Ballesta, S., Shi, W., Conen, K.E., and Padoa-Schioppa, C. (2020). Values encoded in orbitofrontal cortex are causally related to economic choices. Nature *588*, 450-453.

Bartra, O., McGuire, J.T., and Kable, J.W. (2013). The valuation system: a coordinate-based meta-analysis of BOLD fMRI experiments examining neural correlates of subjective value. Neuroimage *76*, 412-427.

Baxter, M.G., Parker, A., Lindner, C.C., Izquierdo, A.D., and Murray, E.A. (2000). Control of response selection by reinforcer value requires interaction of amygdala and orbital prefrontal cortex. J Neurosci *20*, 4311-4319.

Bonaiuto, J.J., de Berker, A.O., and Bestmann, S. (2016). Response repetition biases in human perceptual decisions are explained by activity decay in competitive attractor models. eLife *5*.

Breslow, N.E., and Day, N.E. (1980). Statistical methods in cancer research. Vol. 1. The analysis of case-control studies., Vol 1 (Distributed for IARC by WHO, Geneva, Switzerland).

Britten, K.H., Newsome, W.T., and Saunders, R.C. (1992). Effects of inferotemporal cortex lesions on form-from-motion discrimination in monkeys. Exp Brain Res *88*, 292-302.

Britten, K.H., Newsome, W.T., Shadlen, M.N., Celebrini, S., and Movshon, J.A. (1996). A relationship between behavioral choice and the visual responses of neurons in macaque MT. Vis Neurosci *13*, 87-100.

Brunel, N., and Wang, X.J. (2001). Effects of neuromodulation in a cortical network model of object working memory dominated by recurrent inhibition. J Comput Neurosci *11*, 63-85.

Cai, X., Kim, S., and Lee, D. (2011). Heterogeneous coding of temporally discounted values in the dorsal and ventral striatum during intertemporal choice. Neuron *69*, 170-182.

Cai, X., and Padoa-Schioppa, C. (2012). Neuronal encoding of subjective value in dorsal and ventral anterior cingulate cortex. J Neurosci *32*, 3791-3808.

Cai, X., and Padoa-Schioppa, C. (2014). Contributions of orbitofrontal and lateral prefrontal cortices to economic choice and the good-to-action transformation. Neuron *81*, 1140-1151.

Camerer, C. (2008). Neuroeconomics: Using neuroscience to make economic predictions. In The philosophy of economics: an antology, 3rd edition, D.M. Hausman, ed. (Cambridge University Press), pp. 356-377.

Camerer, C.F., Loewenstein, G., and Prelec, D. (2005). Neuroeconomics: How neuroscience can inform economics. J Econ Lit *43*, 9-64.

Camille, N., Griffiths, C.A., Vo, K., Fellows, L.K., and Kable, J.W. (2011). Ventromedial frontal lobe damage disrupts value maximization in humans. J Neurosci *31*, 7527-7532.

Carmichael, S.T., Clugnet, M.C., and Price, J.L. (1994). Central olfactory connections in the macaque monkey. J Comp Neurol *346*, 403-434.

Carmichael, S.T., and Price, J.L. (1994). Architectonic subdivision of the orbital and medial prefrontal cortex in the macaque monkey. J Comp Neurol *346*, 366-402.

Carmichael, S.T., and Price, J.L. (1995a). Limbic connections of the orbital and medial prefrontal cortex in macaque monkeys. J Comp Neurol *363*, 615-641.

Carmichael, S.T., and Price, J.L. (1995b). Sensory and premotor connections of the orbital and medial prefrontal cortex of macaque monkeys. J Comp Neurol *363*, 642-664.

Cavedini, P., Gorini, A., and Bellodi, L. (2006). Understanding obsessive-compulsive disorder: focus on decision making. Neuropsychol Rev *16*, 3-15.

Cisek, P. (2012). Making decisions through a distributed consensus. Curr Opin Neurobiol *22*, 927-936.

Cohen, M.R., and Newsome, W.T. (2009). Estimates of the contribution of single neurons to perception depend on timescale and noise correlation. J Neurosci *29*, 6635-6648.

Colwill, R.M., and Rescorla, F.J. (1985). Postconditioning devaluation of reinforcer affects instrumental responding. J Exp Psychol Anim Behav Process *11*, 120-132.

Conen, K.E., and Padoa-Schioppa, C. (2015). Neuronal variability in orbitofrontal cortex during economic decisions. J Neurophysiol *114*, 1367-1381.

Conen, K.E., and Padoa-Schioppa, C. (2018). Neuronal adaptation to the value range in macaque orbitofrontal cortex. bioRxiv.

Conen, K.E., and Padoa-Schioppa, C. (2019). Partial adaptation to the value range in the macaque orbitofrontal cortex. J Neurosci *39*, 3498-3513.

Cox, K.M., and Kable, J.W. (2014). BOLD subjective value signals exhibit robust range adaptation. J Neurosci *34*, 16533-16543.

Damasio, H., Grabowski, T., Frank, R., Galaburda, A.M., and Damasio, A.R. (1994). The return of Phineas Gage: clues about the brain from the skull of a famous patient. Science *264*, 1102-1105.

Daw, N.D., Niv, Y., and Dayan, P. (2005). Uncertainty-based competition between prefrontal and dorsolateral striatal systems for behavioral control. Nat Neurosci *8*, 1704-1711.

Eldridge, M.A., Lerchner, W., Saunders, R.C., Kaneko, H., Krausz, K.W., Gonzalez, F.J., Ji, B., Higuchi, M., Minamimoto, T., and Richmond, B.J. (2016). Chemogenetic disconnection of monkey orbitofrontal and rhinal cortex reversibly disrupts reward value. Nat Neurosci *19*, 37-39.

Ethier, C., Brizzi, L., Darling, W.G., and Capaday, C. (2006). Linear summation of cat motor cortex outputs. J Neurosci *26*, 5574-5581.

Fellows, L.K. (2011). Orbitofrontal contributions to value-based decision making: evidence from humans with frontal lobe damage. Ann N Y Acad Sci *1239*, 51-58.

Fellows, L.K., and Farah, M.J. (2007). The role of ventromedial prefrontal cortex in decision making: judgment under uncertainty or judgment per se? Cereb Cortex *17*, 2669-2674.

Friedrich, J., and Lengyel, M. (2016). Goal-directed decision making with spiking neurons. J Neurosci *36*, 1529-1546.

Gallagher, M., McMahan, R.W., and Schoenbaum, G. (1999). Orbitofrontal cortex and representation of incentive value in associative learning. J Neurosci *19*, 6610-6614.

Gardner, M.P.H., Conroy, J.S., Shaham, M.H., Styer, C.V., and Schoenbaum, G. (2017). Lateral orbitofrontal inactivation dissociates devaluation-sensitive behavior and economic choice. Neuron *96*, 1192-1203 e1194.

Gardner, M.P.H., Sanchez, D., Conroy, J.C., Wikenheiser, A.M., Zhou, J., and Schoenbaum, G. (2020). Processing in lateral orbitofrontal cortex is required to estimate subjective preference during initial, but not established, economic choice. Neuron.

Glimcher, P.W., and Rustichini, A. (2004). Neuroeconomics: the consilience of brain and decision. Science *306*, 447-452.

Goodwin, P.B. (1977). Habit and hysteresis in mode choice. Urban Studies *14*, 95-98.

Gore, F., Ramakrishnan, C., Malenka, R., and Deisseroth, K. (2019). The role of fronto-striatal connectivity in value-based decision-making. Society for Neuroscience Abstract, 253.203.

Green, D.M., and Swets, J.A. (1966). Signal detection theory and psychophysics (New York,: Wiley).

Gremel, C.M., and Costa, R.M. (2013). Orbitofrontal and striatal circuits dynamically encode the shift between goal-directed and habitual actions. Nat Commun *4*, 2264.

Griffin, D.M., Hudson, H.M., Belhaj-Saif, A., and Cheney, P.D. (2011). Hijacking cortical motor output with repetitive microstimulation. J Neurosci *31*, 13088-13096.

Hare, T.A., O'Doherty, J., Camerer, C.F., Schultz, W., and Rangel, A. (2008). Dissociating the role of the orbitofrontal cortex and the striatum in the computation of goal values and prediction errors. J Neurosci *28*, 5623-5630.

Hayden, B.Y. (2018). The foraging perspective on economic choice. Current opinion in behavioral sciences *24*, 1-6.

Hayden, B.Y., and Moreno-Bote, R. (2018). A neuronal theory of sequential economic choice. Brain and Neuroscience Advances, 1-15.

Hirokawa, J., Vaughan, A., Masset, P., Ott, T., and Kepecs, A. (2019). Frontal cortex neuron types categorically encode single decision variables. Nature *576*, 446-451.

Histed, M.H., Bonin, V., and Reid, R.C. (2009). Direct activation of sparse, distributed populations of cortical neurons by electrical microstimulation. Neuron *63*, 508-522.

Hosokawa, T., Kennerley, S.W., Sloan, J., and Wallis, J.D. (2013). Single-neuron mechanisms underlying cost-benefit analysis in frontal cortex. J Neurosci *33*, 17385-17397.

Howard, J.D., Gottfried, J.A., Tobler, P.N., and Kahnt, T. (2015). Identity-specific coding of future rewards in the human orbitofrontal cortex. Proc Natl Acad Sci U S A.

Hunt, L.T., Malalasekera, W.M.N., de Berker, A.O., Miranda, B., Farmer, S.F., Behrens, T.E.J., and Kennerley, S.W. (2018). Triple dissociation of attention and decision computations across prefrontal cortex. Nat Neurosci *21*, 1471-1481.

Hunt, L.T., Woolrich, M.W., Rushworth, M.F., and Behrens, T.E. (2013). Trial-type dependent frames of reference for value comparison. PLoS Comput Biol *9*, e1003225.

Hussin, A.T., Boychuk, J.A., Brown, A.R., Pittman, Q.J., and Teskey, G.C. (2015). Intracortical microstimulation (ICMS) activates motor cortex layer 5 pyramidal neurons mainly transsynaptically. Brain Stimul *8*, 742-750.

Hwang, J., Mitz, A.R., and Murray, E.A. (2019). NIMH MonkeyLogic: Behavioral control and data acquisition in MATLAB. J Neurosci Meth *323*, 13-21.

Izquierdo, A., and Murray, E.A. (2004). Combined unilateral lesions of the amygdala and orbital prefrontal cortex impair affective processing in rhesus monkeys. J Neurophysiol *91*, 2023-2039.

Izquierdo, A., Suda, R.K., and Murray, E.A. (2004). Bilateral orbital prefrontal cortex lesions in rhesus monkeys disrupt choices guided by both reward value and reward contingency. J Neurosci *24*, 7540-7548.

Jensen, A.L., and Durand, D.M. (2009). High frequency stimulation can block axonal conduction. Exp Neurol *220*, 57-70.

Jezzini, A., and Padoa-Schioppa, C. (2020). Neuronal activity in the primate amygdala during economic choice. J Neurosci *40*, 1286-1301.

Kable, J.W., and Glimcher, P.W. (2007). The neural correlates of subjective value during intertemporal choice. Nat Neurosci *10*, 1625-1633.

Kable, J.W., and Glimcher, P.W. (2009). The neurobiology of decision: consensus and controversy. Neuron *63*, 733-745.

Kacelnik, A., Vasconcelos, M., and Monteiro, T. (2011). Darwin's "tug-of-war" vs. starling's "horse-racing": how adaptations for sequential encounters drive simultaneous choice. Behav Ecol Sociobiol *65*, 547-558.

Kahneman, D., Slovic, P., and Tversky, A., eds. (1982). Judgment under uncertainty: heuristics and biases (Cambridge, UK; New York, NY: Cambridge University Press).

Kahneman, D., and Tversky, A. (1979). Prospect theory: an analysis of decision under risk. Econometrica *47*, p 263-291.

Kahneman, D., and Tversky, A., eds. (2000). Choices, values and frames (Cambridge, UK; New York, NY: Russell Sage Foundation - Cambridge University Press).

Kang, I., and Maunsell, J.H. (2012). Potential confounds in estimating trial-to-trial correlations between neuronal response and behavior using choice probabilities. J Neurophysiol *108*, 3403-3415.

Kennerley, S.W., Dahmubed, A.F., Lara, A.H., and Wallis, J.D. (2009). Neurons in the frontal lobe encode the value of multiple decision variables. J Cogn Neurosci *21*, 1162-1178.

Kennerley, S.W., Walton, M.E., Behrens, T.E., Buckley, M.J., and Rushworth, M.F. (2006). Optimal decision making and the anterior cingulate cortex. Nat Neurosci *9*, 940-947.

Kim, S., Hwang, J., and Lee, D. (2008). Prefrontal coding of temporally discounted values during intertemporal choice. Neuron *59*, 161-172.

Knudsen, E.B., and Wallis, J.D. (2020). Closed-Loop Theta Stimulation in the Orbitofrontal Cortex Prevents Reward-Based Learning. Neuron *106*, 537-547 e534.

Kobayashi, S., Pinto de Carvalho, O., and Schultz, W. (2010). Adaptation of reward sensitivity in orbitofrontal neurons. J Neurosci *30*, 534-544.

Kolling, N., Behrens, T.E., Mars, R.B., and Rushworth, M.F. (2012). Neural mechanisms of foraging. Science *336*, 95-98.

Krajbich, I., Armel, C., and Rangel, A. (2010). Visual fixations and the computation and comparison of value in simple choice. Nat Neurosci *13*, 1292-1298.

Krajbich, I., Lu, D., Camerer, C., and Rangel, A. (2012). The attentional drift-diffusion model extends to simple purchasing decisions. Front Psychol *3*, 193.

Krajbich, I., and Rangel, A. (2011). Multialternative drift-diffusion model predicts the relationship between visual fixations and choice in value-based decisions. Proc Natl Acad Sci U S A *108*, 13852-13857.

Kreps, D.M. (1990). A course in microeconomic theory (Princeton, NJ: Princeton University Press).

Kuwabara, M., Kang, N., Holy, T.E., and Padoa-Schioppa, C. (2020). Neural mechanisms of economic choices in mice. eLife *9*.

La Camera, G., Giugliano, M., Senn, W., and Fusi, S. (2008). The response of cortical neurons to in vivo-like input current: theory and experiment : I. Noisy inputs with stationary statistics. Biol Cybern *99*, 279-301.

Lak, A., Stauffer, W.R., and Schultz, W. (2014). Dopamine prediction error responses integrate subjective value from different reward dimensions. Proc Natl Acad Sci U S A *111*, 2343-2348.

Lee, S.W., Eddington, D.K., and Fried, S.I. (2013). Responses to pulsatile subretinal electric stimulation: effects of amplitude and duration. J Neurophysiol *109*, 1954-1968.

Levy, I., Snell, J., Nelson, A.J., Rustichini, A., and Glimcher, P.W. (2010). Neural representation of subjective value under risk and ambiguity. J Neurophysiol *103*, 1036-1047.

Louie, K., and Glimcher, P.W. (2010). Separating value from choice: delay discounting activity in the lateral intraparietal area. J Neurosci *30*, 5498-5507.

McGinty, V.B., Rangel, A., and Newsome, W.T. (2016). Orbitofrontal cortex value signals depend on fixation location during free viewing. Neuron *90*, 1299-1311.

Murasugi, C.M., Salzman, C.D., and Newsome, W.T. (1993). Microstimulation in visual area MT: effects of varying pulse amplitude and frequency. J Neurosci *13*, 1719-1729.

Niehans, J. (1990). A history of economic theory: classic contributions, 1720-1980 (Baltimore: Johns Hopkins University Press).

Nienborg, H., and Cumming, B.G. (2006). Macaque V2 neurons, but not V1 neurons, show choice-related activity. J Neurosci *26*, 9567-9578.

Nienborg, H., and Cumming, B.G. (2014). Decision-related activity in sensory neurons may depend on the columnar architecture of cerebral cortex. J Neurosci *34*, 3579-3585.

O'Doherty, J.P. (2014). The problem with value. Neuroscience and biobehavioral reviews *43*, 259-268.

Ongur, D., An, X., and Price, J.L. (1998). Prefrontal cortical projections to the hypothalamus in macaque monkeys. J Comp Neurol *401*, 480-505.

Ongur, D., Ferry, A.T., and Price, J.L. (2003). Architectonic subdivision of the human orbital and medial prefrontal cortex. J Comp Neurol *460*, 425-449.

Ongur, D., and Price, J.L. (2000). The organization of networks within the orbital and medial prefrontal cortex of rats, monkeys and humans. Cereb Cortex *10*, 206-219.

Onken, A., Xie, J., Panzeri, S., and Padoa-Schioppa, C. (2019). Categorical encoding of decision variables in orbitofrontal cortex. PLoS Comput Biol *15*, e1006667.

Ostlund, S.B., and Balleine, B.W. (2008). Differential involvement of the basolateral amygdala and mediodorsal thalamus in instrumental action selection. J Neurosci *28*, 4398-4405.

Padoa-Schioppa, C. (2007). Orbitofrontal cortex and the computation of economic value. Ann N Y Acad Sci *1121*, 232-253.

Padoa-Schioppa, C. (2009). Range-adapting representation of economic value in the orbitofrontal cortex. J Neurosci *29*, 14004-14014.

Padoa-Schioppa, C. (2011). Neurobiology of economic choice: a good-based model. Annu Rev Neurosci *34*, 333-359.

Padoa-Schioppa, C. (2013). Neuronal origins of choice variability in economic decisions. Neuron *80*, 1322-1336.

Padoa-Schioppa, C., and Assad, J.A. (2006). Neurons in orbitofrontal cortex encode economic value. Nature *441*, 223-226.

Padoa-Schioppa, C., and Assad, J.A. (2008). The representation of economic value in the orbitofrontal cortex is invariant for changes of menu. Nat Neurosci *11*, 95-102.

Padoa-Schioppa, C., and Cai, X. (2011). The orbitofrontal cortex and the computation of subjective value: consolidated concepts and new perspectives. Ann N Y Acad Sci *1239*, 130-137.

Padoa-Schioppa, C., and Conen, K.E. (2017). Orbitofrontal cortex: A neural circuit for economic decisions. Neuron *96*, 736-754.

Pastor-Bernier, A., Stasiak, A., and Schultz, W. (2019). Orbitofrontal signals for two-component choice options comply with indifference curves of Revealed Preference Theory. Nat Commun *10*, 4885.

Paus, T. (2001). Primate anterior cingulate cortex: where motor control, drive and cognition interface. Nat Rev Neurosci *2*, 417-424.

Perkins, A.Q., and Rich, E. (2021). Identifying identity and attributing value to attributes: reconsidering mechanisms of preference decisions. Current opinion in behavioral sciences *41*, 98-105.

Petrides, M., and Pandya, D.N. (2006). Efferent association pathways originating in the caudal prefrontal cortex in the macaque monkey. J Comp Neurol *498*, 227-251.

Pickens, C.L., Saddoris, M.P., Setlow, B., Gallagher, M., Holland, P.C., and Schoenbaum, G. (2003). Different roles for orbitofrontal cortex and basolateral amygdala in a reinforcer devaluation task. J Neurosci *23*, 11078-11084.

Plassmann, H., O'Doherty, J., and Rangel, A. (2007). Orbitofrontal cortex encodes willingness to pay in everyday economic transactions. J Neurosci *27*, 9984-9988.

Price, J.L. (2007). Definition of the orbital cortex in relation to specific connections with limbic and visceral structures and other cortical regions. Ann N Y Acad Sci *1121*, 54-71.

Raghuraman, A.P., and Padoa-Schioppa, C. (2014). Integration of multiple determinants in the neuronal computation of economic values. J Neurosci *34*, 11583-11603.

Rahman, S., Sahakian, B.J., Cardinal, R.N., Rogers, R., and Robbins, T. (2001). Decision making and neuropsychiatry. Trends Cogn Sci *5*, 271-277.

Rahman, S., Sahakian, B.J., Hodges, J.R., Rogers, R.D., and Robbins, T.W. (1999). Specific cognitive deficits in mild frontal variant of frontotemporal dementia. Brain *122 (Pt 8)*, 1469-1493.

Rangel, A., Camerer, C., and Montague, P.R. (2008). A framework for studying the neurobiology of value-based decision making. Nat Rev Neurosci *9*, 545-556.

Rhodes, S.E., and Murray, E.A. (2013). Differential effects of amygdala, orbital prefrontal cortex, and prelimbic cortex lesions on goal-directed behavior in rhesus macaques. J Neurosci *33*, 3380-3389.

Rich, E.L., and Wallis, J.D. (2016). Decoding subjective decisions from orbitofrontal cortex. Nat Neurosci *19*, 973-980.

Roesch, M.R., and Olson, C.R. (2005). Neuronal activity in primate orbitofrontal cortex reflects the value of time. J Neurophysiol *94*, 2457-2471.

Roesch, M.R., and Olson, C.R. (2007). Neuronal activity related to anticipated reward in frontal cortex: does it represent value or reflect motivation? Ann N Y Acad Sci *1121*, 431-446.

Roesch, M.R., Taylor, A.R., and Schoenbaum, G. (2006). Encoding of time-discounted rewards in orbitofrontal cortex is independent of value representation. Neuron *51*, 509-520.

Romo, R., Hernandez, A., Zainos, A., Lemus, L., and Brody, C.D. (2002). Neuronal correlates of decision-making in secondary somatosensory cortex. Nat Neurosci *5*, 1217-1225.

Rudebeck, P.H., Behrens, T.E., Kennerley, S.W., Baxter, M.G., Buckley, M.J., Walton, M.E., and Rushworth, M.F. (2008). Frontal cortex subregions play distinct roles in choices between actions and stimuli. J Neurosci *28*, 13775-13785.

Rudebeck, P.H., and Murray, E.A. (2008). Amygdala and orbitofrontal cortex lesions differentially influence choices during object reversal learning. J Neurosci *28*, 8338-8343.

Rudebeck, P.H., and Murray, E.A. (2011). Dissociable effects of subtotal lesions within the macaque orbital prefrontal cortex on reward-guided behavior. J Neurosci *31*, 10569-10578.

Rushworth, M.F., Behrens, T.E., Rudebeck, P.H., and Walton, M.E. (2007). Contrasting roles for cingulate and orbitofrontal cortex in decisions and social behaviour. Trends Cogn Sci *11*, 168-176.

Rustichini, A., Conen, K.E., Cai, X., and Padoa-Schioppa, C. (2017). Optimal coding and neuronal adaptation in economic decisions. Nat Commun *8*, 1208.

Rustichini, A., Domenech, P., Civai, C., and deYoung, C. (2021). Working memory and attention in choice. preprint.

Rustichini, A., and Padoa-Schioppa, C. (2015). A neuro-computational model of economic decisions. J Neurophysiol *114*, 1382-1398.

Saez, R.A., Saez, A., Paton, J.J., Lau, B., and Salzman, C.D. (2017). Distinct roles for the amygdala and orbitofrontal cortex in representing the relative amount of expected reward. Neuron *95*, 70-77 e73.

Saleem, K.S., Miller, B., and Price, J.L. (2013). Subdivisions and connectional networks of the lateral prefrontal cortex in the macaque monkey. J Comp Neurol.

Salzman, C.D., Britten, K.H., and Newsome, W.T. (1990). Cortical microstimulation influences perceptual judgements of motion direction. Nature *346*, 174-177.

Samuelson, P.A. (1938). A note on the pure theory of consumers' behavior. Economica *5*, 61-71.

Samuelson, P.A. (1947). Foundations of economic analysis (Cambridge, MA: Harvard University Press).

Sasikumar, D., Emeric, E., Stuphorn, V., and Connor, C.E. (2018). First-pass processing of value cues in the ventral visual pathway. Current Biology *28*, 538-+.

Schoemann, M., and Scherbaum, S. (2019). Choice history bias in intertemporal choice (https://doi.org/10.31234/osf.io/7h9zj).

Schultz, W. (2015). Neuronal reward and decision signals: from theories to data. Physiol Rev *95*, 853-951.

Senftleben, U., Schoemann, M., Rudolf, M., and Scherbaum, S. (2021). To stay or not to stay: The stability of choice perseveration in value-based decision making. Q J Exp Psychol (Hove) *74*, 199-217.

Shenhav, A., and Greene, J.D. (2010). Moral judgments recruit domain-general valuation mechanisms to integrate representations of probability and magnitude. Neuron *67*, 667-677.

Shi, W., Ballesta, S., and Padoa-Schioppa, C. (2021). Economic choices under simultaneous or sequential offers rely on the same neural circuit. J Neurosci, in press.

So, N.Y., and Stuphorn, V. (2010). Supplementary eye field encodes option and action value for saccades with variable reward. J Neurophysiol *104*, 2634-2653.

Solway, A., and Botvinick, M.M. (2012). Goal-directed decision making as probabilistic inference: a computational framework and potential neural correlates. Psychol Rev *119*, 120-154.

Song, H.F., Yang, G.R., and Wang, X.J. (2017). Reward-based training of recurrent neural networks for cognitive and value-based tasks. In eLife.

Stalnaker, T.A., Cooch, N.K., and Schoenbaum, G. (2015). What the orbitofrontal cortex does not do. Nat Neurosci *18*, 620-627.

Stoney, S.D., Jr., Thompson, W.D., and Asanuma, H. (1968). Excitation of pyramidal tract cells by intracortical microstimulation: effective extent of stimulating current. J Neurophysiol *31*, 659-669.

Strauss, G.P., Waltz, J.A., and Gold, J.M. (2014). A review of reward processing and motivational impairment in schizophrenia. Schizophrenia bulletin *40 Suppl 2*, S107-116.

Takahara, D., Inoue, K.I., Hirata, Y., Miyachi, S., Nambu, A., Takada, M., and Hoshi, E. (2012). Multisynaptic projections from the ventrolateral prefrontal cortex to the dorsal premotor cortex in macaques - anatomical substrate for conditional visuomotor behavior. Eur J Neurosci.

Tolias, A.S., Sultan, F., Augath, M., Oeltermann, A., Tehovnik, E.J., Schiller, P.H., and Logothetis, N.K. (2005). Mapping cortical activity elicited with electrical microstimulation using FMRI in the macaque. Neuron *48*, 901-911.

Tremblay, L., and Schultz, W. (1999). Relative reward preference in primate orbitofrontal cortex. Nature *398*, 704-708.

Tukey, J.W. (1977). Exploratory data analysis (Reading, Mass.: Addison-Wesley Pub. Co.).

Van Acker, G.M., 3rd, Amundsen, S.L., Messamore, W.G., Zhang, H.Y., Luchies, C.W., Kovac, A., and Cheney, P.D. (2013). Effective intracortical microstimulation parameters applied to primary motor cortex for evoking forelimb movements to stable spatial end points. J Neurophysiol *110*, 1180-1189.

Volkow, N.D., and Li, T.K. (2004). Drug addiction: the neurobiology of behaviour gone awry. Nat Rev Neurosci *5*, 963-970.

Wallis, J.D. (2007). Orbitofrontal cortex and its contribution to decision-making. Annu Rev Neurosci *30*, 31-56.

Wallis, J.D. (2012). Cross-species studies of orbitofrontal cortex and value-based decision-making. Nat Neurosci *15*, 13-19.

Wallis, J.D., and Miller, E.K. (2003). Neuronal activity in primate dorsolateral and orbital prefrontal cortex during performance of a reward preference task. Eur J Neurosci *18*, 2069-2081.

Wallis, J.D., and Rich, E.L. (2011). Challenges of Interpreting Frontal Neurons during Value-Based Decision-Making. Front Neurosci *5*, 124.

Wang, X.J. (2002). Probabilistic decision making by slow reverberation in cortical circuits. Neuron *36*, 955-968.

Way, B.M., Lacan, G., Fairbanks, L.A., and Melega, W.P. (2007). Architectonic distribution of the serotonin transporter within the orbitofrontal cortex of the vervet monkey. Neuroscience *148*, 937-948.

Wellman, L.L., Gale, K., and Malkova, L. (2005). GABAA-mediated inhibition of basolateral amygdala blocks reward devaluation in macaques. J Neurosci *25*, 4577-4586.

West, E.A., DesJardin, J.T., Gale, K., and Malkova, L. (2011). Transient inactivation of orbitofrontal cortex blocks reinforcer devaluation in macaques. J Neurosci *31*, 15128-15135.

Wolff, S.B., and Olveczky, B.P. (2018). The promise and perils of causal circuit manipulations. Curr Opin Neurobiol *49*, 84-94.

Wong, K.F., and Wang, X.J. (2006). A recurrent network mechanism of time integration in perceptual decisions. J Neurosci *26*, 1314-1328.

Xie, J., and Padoa-Schioppa, C. (2016). Neuronal remapping and circuit persistence in economic decisions. Nat Neurosci *19*, 855-861.

Yim, M.Y., Cai, X., and Wang, X.J. (2019). Transforming the Choice Outcome to an Action Plan in Monkey Lateral Prefrontal Cortex: A Neural Circuit Model. Neuron *103*, 520-532 e525.

Yu, L.Q., Dana, J., and Kable, J.W. (2018). Individuals with ventromedial frontal damage have more unstable but still fundamentally transitive preferences. bioRxiv.

Zhang, Z., Cheng, Z., Lin, Z., Nie, C., and Yang, T. (2018). A neural network model for the orbitofrontal cortex and task space acquisition during reinforcement learning. PLoS Comput Biol *14*, e1005925.